DEVELOPMENT OF ALUMINIUM ALLOY BASED CARBON FIBRE REINFORCED METAL MATRIX COMPOSITES

A THESIS

Submitted in fulfilment of the
requirements for the award of the degree
of
DOCTOR OF PHILOSOPHY
in
METALLURGICAL AND MATERIALS ENGINEERING

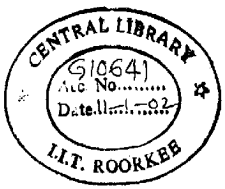

By

RAJNISH GARG

DEPARTMENT OF METALLURGICAL AND MATERIALS ENGINEERING
UNIVERSITY OF ROORKEE
ROORKEE–247 667 (INDIA)

AUGUST, 2000

UNIVERSITY OF ROORKEE
ROORKEE
CANDIDATE'S DECLARATION

I hereby certify that the work which is being presented in the thesis entitled **"DEVELOPMENT OF ALUMINIUM ALLOY BASED CARBON FIBRE REINFORCED METAL MATRIX COMPOSITES"** in fulfilment of the requirement for the award of the Degree of Doctor of Philosophy and submitted in the Department of Metallurgical and Materials Engineering of the University is an authentic record of my own work carried out during a period from August 1994 to August 2000 under the supervision of Dr. R.C. Agarwala and Dr. (Mrs.) V. Agarwala.

The matter presented in this thesis has not been submitted by me for the award of any other degree of this or any other University.

Rajnish

(RAJNISH GARG)

Dated: 26/08/2000

This is to certify that the above statement made by the candidate is correct to the best of our knowledge.

V. Agarwala

Dr. (Mrs.) V. AGARWALA
Asst. Professor
Met. & Matls. Engg., UOR

Kagarwala.

Dr. R. C. AGARWALA
Asst. Professor
Met. & Matls. Engg.,UOR

The Ph.D. Viva-Voce examination of **RAJNISH GARG**, Research Scholar, has been held on 21.04.2001

Kagarwal

V. Agarwal 21/4/2001

Signature of Supervisor(s)

Signature of H.O.D.

Signature of External Examiner

ABSTRACT

Fibre reinforced metal matrix composites (FMMCs), are a new range of advanced engineering materials used mainly at elevated temperatures where existing materials are not suitable for use. The FMMCs can be tailored to produce various combinations of stiffness and strength. The FMMCs are generally anisotropic, but show very high strength and modulus along the direction of fibre alignment.

When costly fibres are reinforced in metal matrices by relatively costlier processing route of powder metallurgy and diffusion bonding, then very expensive FMMCs are produced. These can only be used in aerospace and military industries as these industries offer a large premium on weight saving. Aluminium and its alloys when reinforced with low cost and low density carbon fibres, by relatively economical solidification processing route, produce cheap FMMCs having specific strength and specific modulus far superior to those of steels. Therefore, aluminium-carbon fibre (Al/CF) composites may have a high potential to be used even in automotive industries where premium on weight saving is very less as compared to aerospace and military industries.

Carbon fibres are poorly wetted by aluminium and its alloys at low temperatures and aluminium reacts with carbon fibres at high temperature resulting in poor infiltration and degraded fibres respectively. The problem of poor wettability can be solved by adding sufficient amounts of surface active or reactive elements to aluminium, whereas the degradation of fibres can be minimised by using squeeze casting technique for the solidification synthesis of the Al/CF composite. Thus, it is possible to reinforce the carbon fibres uniformly by the solidification processing in aluminium alloy matrices without substantial degradation of fibres.

The mechanical properties of FMMC largely depend upon the distribution of the fibres, volume fraction of the fibres and interfacial bonding between the fibres and the matrix. Other microstructural features, like uneven solute distribution in the composite

matrix, grain size of the matrix and thermal stresses, developed due to the difference in the thermal expansion coefficients of the constituents, can also alter the mechanical behaviour of the FMMC.

In the present study, wetting of three aluminium alloys containing Cu, Li and Zr as alloying additions respectively, on vitreous carbon substrate has been investigated as a function of temperature and of Li and Zr content in the alloys (in case of Al-Li and Al-Zr alloys). The selected alloys have been reinforced with high strength carbon fibres by solidification processing. These FMMCs have been characterized by their microstructures. The mechanical properties of these composites have been determined in as cast condition at ambient temperature. Finally, a theoretical model has been developed to predict the compressive behaviour of carbon fibres during squeeze casting. An expression for limiting fibre thickness reduction is also established.

Chapter- 1 outlines the introductory remarks underscoring the purpose and technological importance of the problem under investigation.

Chapter- 2 contains critical review of the existing literature on the solidification processing and mechanical properties of FMMCs.

The various problems and their remedies as pointed out by early workers have been critically reviewed. The various fabrication methods that have been used so far for FMMCs have been discussed in general and squeeze casting technique in particular as this technique has been used for the synthesis of FMMCs in the present study. A critical review on the fabrication of Al/CF composites by various methods and their microstructure as observed by other workers earlier has also been given in this chapter. Finally, this chapter reviews the existing knowledge base on the mechanical and physical properties of Al/CF composites.

Chapter- 3 deals with the details of the experimental procedure followed in the present study for evaluating the wettability of aluminium alloys with vitreous carbon, the

fabrication of composites by squeeze casting, microstructural characterization of the composites and determination of mechanical properties of the composites.

The detailed description of sessile drop setup used in the present study to investigate the wetting of various aluminium alloys with vitreous carbon substrate has been outlined. The pilot experiments on Al/Al_2O_3 system, conducted for the selection of holding time for aluminium alloy-vitreous carbon ($Al\text{-}X/C_v$) system in the present study, have been outlined. The wetting of aluminium alloys containing Cu, Li and Zr with vitreous carbon have been evaluated by measuring the contact angle 'θ' of the aluminium alloy drop as a function of temperature for a holding time of 10 mins after melting in argon atmosphere. The work of adhesion 'w_a' has been measured, by determining the surface tension of the alloys at specific temperatures, as a function of Li and Zr contents in the alloys.

The experimental procedure followed in the present investigation for the fabrication of the composites has been described in this chapter. The die and plunger have been designed and fabricated according to the requirement. A proper heat treatment has been given to die and plunger to increase their hardness and to relieve the stresses developed during machining. A proper description of the designing, fabrication and heat treatment process for die and plunger has been given in this chapter. The method used for the preparation of fibre preform has been described. The details of the squeeze casting setup and the parameters used for the synthesis of the composites have been outlined. A brief description of the methods used for the determination of chemical composition of matrix alloys and fibre volume fraction in the composites has been presented.

The standard techniques used for the microstructural characterization of the composites have also been outlined in this chapter. Scanning electron microscopy (SEM), electron probe microanalysis (EPMA), X-ray diffraction analysis (XRD) and transmission electron microscopy (TEM) have been described in detail. The phases identified by XRD analysis have been supplemented by the results of electron probe

microanalysis (EPMA) and selected area diffraction patterns (SAD) of selected regions in the composite microstructures.

This chapter also describes the experimental procedure followed in the present study to determine the physical and mechanical properties of different Al/CF composites in as cast condition at ambient temperature. The extent of interaction between carbon fibres and different aluminium alloy matrices has been determined by the fibre strength degradation in different aluminium alloy composites. The fibres have been extracted from the composites and their strength has been determined by single fibre tensile tests. Real transfer efficiency of fibre strength has been calculated for different composites. Methods followed for the determination of fibre strength, physical and mechanical properties alongwith the specifications of the specimens used in this study have been outlined.

Chapter- 4 deals with the results and discussion on the wetting behaviour of various aluminium alloys with vitreous carbon.

The contact angle 'θ' is found to decrease with the increase in temperature for all the aluminium alloys investigated in the present study. In low temperature range of 700^0C to 925^0C, the contact angle is very large (160^o to 135^o) for Al-Cu and Al-Zr alloys and decreases very slowly to reach a value of about 135^o at 850^0C. However, in the same temperature range, Al-Li alloys show a considerable decrease in the contact angle by having a value of about 100^o at 850^0C. The contact angle decreases rather rapidly in low temperature range for Al-Li alloys. At high temperatures, i.e., above 1000^0C, all the alloys wet the carbon substrate by attaining a value of θ less than 90^o. However, the contact angle decreases very rapidly in this temperature range for Al-Cu and Al-Zr alloys whereas it decreases slowly in this temperature range for Al-Li alloys. With increasing Zr content, the contact angle remains nearly unchanged at low temperatures whereas it decreases significantly with increase in Zr content at high temperatures. The effect of Li content is more pronounced at low temperatures as contact angle varies significantly for different Al-Li alloys, but it has a negligible effect at high temperatures as the contact angles are very close to each other for different Al-Li alloys.

At low temperatures, the work of adhesion 'w_a' is found to increase very slowly with temperature for Al-Cu and Al-Zr alloys. The values of w_a measured in the low temperature range varies from 100 mJ/m^2 to 150mJ/m^2 for Al-Cu and Al-Zr alloys. The work of adhesion 'w_a' increases rapidly with increasing temperature in low temperature range for Al-Li alloys. The values of w_a measured for Al-Li /C_v system in low temperature range varies from 250 mJ/m^2 to 500 mJ/m^2, depending upon the temperature and composition of the alloys. At high temperatures, w_a increases very rapidly with temperature for Al-Cu and Al-Zr alloys whereas it increases slowly with temperature for Al-Li alloys. At high temperatures, w_a attains values between 500 ~ 1100 mJ/m^2, depending upon the temperature and composition of Al-Cu and Al-Zr alloys whereas it shows values between 650 ~ 800 mJ/m^2 for Al-Li alloys at these temperatures. At low temperatures, w_a increases with Li content for Al-Li/C_v system while it remains constant for Al-Zr/C_v system with increasing Zr content in the alloy. At intermediate and high temperatures, w_a increases very rapidly with Zr content for Al-Zr/C_v system while it remains nearly constant with Li content for Al-Li/C_v system.

Although, all the investigated alloys show wettability with vitreous carbon substrate at about 1000^{0}C, from a practical point of view, none of the investigated alloys wets the carbon substrate for a short holding time of 2 minutes at 1000^{0}C and above. The contact angle measured for Al-Li/C_v and Al-Zr/C_v systems in the present study is higher than the contact angle of Al-Li/C_v and Al-Ti/C_v systems respectively, as measured by other workers. The discrepancy can be attributed to the low concentration of alloying elements and different experimental conditions used in the present study.

Chapter- 5 deals with the results and discussion regarding the fabrication and microstructural characterization of the composites.

The quality of the castings is found to be very good for the unreinforced alloys and the composites. The chemical composition of the alloy matrices in the composites, as determined by inductive coupled plasma (ICP), shows very little variation in the concentration of primary alloying elements, i.e., Cu and Zr after squeeze casting in case

of Al-Cu/CF and Al-Zr/CF composites respectively. The lithium concentration decreases considerably after squeeze casting in Al-Li/CF composites. The optical microscopy, carried out to determine the fibre volume fraction, shows little increase in the actual fibre volume fraction of the composites over precalculated fibre volume fraction. The fibre distribution observed in Al-Li/CF composites is more uniform than that observed in Al-Cu/CF and Al-Zr/CF composites.

The scanning electron microscopy (SEM) reveals the extent of infiltration of different aluminium alloys in the carbon fibre reinforcement. The SEM analysis shows the presence of reaction interface in Al-Cu/CF and Al-Zr/CF composites but no trace of reaction is detected at the interface of Al-Li/CF composite. The EDS and EPMA analysis of the interfibre region confirms the uniform distribution of alloying elements in the matrices of Al-Cu/CF and Al-Li/CF composites respectively. The EPMA line analysis of the interfibre region also confirms the uniform distribution of alloying elements in the matrix and the presence of Zr at the interface of Al-Zr/CF composite. The EPMA analysis of Li in Al-Li/CF composite could not be conducted, as EPMA equipment (model JEOL 8600M) is unable to detect the Li element. The XRD analysis shows the presence of Al_4C_3 in Al-Cu/CF and Al-Zr/CF composites, however, Al-Zr/CF composite also has ZrC phase. Intercalation compound LiC_{16}, lithium carbide (Li_2C_2) and lithium oxide (Li_2O) phases have been detected in Al-Li/CF composite alongwith other primary phases present in Al-Li alloy. The TEM study of Al-Cu/CF composites reveals the presence of Al_4C_3, $CuAl_2$ and AlFeSi phases at the interface.

Chapter- 6 contains the results and discussion on the observed mechanical properties and fracture behaviour of different composites fabricated in the present study.

The fibre strength is found to decrease by about 11% after preheating at 650^0C in argon atmosphere. The fibre strength degradation is about 31% and 37% in Al-Cu/CF and Al-Zr/CF composites respectively. The fibre strength degradation is relatively less and about 23% in Al-Li/CF composites. Depending upon the fibre volume fraction of the composites, the fibre strength transfer efficiency varies from 0.310 to 0.253, 0.298 to

0.270 and 0.329 to 0.245 for Al-Cu/CF, Al-Li/CF and Al-Zr/CF composites respectively. The high transfer efficiency of the fibres corresponds to low volume fraction of carbon fibres in the composites.

Depending upon the fibre volume fraction of the composites, the density of the composites varies from 2203 to 2669, 2154 to 2523 and 2262 to 2723 kg/m^3 for Al-Cu/CF, Al-Li/CF and Al-Zr/CF composites respectively. These values are slightly higher than the theoretical density values, estimated by law of mixtures.

The Brinell hardness values as determined are found to be higher for Al-Zr/CF composites than those for Al-Cu/CF and Al-Li/CF composites. Depending upon the fibre volume fraction, the Brinell hardness values vary from 89 to119, 97 to 114 and 84 to 127 kg/mm^2 for Al-Cu/CF, Al-Li/CF and Al-Zr/CF composites respectively. The high hardness values correspond to high volume fraction of carbon fibres in the composites.

The % elongation of the composites is found to decrease with increasing fibre volume fraction. The % elongation of Al-Cu/CF composites is higher than that of Al-Li/CF and Al-Zr/CF composites. Depending upon the fibre volume fraction, % elongation varies from 1.7% to 1.2%, 1.9% to 1.4% and 1.5% to 1.0% for Al-Cu/CF, Al-Li/CF and Al-Zr/CF composites respectively. The high values of % elongation correspond to low volume fraction of carbon fibres in the composites.

The tensile strength of the composites is found to be higher for Al-Li/CF composites than for Al-Cu/CF and Al-Zr/CF composites. Depending upon the volume fraction of the fibres, the tensile strength varies from 309 to 463 MPa, 376 to 562 MPa and 268 to 403 MPa for Al-Cu/CF, Al-Li/CF and Al-Zr/CF composites respectively. The high strength values of these composites correspond to high volume fraction of carbon fibres. These strength values lie between 27~45% of the estimated values based on law of mixtures. The strength values, determined in the present study for Al-Cu/CF and Al-Zr/CF composites are lower while that of Al-Li/CF composite is higher than the strength of the composites having the same volume fraction of carbon fibres, as determined by

other workers. This difference is attributed to heavy degradation of carbon fibres in Al-Cu and Al-Zr alloy matrices and light degradation in Al-Li alloy matrix.

Chapter- 7 describes the theoretical model developed to investigate the compressive behaviour of carbon fibres during squeeze casting. This model is based on hexagonal distribution of the carbon fibres in the squeeze cast composite. On the basis of this model, an analytical expression for relating the fibre volume fraction and the fibre thickness reduction has been established. A prediction of the limiting fibre thickness reduction is also obtained. The analysis is verified by experimental data obtained in case of Al-Cu/CF composite fabricated by squeeze casting technique. The results of this study also have significant implication in the understanding of preform permeability during squeeze casting of the composites.

Chapter- 8 presents the major conclusions of the current study on the wettability of different aluminium alloys with vitreous carbon, solidification processing, microstructural characterization and the physical and mechanical properties of aluminium alloys based carbon fibre reinforced metal matrix composites.

ACKNOWLEDEGMENTS

I express my deep sense of gratitude to **Dr. R.C. Agarwala** and **Dr. (Mrs.) V. Agarwala**, Assistant Professor, Metallurgical and Materials Engineering for their valuable guidance and insightful advice. I have greatly benefited from their knowledge and experience throughout this work.

I am grateful to Dr. S. Ray, Professor & Head, Metallurgical and Materials Engineering Department for his co-operation and facilities provided by him throughout my research work. I am also grateful to the faculty members of the department especially Dr. M.L. Kapoor, Dr. Satyaprakash, Dr. R.P. Ram, Dr. G.C. Kaushal, Dr. S.K. Nath and Dr. D. Puri for their suggestions time to time during my research work.

I can not forget Dr. K. Chandra, Director, USIC and his staff members especially Mr. J.S. Saini, Mr. R. Juyal, Mr. T. Ghosh, Mr. S. Kumar and Mrs. R. Sharma for their help in analysing the specimens during my research work.

I am thankful to the technical staff of the department especially Mr. A. Singh, Mr. M.K. Singh, Mr. S.S. Gupta and Mr. Vidya for their help during this research work. I am also thankful to Mr. A.K. Jethi, Incharge Photographic Section, C.B.R.I, Roorkee, Mr. A.K. Gaur, Incharge CAD Lab, Civil Engineering, U.O.R, and Mr. Y. Atray, WRL, U.O.R for the help extended by them in carrying out this research work successfully.

Lastly, I would like to thank my friend Mr. I. Singh, Research Scholar, NPL, Delhi for providing me the necessary testing facilities to carryout this research work. I am extremely thankful to my parents, my in laws, my wife Neetika Garg and my daughter Khushbu Garg for their patience, encouragement and support I received during this research work. Last but not least, I want to thank my friends especially Mr. S. Juyal and Mr. R. Kumar for their moral support to me throughout this work.

RAJNISH GARG

CONTENTS

Page No.

LIST OF FIGURES

LIST OF TABLES

NOMENCLATURE

θ	Contact angle
w_a	Work of adhesion
γ_{sl}	Solid-liquid interfacial energy
γ_{sv}	Surface energy of solid
γ_{lv}	Surface energy of liquid
η	Shape factor
b	Radius of curvature
ρ	Density of the alloy
g	Acceleration due to gravity
m	Magnification
ΔT	Increase in freezing temperature
T_m	Melting temperature of the alloy
V_1	Specific volume of solid phase
V_2	Specific volume of liquid phase
ΔP	Increase in pressure
ΔP_T	Applied pressure
ΔP_γ	Pressure required for preform penetration
ΔP_μ	Pressure required for preform infiltration
γ_{fl}	Fibre-liquid surface energy
γ_{fv}	Surface energy of fibre
S_f	Surface area per unit volume infiltrated at time t

V_f	Fibre volume fraction
r_f	Radius of the fibre
V_o	Superficial velocity
μ	Viscosity of the liquid metal
K	Permeability of the preform
P_μ	Pressure in the liquid metal
ρ_m	Density of the matrix
V_{sf}	Volume fraction of solid phase
r_{sf}	Radius of the solid phase
L	Infiltration length
t	Time
H	Latent heat of solidfication of the matrix
ΔG	Gibbs standard free energy
E_c	Modulus of the composite
E_f	Modulus of the fibre
E_m	Modulus of the matrix
σ_c	Tensile strength of the composite
σ_f	Tensile strength of the fibres
σ_m	Tensile strength of the matrix
V_m	Volume fraction of the matrix
ε_c	Fracture strain of the composite
ε_f	Fracture strain of the fibre
ε_m	Fracture strain of the matrix

σ_{my}	Matrix yield strength
ε_{my}	Matrix yield strain
$\left(\sigma_{my}\right)_f$	Matrix stress at the fracture strain of the fibre
V_{min}	Minimum fibre volume fraction
V_{crit}	Critical fibre volume fraction
l	Fibre length
l_c	Critical fibre length
$F(\sigma_f)$	Cumulative distribution function
α	Scale parameter
β	Shape parameter
S_d	Standard deviation
C_v	Coefficient of variation
Γ	Gamma function
λ	Wavelength
d	Interplanar spacing
B	Beam direction
ρ_c	Density of the composite
ρ_l	Density of the liquid
w_1	Weight in air
w_2	Weight in liquid
HB	Brinell hardness
P	Applied load
D	Diameter of the indentor

D_t	Diameter of the indentation
s	Distance between two adjacent fibres
S	Distance between the centres of the two fibres
υ_{av}	Average shear strain
υ_{max}	Maximum shear strain
τ	Interfacial shear strength
V_f^0	Fibre volume fraction before compaction
V_f^{max}	Limiting value of fibre volume fraction
V_a	Yarn packing fraction
V_y	Fibre volume
V_u	Volume of the unit cell
r_z	Thickness reduction
r_z^{max}	Maximum thickness reduction
$\left(\frac{d\sigma_m}{d\varepsilon_m}\right)_{\varepsilon_f}$	Slope of stress-strain curve at the fracture strain of fibres

INTRODUCTION

Enhanced performance and cost effectiveness are two major conflicting, yet driving forces leading to the development of new materials. This may be achieved by adopting advanced processing techniques and also by combining two or more materials with superior qualities. Most of the engineering materials derive superior properties from a combination of components rather than a single component. These materials, mainly made up of a combination of two or more phases dispersed on a microscopic scale to obtain the optimum properties, are called composite materials.

Fibre reinforced metal matrix composite (FMMC) is one of the various types of composites where metal acts as the matrix, i.e., the bonding element and fibres act as the load bearing elements. The main function of the metal matrix is to transfer and distribute the load to fibres. The continuous fibre reinforced MMCs have a combination of different superior properties like high strength, high elastic modulus, high service temperature, good wear resistance, high electrical and thermal conductivity, low coefficient of thermal expansion, high vacuum environmental resistance etc. as compared to unreinforced metal matrix (1). The spectrum of properties that one can achieve in these composites is a result of synergy between the constituents. Thus, these composites have extended the horizon of engineering materials and significant research efforts have been directed to develop different fibre reinforced MMCs and to determine their potential as future engineering materials.

Development of fibre reinforced MMCs is continuing for the past forty years. Initial MMC work was stimulated by the high performance needs of the aerospace industry, which places performance ahead of price, at least in development programs. Initially, the development of FMMC was mainly directed towards diffusion bonding processes. Several factors like efficiency, cost, limited number of foil alloys, limitation on product geometry and the size, placed limitations on the potential of the hot-press diffusion-bonding processes. The only aerospace application at that time was of boron/aluminium FMMC, used as tubing for cargo bay stiffeners on the space

shuttle (2). After twenty years of development, because of insignificant commercial application (other than the shuttle tubes), it was obvious that a MMC must also be cost competitive with other materials. Thus, the emphasis of the 80s was towards cheaper reinforcement and net shape technology including rapid and simple production techniques. In comparison with other techniques, for FMMC fabrication, solidification processing stands out as potentially simple and economical. This has driven the developers towards casting processes with modern multifilament yarns, as the reinforcement.

A major thrust in the development of fibre reinforced composites technology has come from the efforts to substitute relatively heavy conventional components by those made of light weight composites. However, depending on the quantum of economic advantage, the premium on weight savings is different in land, air and space transportation. A common figure for the value of weight savings in aerospace is $2000/kg or more and for civil aircraft is $100-1000/kg (3). The automobile industry may be able to afford an additional expenditure of $10/kg against the $10000/kg for the missile industry (4). The quality and reliability of the components and access to the technologies, for the manufacturers of composite components, are limited by the extent of economic advantage.

The continuous fibre reinforced composites are very expensive because of the high cost of continuous fibres and of the production/development. They are not competitive, if the value of weight savings is not taken into account. Though, aerospace and military industries are low volume user of composite materials but due to the high premium on weight saving, continuous fibre reinforced composites find application mainly in these industries and slightly in automobile industries. The main reason, of these composites being more profitable in aerospace and military areas than conventional materials, lies in the fact that fuel can be saved due to light weight of the structure. It is also possible to add additional weight into a system such as the space shuttle and the range of a missile can be increased for the same payload (5).

Today, the main focus is on aluminium as matrix in FMMCs because of its unique combination of good corrosion resistance, low electrical resistance and excellent mechanical properties (6). To obtain good bonding and strength in the

composites, aluminium alloys are used as the matrix instead of pure aluminium. The 2xxx, 6xxx and 7xxx alloys have been used widely as matrices, for making FMMCs. Recently, Al-Li alloy (8xxx) has been attracting the attention of researchers due to its good wettability characteristics resulting in improved interfacial bonding with the reinforcement. The 2xxx alloys provide excellent combinations of strength and damage tolerance whereas 8xxx alloys provide the opportunity for high temperature performance (7).

Many kinds of continuous fibres such as boron, alumina, silicon carbide and carbon fibres have been reinforced in different metal matrices. But carbon fibre reinforced aluminium composites have been an area of considerable interest over the last three decades, primarily for their high specific strength, high specific modulus, high temperature applications and excellent thermal and electrical conductivity. They have many applications in aircraft, missiles, rocket propulsion systems, spacecraft and electrical machinery (8). Aluminium alloys reinforced with continuous fibres of graphite/carbon have good high temperature properties, which makes them interesting for tactical missile skin, stiffeners and launch tubes (9).

Carbon fibres have been classified into two main categories according to their mechanical properties, i.e., high strength carbon fibre and high modulus carbon fibre. The mechanical properties of carbon fibres depend upon their microstructure and the degree of crystallite orientation. High modulus carbon fibres, having a density about 1.8 to 2.2 g/cm^3, are highly graphitized at a temperature above 2000^0C and are characterized by a high modulus. They have the long distance order of graphite crystallites, mainly parallel to the fibre axis. High strength fibres, which are heat treated at a temperature lower than 1500^0C, have a low modulus but very high strength. Although, high strength carbon fibres also have crystallite orientation mainly parallel to the fibre axis, the size of the crystallites is very small as compared to that of high modulus carbon fibres (10). The high strength carbon fibres are the cheapest (except alumina fibres) and easily available (6).

Design of composite materials, for a given application, may address primary issues like the selection of the reinforcement and the matrix, their wettability, the nature of interface to attain good bonding and reproducibility. The wettability of the

fibre reinforcement by metal matrix generally determines the bonding at the interface. Most of the fibre reinforcements are poorly wetted by the molten metal. It is the bonding at the interface, which plays an important role in determining the properties of a composite. Normally, in continuous fibre reinforced MMCs, employed in static or dynamic structures, it is desirable to have a sufficiently strong interface which could transfer and distribute the load from matrix to the fibres. The composites with weak interfaces generally have low strength and stiffness but high fracture toughness while a strong interface usually leads to high strength and stiffness but poor fracture toughness. A medium strength bonding at the interface results in high strength and stiffness with good fracture toughness. These properties are related to the ease of debonding and pullout of fibres from the matrix, during crack propagation (11). In the ideal case, the bonding should be a continuum across the interface, involving coherency of bonds at the atomic level but a chemical discontinuity requiring absence of any interdiffusion between the constituents.

The fabrication of Al/CF composites by liquid phase fabrication methods is limited mainly due to two recurrent problems: Molten aluminium and its alloys do not wet carbon up to 950^0C and carbon reacts with aluminium to form aluminium carbide above 950^0C resulting in poor infiltration and degraded fibres respectively. It has been reported by many workers that high modulus carbon fibres are less degraded than high strength carbon fibres due to the differences in crystal structure and surface properties, as these determine the reactivity of carbon fibres with aluminium and its alloys (12,13). However, some workers have shown that high strength carbon fibres are less degraded when reinforced in aluminium alloy matrices containing sufficient amount of surface active elements like Li, Mg and Ca (14).

The wettability of carbon reinforcement by aluminium and its alloys can be enhanced by various methods. The most simple and economical method is to modify the aluminium matrix by alloying additions. Two types of alloying additions have been used for enhancing the wettability of carbon by aluminium. The first alloying additions are those, which promote reaction between carbon and aluminium whereas the second alloying additions modify the characteristics of oxide layer present on the surface of molten aluminium (15-17). It has been reported that these alloying additions must have sufficient concentration in aluminium to produce a significant

improvement in the wettability (18,19). This also helps, as the liquidus temperature of highly alloyed aluminium matrix is relatively lower than that of aluminium, however, the addition of reactive elements increases the liquidus temperature of the aluminium alloy (20).

The primary methods for solidification processing of metal matrix composites having continuous fibre reinforcement, as established over recent years, are (i) liquid metal infiltration and (ii) squeeze casting. The application of liquid metal infiltration is limited because of the wettability problem of most of the fibre reinforcements with all liquid metals at low temperatures and the degradation of the fibre reinforcement at high temperatures. However, both the methods as well as several variations of these two have been used to make continuous carbon fibre reinforced aluminium alloy matrix composites (21-23).

In squeeze casting, a hydrostatic pressure is applied to the entire volume of liquid metal in a die cavity which contains the preheated fibre perform. The high pressure assures the wetting of the fibres by the liquid metal and a casting free of shrinkage and porosity is produced due to expulsion of all the absorbed and trapped gases. The high pressure also ensures the elimination of the air film at the liquid-die interface so as to enhance the heat transfer across the die wall and results in a rapid solidification of the composite casting. Another advantage of the high pressure application in squeeze casting is that the freezing temperature of the metal matrix is increased according to the Clausius-Clapeyron equation (23).

At high temperatures, the degradation of carbon fibres in aluminium matrix often results due to the chemical reaction forming compounds like Al_4C_3 (24,25). Thus, the degradation of fibres is associated with the reaction kinetics between fibres and aluminium matrix. In other words, it depends upon processing time and temperature of composite fabrication as reaction kinetics is governed by these two parameters.

The advantage of highly alloyed aluminium matrices is their lower liquidus temperature as compared to pure aluminium. In these conditions, the reaction kinetics between aluminium and carbon can be slowed down during processing of the

composite. On the other hand, by using squeeze casting technique, the processing time can be reduced due to rapid solidification under high hydrostatic pressure as well as due to increase in the freezing temperature of the aluminium alloy matrix. Thus, it is possible to fabricate continuous carbon fibre reinforced aluminium alloy matrix composites by squeeze casting at high pressure and moderate temperatures (700-800^{0}C) without degrading the carbon fibres. At the same time, one may overcome the problem of poor wetting of carbon fibres by aluminium alloys at these temperatures.

The addition of reinforcements generally has a strong effect on the microstructure of composite matrix. The presence of reinforcements within the matrix can cause a variety of phenomena including localized plastic flow, interfacial precipitation, grain size refinement and uneven solute distribution. Several of these effects are found in aluminium alloys reinforced with carbon fibres (26). Most of these factors largely influence the mechanical properties of the composites. So, microstructural characterization of aluminium alloy reinforced with continuous fibres is a necessary step in determining the effect of processing parameters on mechanical behaviour and in understanding the fundamental mechanisms of its failure.

In fibre reinforced aluminium alloy composites, most of the mechanical properties like hardness, tensile strength and tensile modulus increase with increasing fibre volume fraction (27). On the other hand, the ductility and density of these composites decrease with increasing fibre volume fraction. So, one has to compromise with low ductility of these composites against the advantage of weight saving; but the span to tailor the properties according to the requirement is quite large to adjust the low ductility. Thus, these composites may have the potential to be used in aeronautical and military areas, where weight saving is of prime interest in addition to high specific strength and high specific stiffness.

To summarize, the present study is an attempt to explore the possibilities of developing high strength carbon fibre reinforced aluminium alloy matrix composites having superior mechanical properties. The effect of two types of alloying additions to aluminium is investigated to evaluate the improvement in the wettability of aluminium with carbon. The concentration of these alloying additions has been optimized to produce sufficient wettability and bonding by keeping the density of the

alloys nearly equal to that of aluminium. The contact angle of aluminium alloys containing different concentrations of these alloying additions has been compared with the contact angle of an aluminium alloy containing neutral alloying addition. The solidification processing method and alloy matrices have been selected on the basis of wettability studies to reinforce the carbon fibres. The processing parameters have been selected by optimizing 'complete infiltration' and 'minimum degradation' of fibres.

The microstructural characterization of these composites has been carried out to observe the effect of fibre addition in different aluminium alloy matrices. The extent of interaction and bonding between carbon fibres and different aluminium alloy matrices has been evaluated in terms of fibre strength degradation during solidification processing of the composites. These microstructural features alongwith the extent of fibre degradation have been correlated to the observed mechanical behaviour of different composites. Finally, a theoretical model has been developed to predict the compressive behaviour of carbon fibres during squeeze casting.

The knowledge base generated through this study is expected to offer a better understanding regarding the fabrication and mechanical behaviour of continuous fibre reinforced metal matrix composites. It also helps in tailoring the various properties of continuous fibre reinforced metal matrix composites so as to utilize their potential as structural materials for future applications in aeronautical and military areas.

LITERATURE REVIEW

2.1 INTRODUCTION

The art and science of combining molten aluminium and its alloys with carbon fibres mainly consists of two recurrent problems: Molten aluminium and its alloys do not wet carbon fibres at low temperatures and aluminium reacts with carbon to form Al_4C_3 at high temperatures. The wetting of carbon by aluminium using the sessile drop method was initially investigated by Naidich and Kolesnichenko (28) in 1965. Later, Eustathopoulos et al. (29), in their pioneering work on the wettability of aluminium with carbon, have pointed out that the poor wettability of carbon by aluminium is due to the oxide layer present on the molten aluminium surface, which prevents the direct contact of aluminium with carbon.

Several methods have been developed to overcome the problem of poor wettability of carbon by aluminium. Manning et al. (18) and Nicholas et al. (30) have tried to improve the wettability by alloying additions whereas several others have used metallic coatings on carbon fibre surface to improve the wettability (31-33).

Many methods have been developed for the solidification processing of carbon fibre reinforced aluminium matrix composites. Pepper et al. (34) were the first to successfully infiltrate the carbon fibres by aluminium-silicon alloy through liquid metal infiltration technique and most probably, first to take a patent (35) on the solidification processing of these composites. Afterwards, early workers have developed many methods based on pressure casting. These include vacuum infiltration (36), squeeze casting (37), pressure infiltration (12) and pressure assisted network infiltration (38).

2.2 WETTABILITY

Wettability is described by the contact angle 'θ' formed at the line of contact of three phases-solid (s), liquid (l) and vapour (v). The contact angle 'θ' is defined as the angle included between the tangent to the surface of the liquid and the tangent to the surface of the solid at any point, along their line of contact.

If a liquid drop rests on a solid substrate, as shown in Fig.2.1, the wetting angle 'θ' characterizes the wetting of solid by liquid. The fundamental relationship between wetting angle and the surface energy in equilibrium is given by Young's (39) equation as,

$$\gamma_{sv} = \gamma_{sl} + \gamma_{lv} \cos\theta \tag{2.1}$$

where, γ_{sv} is the surface energy of solid, γ_{sl} is the solid-liquid interfacial energy, γ_{lv} is the surface energy of liquid and θ is the wetting angle. For wetting systems, θ should be less than 90°. The wetting angle 'θ' characterizes the degree of spreading/wetting in the system.

The work of adhesion 'w_a' of the liquid on the solid is given by Dupre's (40) equation as,

$$w_a = \gamma_{sv} + \gamma_{lv} - \gamma_{sl} \tag{2.2}$$

work of adhesion 'w_a' and wetting angle 'θ' are related to each other according to classical Young-Dupre equation as,

$$\cos\theta = \frac{w_a}{\gamma_{lv}} - 1 \tag{2.3}$$

The work of adhesion 'w_a' quantifies the strength of the interactions between the liquid and solid at the interface. So, it characterizes the bonding between liquid

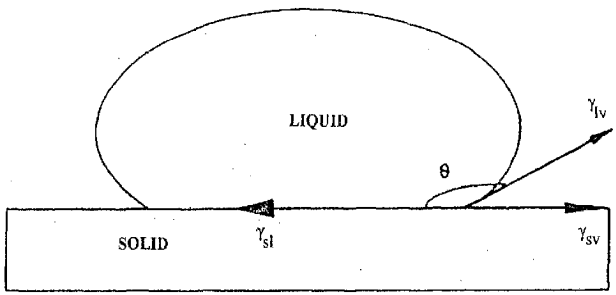

(a)

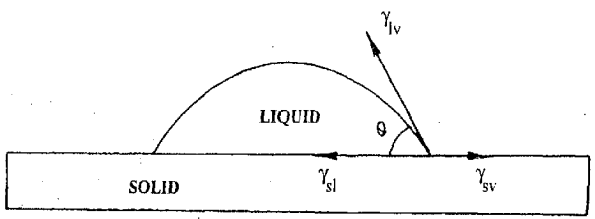

(b)

Fig. 2.1 Schematic diagram of a liquid drop on the solid surface showing the interfacial forces and wetting angle (a) nonwetting system (b) wetting system.

and solid and is invariably taken into account when modeling the mechanical properties of metal-ceramic composites (41,42).

Oh et al. (43) have proposed the concept of immersional wetting. When a solid is immersed into liquid, the solid-gas interface is replaced by a solid-liquid interface without changing the area of liquid-gas interface. The free energy change or the work performed 'w_i' is given as,

$$w_i = \gamma_{sl} - \gamma_{sv} \tag{2.4}$$

Equation (2.4) defines the work of immersion 'w_i' as the change in free energy on immersing the solid in the liquid, so that $w_i < 0$ indicates spontaneous wetting. When $w_i > 0$, the solid would tend to float and must be forced into the liquid. Capillary rise and pressure infiltration of liquid metal into a solid preform are two practical examples of immersional wetting. Immersional wetting may be affected only by changes either in γ_{sl} and γ_{sv} or both.

2.2.1 Measurement of Wettability

The sessile drop method allows simultaneous measurement of the contact angle 'θ' and the liquid metal surface tension 'γ_{lv}' and therefore, allows measurement of wettability by virtue of Young's equation.

In sessile drop method, conventional experimental approach to wettability consists of measuring the contact angle of a drop of the liquid metal matrix resting on a flat substrate of the ceramic reinforcement material. Some investigators (29) have measured the contact angle 'θ' directly with the help of a protractor through the construction of tangent on the drop profile at the point of contact of drop profile and the substrate. However, several investigators (44-48) have successfully used other geometrical processes to obtain the contact-angle from the drop profile.

The measurement of surface tension by sessile drop method is essentially based on the determination of the shape factor 'η' and of the radius of curvature 'b' at the drop apex. The two parameters are related as,

$$\eta = \frac{g\rho b^2}{\gamma_{lv}} \tag{2.5}$$

Kozakevitch and Urbain (49) have given a technique by simultaneously measuring the h/r_{max} ratio for four different values of ϕ (45°, 60°, 120°, 135°) as shown in Fig. 2.2 where, OM=h and EB=r_{max}. Four η values are then found by interpolating from the Table-A1 in Appendix-A. Weightage factor 'k' to these η values is given in Table-A2 in Appendix-A. The average shape factor '$\bar{\eta}$' is then calculated by the ratio of the sum of the product of all η value by their respective weightage factors k to the sum of all weightage factors corresponding to different η values. After calculating the average shape factor '$\bar{\eta}$', the value of $p = r/b$ is taken from Table-A3 in Appendix-A. The value of b is calculated as $b = \frac{p}{r} x \frac{1}{m}$, where m is the magnification of the drop profile. The surface tension of the liquid metal is then calculated as,

$$\gamma_{lv} = \frac{gp^2}{\eta(rm)^2} \tag{2.6}$$

After calculating the surface tension and contact angle, the bonding strength is determined by calculating the work of adhesion from Eqn. (2.3). Bonding properties are some times calculated as the fraction of work of cohesion, which is equal to 2 γ_{lv}. To achieve good interfacial properties in metal matrix composites, the work of adhesion should be about 50 to 60% to the work of cohesion of liquid metal (19).

2.2.2 Wettability of Al/C system

Due to the importance of the aluminium/carbon system as a candidate for metal matrix composites (50), the wetting of carbon by aluminium has been studied

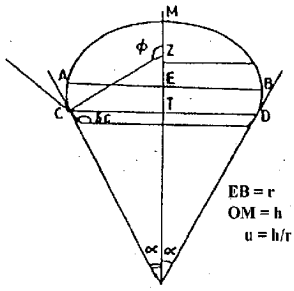

(a)

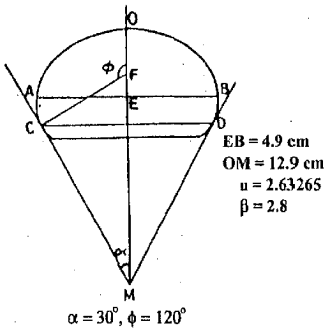

α = 30°, ϕ = 120°

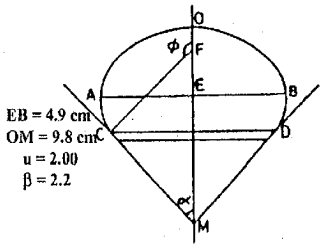

α = 45°, ϕ = 135°

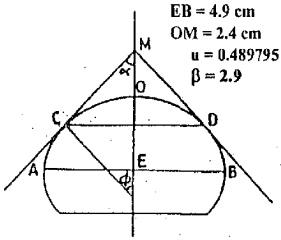

α = 45°, β = 45°

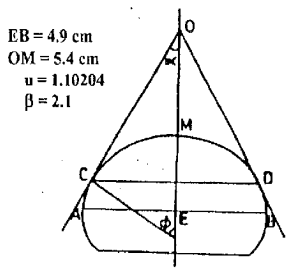

α = 30°, ϕ = 60°

(b)

Fig. 2.2 Schematic diagram showing a sessile drop profile (a) general profil(b) different positions showing four combinations of angles to measure average shape factor.

extensively during the last three decades (19,28,29). Indeed, wetting properties are needed to describe the liquid-state processing of the composites.

The wettability of carbon by aluminium has been found poor below 950^0C as investigated by several workers (28-30). Eustathopoulos et al. (29) have shown that this phenomenon is due to the presence of aluminium oxide layer on the metal drop preventing the actual contact of aluminium with carbon substrate. The same phenomenon is observed by other workers (51,52) during their studies on wetting of aluminium with other substrates.

The presence of wetting/nonwetting transition temperature, which is relatively independent of the substrate but dependent on the partial pressure of oxygen in the chamber, indicates that wettability is largely dictated by this oxide layer (2). Eustathopoulos et al. (29) have pointed out that at about 860^0C, compactness of the oxide layer is reduced due to the dissolution of oxide particles in molten aluminium and the defects in the oxide layer occur due to the formation of gaseous substance Al_2O according to the reaction $4Al + Al_2O_3 \rightarrow 3Al_2O$ at about 1000^0C. As a result, liquid aluminium penetrates the oxide layer to make actual contact with carbon substrate. The contact angle then sharply reduces to 65° from 95° at 1000^0C with the formation of a thick layer of Al_4C_3 at the liquid-solid interface. They have marked the observed contact angle as dynamic as it depends upon the rate of reaction of Al_4C_3 formation.

Zhongyu et al. (53) have experimentally measured the contact angle of aluminium on polycrystalline graphite substrate by sessile drop method and have reported that the contact angle changes with the melt temperatures at two different stages showing different features. The initial stage covers the temperatures ranging from 660^0C to 850^0C where the contact angle of the system decreases slowly with the increase in temperature and the second stage covers the temperatures ranging from 850^0C to 1100^0C where the contact angle drops sharply with the rise in temperature. They have observed a nonwetting angle (~160°) at 800^0C followed by wetting of graphite after attaining the wetting angle (~55°) at about 1000^0C.

extensively during the last three decades (19,28,29). Indeed, wetting properties are needed to describe the liquid-state processing of the composites.

The wettability of carbon by aluminium has been found poor below 950^0C as investigated by several workers (28-30). Eustathopoulos et al. (29) have shown that this phenomenon is due to the presence of aluminium oxide layer on the metal drop preventing the actual contact of aluminium with carbon substrate. The same phenomenon is observed by other workers (51,52) during their studies on wetting of aluminium with other substrates.

The presence of wetting/nonwetting transition temperature, which is relatively independent of the substrate but dependent on the partial pressure of oxygen in the chamber, indicates that wettability is largely dictated by this oxide layer (2). Eustathopoulos et al. (29) have pointed out that at about 860^0C, compactness of the oxide layer is reduced due to the dissolution of oxide particles in molten aluminium and the defects in the oxide layer occur due to the formation of gaseous substance Al_2O according to the reaction $4Al + Al_2O_3 \rightarrow 3Al_2O$ at about 1000^0C. As a result, liquid aluminium penetrates the oxide layer to make actual contact with carbon substrate. The contact angle then sharply reduces to 65^o from 95^o at 1000^0C with the formation of a thick layer of Al_4C_3 at the liquid-solid interface. They have marked the observed contact angle as dynamic as it depends upon the rate of reaction of Al_4C_3 formation.

Zhongyu et al. (53) have experimentally measured the contact angle of aluminium on polycrystalline graphite substrate by sessile drop method and have reported that the contact angle changes with the melt temperatures at two different stages showing different features. The initial stage covers the temperatures ranging from 660^0C to 850^0C where the contact angle of the system decreases slowly with the increase in temperature and the second stage covers the temperatures ranging from 850^0C to 1100^0C where the contact angle drops sharply with the rise in temperature. They have observed a nonwetting angle ($\sim 160^o$) at 800^0C followed by wetting of graphite after attaining the wetting angle ($\sim 55^o$) at about 1000^0C.

on different types of carbon substrates has also revealed that initial contact angle is higher for vitreous carbon substrate than graphite substrate. This behaviour is in good agreement with the classical theory of adhesion due to Vander Waal's interactions (55), according to which the adhesion energy is proportional to the atomic densities of the two phases in contact. Since initial contact angles are related to Vander Waal's interactions, the low atomic density carbon substrate, i.e., vitreous carbon in contact with aluminium has low adhesion energy hence, high contact angle.

The final contact angle of aluminium on vitreous carbon substrate is lower than that on other carbon substrates because spreading kinetics is related directly to reaction kinetics and the reactivity varies with carbon substrates. As the reactive carbon atoms are present inside the prismatic planes of graphite materials, a high parallelism of the graphite basal planes with respect to the substrate surface leads to a low fraction of exposed prismatic planes and thus, a lower reactivity. The higher reactivity of vitreous carbon substrate than graphite substrate is responsible for the low final contact angle of aluminium on vitreous carbon.

The wide differences in the contact angle data of aluminium on carbon at low temperatures may be attributed to the experimental conditions also. Depending upon the particular atmosphere and the substrate roughness, several workers (56-58) have observed the contact angle of aluminium on carbon in the range of 150° to 170° at low temperatures that remains nearly constant with time, whatever is the type of carbon substrate. This behaviour is typical of the oxidised drops and is observed at low temperatures, when a medium vacuum or an atmosphere of inert or even reducing gas is used. The deoxidation of aluminium/aluminium alloy drop is favoured by high temperature, high vacuum ($p< 10^{-2}$ Pa) and by using the capillary purification technique, in which this layer is broken by extrusion of the melt through a capillary (59).

2.2.3 Enhancement of wettability in Al/C system

Though, aluminium shows good wettability with carbon at low temperatures (19), it is of no practical use in the solidification processing of Al/CF composites as molten aluminium reacts with carbon fibres to form aluminium carbide. This results

on different types of carbon substrates has also revealed that initial contact angle is higher for vitreous carbon substrate than graphite substrate. This behaviour is in good agreement with the classical theory of adhesion due to Vander Waal's interactions (55), according to which the adhesion energy is proportional to the atomic densities of the two phases in contact. Since initial contact angles are related to Vander Waal's interactions, the low atomic density carbon substrate, i.e., vitreous carbon in contact with aluminium has low adhesion energy hence, high contact angle.

The final contact angle of aluminium on vitreous carbon substrate is lower than that on other carbon substrates because spreading kinetics is related directly to reaction kinetics and the reactivity varies with carbon substrates. As the reactive carbon atoms are present inside the prismatic planes of graphite materials, a high parallelism of the graphite basal planes with respect to the substrate surface leads to a low fraction of exposed prismatic planes and thus, a lower reactivity. The higher reactivity of vitreous carbon substrate than graphite substrate is responsible for the low final contact angle of aluminium on vitreous carbon.

The wide differences in the contact angle data of aluminium on carbon at low temperatures may be attributed to the experimental conditions also. Depending upon the particular atmosphere and the substrate roughness, several workers (56-58) have observed the contact angle of aluminium on carbon in the range of 150° to 170° at low temperatures that remains nearly constant with time, whatever is the type of carbon substrate. This behaviour is typical of the oxidised drops and is observed at low temperatures, when a medium vacuum or an atmosphere of inert or even reducing gas is used. The deoxidation of aluminium/aluminium alloy drop is favoured by high temperature, high vacuum ($p< 10^{-2}$ Pa) and by using the capillary purification technique, in which this layer is broken by extrusion of the melt through a capillary (59).

2.2.3 Enhancement of wettability in Al/C system

Though, aluminium shows good wettability with carbon at low temperatures (19), it is of no practical use in the solidification processing of Al/CF composites as molten aluminium reacts with carbon fibres to form aluminium carbide. This results

influence of heat treatment of carbon fibres on their infiltration by aluminium or aluminium alloys. However, it has been reported that the carbon fibres are degraded by heat treatment. The extent of degradation depends upon preheating temperature, preheating time, preheating atmosphere and on the type of carbon fibres (12). Rossi et al. (63) have reported that multifilament graphite fibres can be properly infiltrated by molten aluminium only after thorough removal of the contaminants by multiple chemical washings.

Alloying additions to the aluminium have shown to affect the wetting angle of Al/C system and ease of infiltration into carbon fibre preforms. Effective alloying additions fall in two categories. The first are additions that promote reactions between carbon reinforcement and aluminium matrix. Several investigators have observed wetting angle and ease of infiltration into carbon preforms by aluminium having reactive alloying additions. Sobczak et al. (64) have observed a wetting angle of Al-6wt.%Ti alloy on graphite substrate in seven minutes at 950^0C, in one minute at 1050^0C and instantaneously at 1150^0C after the melting of the alloy. Delamotte et al. 65) have observed good infiltration and uniform distribution of carbon fibres by luminium-nickel alloy matrix. Similar observations have been reported by Kuniya et l. (66) during the infiltration of carbon fibres by aluminium alloys having the lloying additions of titanium, chromium and zirconium respectively. Sara (67) has lso observed the complete infiltration of carbon fibres by aluminium when alloyed vith tantalum and hafnium respectively.

Naidich (68), in an extensive study, has pointed out that the transition metals metals with an unfilled d-electron shell) react strongly with carbon to form carbides vhere bonding involves some electron transfer from carbon to the d-shell of the netal. The reactivity increases with increasing temperature and with decreasing number of d-shell electrons (Ti > V > ---- > Ni). This tendency agrees well with vetting angle data, obtained by Mortimer et al. (69) in a detailed study on the vettability of vitreous carbon and graphite substrate with copper alloys. This indicates hat in general alloying additions that promote reactivity between metal and the carbon substrate decrease the wetting angle due to formation of carbides at the nterface.

influence of heat treatment of carbon fibres on their infiltration by aluminium or aluminium alloys. However, it has been reported that the carbon fibres are degraded by heat treatment. The extent of degradation depends upon preheating temperature, preheating time, preheating atmosphere and on the type of carbon fibres (12). Rossi et al. (63) have reported that multifilament graphite fibres can be properly infiltrated by molten aluminium only after thorough removal of the contaminants by multiple chemical washings.

Alloying additions to the aluminium have shown to affect the wetting angle of Al/C system and ease of infiltration into carbon fibre preforms. Effective alloying additions fall in two categories. The first are additions that promote reactions between carbon reinforcement and aluminium matrix. Several investigators have observed wetting angle and ease of infiltration into carbon preforms by aluminium having reactive alloying additions. Sobczak et al. (64) have observed a wetting angle of Al-6wt.%Ti alloy on graphite substrate in seven minutes at 950^0C, in one minute at 1050^0C and instantaneously at 1150^0C after the melting of the alloy. Delamotte et al. (65) have observed good infiltration and uniform distribution of carbon fibres by aluminium-nickel alloy matrix. Similar observations have been reported by Kuniya et al. (66) during the infiltration of carbon fibres by aluminium alloys having the alloying additions of titanium, chromium and zirconium respectively. Sara (67) has also observed the complete infiltration of carbon fibres by aluminium when alloyed with tantalum and hafnium respectively.

Naidich (68), in an extensive study, has pointed out that the transition metals (metals with an unfilled d-electron shell) react strongly with carbon to form carbides where bonding involves some electron transfer from carbon to the d-shell of the metal. The reactivity increases with increasing temperature and with decreasing number of d-shell electrons (Ti > V > ---- > Ni). This tendency agrees well with wetting angle data, obtained by Mortimer et al. (69) in a detailed study on the wettability of vitreous carbon and graphite substrate with copper alloys. This indicates that in general alloying additions that promote reactivity between metal and the carbon substrate decrease the wetting angle due to formation of carbides at the interface.

vitreous carbon substrate under same experimental conditions as used for aluminium-lithium alloys. They have attributed this improvement in wettability to the reduction in the compactness of the oxide layer on liquid aluminium by these alloying additions. The same effect of these alloying additions on oxide layer covering the liquid metal has also been observed by other workers (73-74).

Lithium is supposed to be beneficial for the impregnation of carbon fibres (16,75). Kimura et al. (17) have studied the dewetting of various aluminium alloy coatings deposited on carbon fibres by vacuum evaporation. These authors have concluded that alloys containing 1 at.% of indium, lead and thallium and 5 at.% of magnesium respectively, show excellent wetting behaviour with carbon fibres. In fact, they have observed that dewetting of carbon fibres coated with these aluminium alloys is prevented after heating sufficiently above the melting points of the alloys. They have attributed the observed behaviour to the lowering of the surface tension of liquid aluminium by the addition of these elements. Their results have been in good agreement with the findings of Manning et al. (18) who has pointed out that wetting is not significantly affected by the addition of small quantities (2 to 3wt.%) of surface active elements such as bismuth and lead.

So, these two classes broadly illustrate the chief methods that have been used in practice to achieve wettability for fabrication of carbon fibre reinforced aluminium matrix composites: reactions at the carbon fibre/aluminium matrix interface and modifications of the oxide layer that usually present at the surface of liquid aluminium matrix. A more sophisticated technique based on the same principles is to modify the carbon fibre surface itself with a coating. This is the most widely explored technique to promote wettability in the fabrication of carbon fibre reinforced aluminium matrix composites.

Coatings are also classified broadly into the two categories that have been employed for alloying additions. Coatings that react with the matrix are numerous and include metallic and carbide coatings for carbon fibre reinforcement in aluminium. Several methods have been developed to deposit these coatings on carbon fibres.

vitreous carbon substrate under same experimental conditions as used for aluminium-lithium alloys. They have attributed this improvement in wettability to the reduction in the compactness of the oxide layer on liquid aluminium by these alloying additions. The same effect of these alloying additions on oxide layer covering the liquid metal has also been observed by other workers (73-74).

Lithium is supposed to be beneficial for the impregnation of carbon fibres (16,75). Kimura et al. (17) have studied the dewetting of various aluminium alloy coatings deposited on carbon fibres by vacuum evaporation. These authors have concluded that alloys containing 1 at.% of indium, lead and thallium and 5 at.% of magnesium respectively, show excellent wetting behaviour with carbon fibres. In fact, they have observed that dewetting of carbon fibres coated with these aluminium alloys is prevented after heating sufficiently above the melting points of the alloys. They have attributed the observed behaviour to the lowering of the surface tension of liquid aluminium by the addition of these elements. Their results have been in good agreement with the findings of Manning et al. (18) who has pointed out that wetting is not significantly affected by the addition of small quantities (2 to 3wt.%) of surface active elements such as bismuth and lead.

So, these two classes broadly illustrate the chief methods that have been used in practice to achieve wettability for fabrication of carbon fibre reinforced aluminium matrix composites: reactions at the carbon fibre/aluminium matrix interface and modifications of the oxide layer that usually present at the surface of liquid aluminium matrix. A more sophisticated technique based on the same principles is to modify the carbon fibre surface itself with a coating. This is the most widely explored technique to promote wettability in the fabrication of carbon fibre reinforced aluminium matrix composites.

Coatings are also classified broadly into the two categories that have been employed for alloying additions. Coatings that react with the matrix are numerous and include metallic and carbide coatings for carbon fibre reinforcement in aluminium. Several methods have been developed to deposit these coatings on carbon fibres.

carbide coatings for several types of carbon fibres by using tin as a transfer agent. Several others (85,86) have coated carbon fibres with chromium carbide and tungsten carbide, using copper as a transfer agent.

Coatings of tantalum, TiN and SiC have also been studied for carbon fibres. Morooka et al. (87) have observed that coating of SiC effectively protects the fibres from the oxidation and prevents the diffusion of aluminium into the fibres. Wang et al.(88) have successfully coated the carbon fibres with SiC by a polycarbosilane solution process and have observed an improvement in the wettability of carbon fibres with aluminium.

Although these coatings are stable in liquid aluminium, they degrade the fibres due to dissolution of carbon fibres necessary for carbide formation. So, an additional coating of nickel is then necessary to provide wetting and to prevent further degradation of carbon fibres (89).

The second types of coatings are those, which react with the oxide layer on the liquid aluminium. A coating derived from the chemical formulas used in conventional fluxing of aluminium alloys has been developed by Naslain and co-workers (90) to eliminate the solid aluminium oxide layer that forms at the metal/air interface during infiltration. A loose coating of K_2 ZrF_6, which is a fluxing agent for aluminium, is deposited between the fibres. The coating of K_2ZrF_6 permits continuous fibre reinforced composites to be cast in permanent moulds at low temperatures without any additional pressure, showing the enhancement in wettability of the fibres by metal matrix. Sanctis et al. (36) have successfully infiltrated the K_2ZrF_6 coated PAN T300 carbon fibres by aluminium silicon alloy at 690^0C. Although the infiltration is aided by applying some vacuum, the infiltration of coated carbon fibres at 690^0C clearly reflects the enhancement in wetting.

Pfeifer (91) has reviewed the technology of liquid metal infiltration of carbon fibres by aluminium, where fibres are precoated either with titanium boride or titanium boride mixed with titanium carbide to enhance the wettability of carbon fibres by aluminium. Materials concept Inc. in a patent (92), utilizes the in-line TiB treatment on tows of carbon fibres for deposition of thin TiB_2 coating by chemical

carbide coatings for several types of carbon fibres by using tin as a transfer agent. Several others (85,86) have coated carbon fibres with chromium carbide and tungsten carbide, using copper as a transfer agent.

Coatings of tantalum, TiN and SiC have also been studied for carbon fibres. Morooka et al. (87) have observed that coating of SiC effectively protects the fibres from the oxidation and prevents the diffusion of aluminium into the fibres. Wang et al.(88) have successfully coated the carbon fibres with SiC by a polycarbosilane solution process and have observed an improvement in the wettability of carbon fibres with aluminium.

Although these coatings are stable in liquid aluminium, they degrade the fibres due to dissolution of carbon fibres necessary for carbide formation. So, an additional coating of nickel is then necessary to provide wetting and to prevent further degradation of carbon fibres (89).

The second types of coatings are those, which react with the oxide layer on the liquid aluminium. A coating derived from the chemical formulas used in conventional fluxing of aluminium alloys has been developed by Naslain and co-workers (90) to eliminate the solid aluminium oxide layer that forms at the metal/air interface during infiltration. A loose coating of K_2 ZrF_6, which is a fluxing agent for aluminium, is deposited between the fibres. The coating of K_2ZrF_6 permits continuous fibre reinforced composites to be cast in permanent moulds at low temperatures without any additional pressure, showing the enhancement in wettability of the fibres by metal matrix. Sanctis et al. (36) have successfully infiltrated the K_2ZrF_6 coated PAN T300 carbon fibres by aluminium silicon alloy at 690^0C. Although the infiltration is aided by applying some vacuum, the infiltration of coated carbon fibres at 690^0C clearly reflects the enhancement in wetting.

Pfeifer (91) has reviewed the technology of liquid metal infiltration of carbon fibres by aluminium, where fibres are precoated either with titanium boride or titanium boride mixed with titanium carbide to enhance the wettability of carbon fibres by aluminium. Materials concept Inc. in a patent (92), utilizes the in-line TiB treatment on tows of carbon fibres for deposition of thin TiB_2 coating by chemical

In case of carbon fibre reinforced aluminium matrix composites, where carbon and aluminium form a reactive system, the physical interaction at low temperature is related to small work of adhesion, which is a small fraction of the work of cohesion of liquid aluminium. This physical interaction, arises due to the dissolution of carbon in aluminium (19), shows that Al/C interface is energetically weak as the solubility of carbon in aluminium at this temperature is only 0.16 wt.% (97). These values of work of adhesion are comparable with those measured in non-reactive systems like Cu/carbon (98,99) and Ag/graphite (68) systems in which adhesion has been attributed to Vander Waal's interactions.

As the physical interactions have weak temperature dependence, it is impossible to obtain a strong interface bonding between carbon and aluminium by physical interactions only, which of course are always present there (100). Thus, it is necessary to induce chemical interaction between fibre and the matrix to get a strong interfacial bonding. Chemical interactions between carbon fibre and aluminium are associated with the formation of aluminium carbide at the interface. The work of adhesion of these chemical interactions is quite large (68) and is about 70 to 80% of the work of cohesion of liquid aluminium (19). Landry et al. (19) have pointed out that this work of adhesion is actually for Al/Al_4C_3 system and not for Al/C system. The Al/Al_4C_3 interface is thus energetically strong and adhesion is interpreted in terms of covalent bonds formed due to chemical interactions.

Transition metals react strongly with carbon to form carbides. The work of adhesion with graphite is very large which increases with increase in temperature and with decrease in number of d-shell electrons. Chemical interactions amount for 90 to 95% of the work of cohesion. In such reactive systems, work of adhesion is a very dynamic quantity. These metal like carbides show highest wetting by transition metals. The chemical interactions, between aluminium (alloyed with transition metal) and carbon, are associated with large work of adhesion because of metallic like carbide formation at the interface. This large work of adhesion is attributed to the formation of metallic bonding across the interface. As soon as the reaction front proceeds in the solid, one deals with an interface of the type liquid metal-metal carbide-carbon rather than liquid metal-carbon (68).

In case of carbon fibre reinforced aluminium matrix composites, where carbon and aluminium form a reactive system, the physical interaction at low temperature is related to small work of adhesion, which is a small fraction of the work of cohesion of liquid aluminium. This physical interaction, arises due to the dissolution of carbon in aluminium (19), shows that Al/C interface is energetically weak as the solubility of carbon in aluminium at this temperature is only 0.16 wt.% (97). These values of work of adhesion are comparable with those measured in non-reactive systems like Cu/carbon (98,99) and Ag/graphite (68) systems in which adhesion has been attributed to Vander Waal's interactions.

As the physical interactions have weak temperature dependence, it is impossible to obtain a strong interface bonding between carbon and aluminium by physical interactions only, which of course are always present there (100). Thus, it is necessary to induce chemical interaction between fibre and the matrix to get a strong interfacial bonding. Chemical interactions between carbon fibre and aluminium are associated with the formation of aluminium carbide at the interface. The work of adhesion of these chemical interactions is quite large (68) and is about 70 to 80% of the work of cohesion of liquid aluminium (19). Landry et al. (19) have pointed out that this work of adhesion is actually for Al/Al_4C_3 system and not for Al/C system. The Al/Al_4C_3 interface is thus energetically strong and adhesion is interpreted in terms of covalent bonds formed due to chemical interactions.

Transition metals react strongly with carbon to form carbides. The work of adhesion with graphite is very large which increases with increase in temperature and with decrease in number of d-shell electrons. Chemical interactions amount for 90 to 95% of the work of cohesion. In such reactive systems, work of adhesion is a very dynamic quantity. These metal like carbides show highest wetting by transition metals. The chemical interactions, between aluminium (alloyed with transition metal) and carbon, are associated with large work of adhesion because of metallic like carbide formation at the interface. This large work of adhesion is attributed to the formation of metallic bonding across the interface. As soon as the reaction front proceeds in the solid, one deals with an interface of the type liquid metal-metal carbide-carbon rather than liquid metal-carbon (68).

coating is necessary to provide satisfactory wetting (89). The coatings of SiO_2 (barrier) and Cu (wetting), deposited in sequence on carbon fibres have been reported to prevent the reaction at the interface (110). Several investigators have reported the prevention of fibre/matrix reactivity by depositing inert coatings on the fibres using chemical vapour deposition (16,104) and various other methods (108,111).

2.4 FABRICATION METHODS FOR FMMCs

Continuous fibre reinforced MMCs can not be fabricated easily by the conventional casting methods. There are several techniques available to fabricate such MMCs. Generally, there are two types of fabrication methods: Solid phase fabrication methods and liquid phase fabrication methods.

2.4.1 Solid-Phase Fabrication Methods

(a) **Diffusion Bonding:** This method is normally used to fabricate fibre reinforced MMC with sheets or foils of matrix. In this method, the metal or metal alloys in the form of sheets and the reinforcement material in the form of fibre are chemically surface treated for the effectiveness of interdiffusion. Alkaline or acid solutions are often used for chemical treatment of fibres while other solutions are used for surface cleaning of matrix sheets or foils eg. carbon tetrachloride for aluminium foils or sheets (112).

The carbon fibres are wound on a drum of a metal having good thermal conductivity (Cu for instance) to deposit the coating of matrix material. Preformed sheets are then cut by shears or die and are laid in predetermined orientations to achieve the fibre volume fraction and thickness required. The major step in the diffusion bonding method is press forming which achieves bonding of fibre and matrix through the application of pressure and temperature. The method enhances the composite density by removing voids and improves composite strength by introducing some plastic deformation in the metal matrix. Basic parameters controlling the forming process are press temperature, pressure, holding time and atmosphere.

coating is necessary to provide satisfactory wetting (89). The coatings of SiO_2 (barrier) and Cu (wetting), deposited in sequence on carbon fibres have been reported to prevent the reaction at the interface (110). Several investigators have reported the prevention of fibre/matrix reactivity by depositing inert coatings on the fibres using chemical vapour deposition (16,104) and various other methods (108,111).

2.4 FABRICATION METHODS FOR FMMCs

Continuous fibre reinforced MMCs can not be fabricated easily by the conventional casting methods. There are several techniques available to fabricate such MMCs. Generally, there are two types of fabrication methods: Solid phase fabrication methods and liquid phase fabrication methods.

2.4.1 Solid-Phase Fabrication Methods

(a) **Diffusion Bonding:** This method is normally used to fabricate fibre reinforced MMC with sheets or foils of matrix. In this method, the metal or metal alloys in the form of sheets and the reinforcement material in the form of fibre are chemically surface treated for the effectiveness of interdiffusion. Alkaline or acid solutions are often used for chemical treatment of fibres while other solutions are used for surface cleaning of matrix sheets or foils eg. carbon tetrachloride for aluminium foils or sheets (112).

The carbon fibres are wound on a drum of a metal having good thermal conductivity (Cu for instance) to deposit the coating of matrix material. Preformed sheets are then cut by shears or die and are laid in predetermined orientations to achieve the fibre volume fraction and thickness required. The major step in the diffusion bonding method is press forming which achieves bonding of fibre and matrix through the application of pressure and temperature. The method enhances the composite density by removing voids and improves composite strength by introducing some plastic deformation in the metal matrix. Basic parameters controlling the forming process are press temperature, pressure, holding time and atmosphere.

refractory metal powders, ceramic powders and cermets. In recent years, the HIP technique has been applied to superalloys, tool steels and titanium/titanium alloy powders. Inert gases such as He, Ar and N_2 are used for applying the pressure. A HIP apparatus with a vessel size of 0.9-1.5m diameter and pressure of 20.6-206 MPa has been reported (118-121). Composites including B/Ti, B/Al, steel wire/Ti and steel wire/Al have been fabricated by this method.

2.4.2 Liquid-Phase Fabrication Methods

Liquid phase fabrication methods are particularly suitable for producing composite parts of complex shapes and the apparatus needed is relatively simple. Uniform fibre distribution can usually be achieved with little porosity in the matrix material. However, the contact of molten metals with fibres often results in interfacial reactions, which are only avoided if the fibre is completely insoluble in the molten metal. Fibre coatings or alloying of matrix materials are then necessary to prevent fibre damage or enhance the interfacial bonding. Several infiltration techniques have been used.

(a) **Liquid Metal Infiltration:** This process can also be called fibre tow infiltration. Fibre tows can be infiltrated by the molten metal, if wetted by the metal (104,122). Usually the fibres must be coated to promote wetting. Once the infiltrated wires are produced, they are assembled into a preform and are given a secondary consolidation process to produce a component. Secondary consolidation is generally accomplished through diffusion bonding or hot moulding in the two phase (solid + liquid) region of the phase diagram (2). The infiltration process can be done under atmospheric pressure, inert gas pressure and in vacuum.

Metals such as aluminium, magnesium, silver and copper have been used as matrix materials in this process because of their low melting temperatures. This method is desirable in producing relatively small size composite specimens having unidirectional properties (123). The application of this process is limited because of the wettability problem of reinforcement

refractory metal powders, ceramic powders and cermets. In recent years, the HIP technique has been applied to superalloys, tool steels and titanium/titanium alloy powders. Inert gases such as He, Ar and N_2 are used for applying the pressure. A HIP apparatus with a vessel size of 0.9-1.5m diameter and pressure of 20.6-206 MPa has been reported (118-121). Composites including B/Ti, B/Al, steel wire/Ti and steel wire/Al have been fabricated by this method.

2.4.2 Liquid-Phase Fabrication Methods

Liquid phase fabrication methods are particularly suitable for producing composite parts of complex shapes and the apparatus needed is relatively simple. Uniform fibre distribution can usually be achieved with little porosity in the matrix material. However, the contact of molten metals with fibres often results in interfacial reactions, which are only avoided if the fibre is completely insoluble in the molten metal. Fibre coatings or alloying of matrix materials are then necessary to prevent fibre damage or enhance the interfacial bonding. Several infiltration techniques have been used.

(a) **Liquid Metal Infiltration:** This process can also be called fibre tow infiltration. Fibre tows can be infiltrated by the molten metal, if wetted by the metal (104,122). Usually the fibres must be coated to promote wetting. Once the infiltrated wires are produced, they are assembled into a preform and are given a secondary consolidation process to produce a component. Secondary consolidation is generally accomplished through diffusion bonding or hot moulding in the two phase (solid + liquid) region of the phase diagram (2). The infiltration process can be done under atmospheric pressure, inert gas pressure and in vacuum.

Metals such as aluminium, magnesium, silver and copper have been used as matrix materials in this process because of their low melting temperatures. This method is desirable in producing relatively small size composite specimens having unidirectional properties (123). The application of this process is limited because of the wettability problem of reinforcement

infiltration and HIP, rolling and hot pressing and combinations of the infiltration methods like vacuum-inert gas infiltration method (21).

(v) **Squeeze Casting:** Squeeze casting is a variant of a pre-existing process employing pressure to enhance casting quality (125,126). The basic principle is to forge a liquid metal into a closed die to produce finished shapes. The liquid metal then solidifies under high pressure (50 to 100 MPa). In addition to rapid solidification, casting quality is enhanced by the collapse of gas and shrinkage porosity under the influence of the high hydrostatic pressure.

For FMMC, a preheated fibre preform is inserted into the die. Liquid metal is metered into the die cavity and a ram (which may be shaped to form part of the near net-shape casting configuration) is inserted to apply pressure. The advantages of this process include simplicity, high speed of operation and high pressures that can easily be maintained throughout solidification to feed shrinkage. A major limitation is the size of parts that can be cast because of the tooling required for such a high pressure (2).

In general, two different kinds of squeeze-casting techniques, known as "direct" and "indirect", have been developed based on different approaches of liquid metal metering and liquid metal movement. The direct squeeze-casting technique is characterized by a direct pressure imposed on the casting without any gating system, as illustrated in Fig.2.2. Since the pressure is directly applied to the entire surface of the molten metal during solidification, this technique gives fully densified components and extremely fast heat transfer which yields fine grain structure alongwith good mechanical properties. In the indirect technique, as shown in Fig.2.3, the pressure is exerted on a gate, which transmits the load to the component (127). Owing to the fact that the pressure is imposed at a distance from the component, it is difficult to maintain a high pressure on the component throughout its solidification and cooling periods. This indicates that it is difficult to cast long freezing range alloys with the indirect technique. Also, metal yield is much lower than that achievable with direct squeeze casting. The mechanical properties of squeeze cast products are controlled to a large extent by the

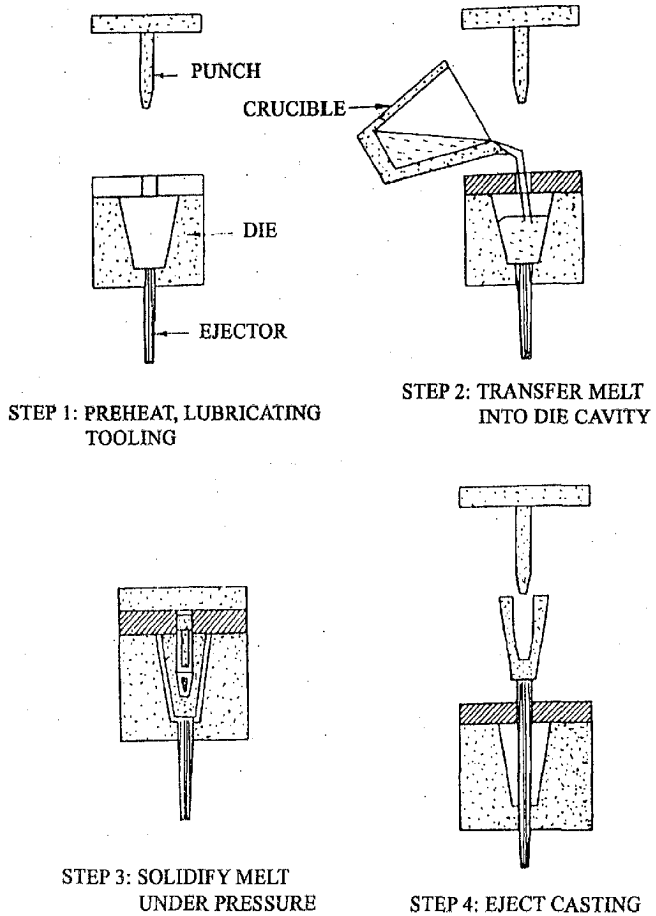

Fig. 2.3 Schematic diagram of the direct squeeze casting process.

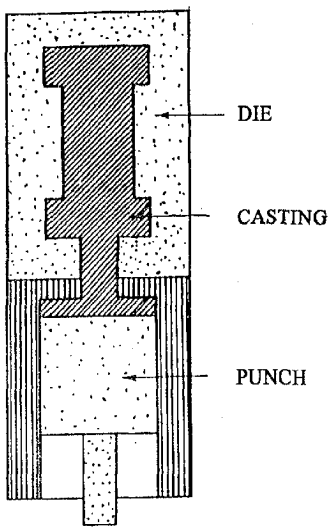

Fig. 2.4 Schematic diagram of the indirect squeeze casting process.

structure and morphology derived during solidification. Extensive nucleation and hence, fine equiaxed grain structure can be obtained due to undercooling below the equilibrium solidification temperature and rapid heat extraction. In squeeze casting, the requirements of both rapid heat extraction and undercooling can be met (128).

The usual equilibrium diagram of an alloy depicts the equilibria at a constant pressure of one atmosphere. During squeeze casting (23), the pressure applied by the punch or upper die can amount to a few thousand atmospheres. The consequent increase in the freezing temperature 'ΔT', for alloys that expand on melting, can be calculated from the Clausius-Clapeyron equation as,

$$\Delta T = \frac{T_m(V_2 - V_1)\Delta P}{H} \tag{2.7}$$

where, H is the latent heat of fusion, T_m is the melting temperature at atmospheric pressure, ΔP is the increase in pressure above one atmosphere and V_2 and V_1 are specific volumes of liquid phase and solid phase respectively.

For Al-base alloys (except high silicon containing alloys which do not show much expansion), the freezing temperature may increase by 10-25^{0}C, depending upon the pressure during squeeze casting.

If pressure is applied on the molten metal, which is only few degrees above the liquidus temperature, undercooling can occur throughout the liquid metal mass. Although the actual temperature may not have decreased below the equilibrium (at one atmospheric pressure) freezing temperature, rapid solidification of the undercooled melt can be realized. Furthermore, the high rate of heat removal achieved in squeeze casting is also helpful to the rate of solidification. This is because the applied pressure tends to force the solidifying metal against the die and eliminates the air gaps between the casting surface and the die wall. The heat transfer coefficient, so achieved in squeeze casting, can be an order of magnitude larger than that in gravity die-

casting. The combination of undercooling with high heat transfer rates ensures a fine grain equiaxed structure (128).

2.4.3 Pressure Infiltration: Processing Fundamentals

The liquid metal infiltration process, for fabricating fibre reinforced MMCs, consists of the flow of liquid metal into the interstices of an array of ceramic fibres by means of a pressure gradient and the subsequent solidification of the liquid metal. This process is generally termed "pressure infiltration" which includes die-casting, gravity casting, counter-gravity casting and squeeze casting.

(a) **The Infiltration Process:** In squeeze casting, molten metal is poured into a cavity, which contains preheated preform of fibres. The metal infiltrates the preform under an applied pressure, ΔP_T, which is equal to the sum of pressure required for preform penetration, ΔP_γ, and the pressure required for preform infiltration, ΔP_μ. So, ΔP_T is given as,

$$\Delta P_T = \Delta P_\gamma + \Delta P_\mu \tag{2.8}$$

In other words, ΔP_T is also equal to the pressure difference between the metal pressure at the entrance of the preform and the pressure at the infiltration front, which is equal to the atmospheric pressure in the non-infiltrated portion of the preform.

(b) **Preform Penetration:** Resistance to melt penetration at the surface of the preform arises from the effect of enforced meniscus curvature. It causes a pressure drop generally called 'capillary back pressure drop' ΔP_γ (in nonwetting systems). Several equations have been proposed for calculating the capillary pressure drop at the infiltration front. On the basis of a simple analysis of the energy required for reversible infiltration of a porous body, Mortenson et al. (60) have proposed an expression for this pressure drop as,

$$\Delta P_\gamma = (\gamma_{fl} - \gamma_{fv})\, S_f \tag{2.9}$$

or,

$$\Delta P_\gamma = - \gamma_{lv} \cos\theta \; S_f$$

in terms of the Young-Kelvin equation. Where γ_{fl} is the fibre-liquid metal interfacial energy, γ_{fv} is the fibre-atmosphere surface energy, γ_{lv} is the surface tension of the liquid metal, θ is the contact angle of the metal on the fibre reinforcement and S_f is the surface area per unit volume of preform being infiltrated at time t. In the limiting case of $\theta = 0$, this equation is identical to that derived by Carman (129) for capillary rise in sands using a force balance at the infiltration front. For fibrous preform consisting of uniform radius r_f, the surface area per unit volume 'S_f' is given as,

$$S_f = 2V_f / r_f (1-V_f) \tag{2.10}$$

(c) **Preform Infiltration:** A second source of resistance to infiltration is expected after initial penetration. This arises from frictional forces experienced by liquid flowing through interstitial channels and depends upon the flow velocity and infiltration distance. Fluid flow within the preform is governed by Darcy's law, provided the Reynold's number is less than one (130,131). This is generally the case in the infiltration of metal matrix composites having fine scale of the reinforcement.

Flow of the fluid can be analyzed on the scale of an elementary volume element that is small on the scale of the casting but comprises at least several fibres, which allows averaging the fluid velocity and pressure over this volume element. Fluid flow is then measured as the superficial velocity 'V_o', a vector given by the average flow direction of the liquid and of magnitude equal to the volume of the liquid flowing per unit time through a unit surface cut into the preform perpendicular to the flow direction. Darcy's law then correlates the pressure gradient in the liquid and the superficial velocity as,

$$V_o = \frac{K}{\mu}[grad(P_\mu) - \rho_m g] \tag{2.11}$$

where, V_o is the superficial velocity, μ is the viscosity of the liquid metal, K is the symmetric permeability tensor of the preform, P_μ is the pressure in the liquid metal, ρ_m is the density of the metal and g is the acceleration due to gravity.

If both the liquid matrix and the preform are assumed to be incompressible, the continuity equation can be given as,

$$div\ (V_o) = 0 \tag{2.12}$$

The pressure drop ΔP_μ is then the integral of the pressure gradient from the preform entrance to the infiltration front and increases with increase in flow velocity of the metal, increase in the viscosity of the metal and decrease in the permeability of the preform. The energy required for the infiltration process is then equal to the volume of metal displaced multiplied by the sum of two terms $(\Delta P_\mu + \Delta P_\gamma)$ of the total driving pressure gradient. ΔP_μ is a measure of the irreversible energy expenditure due to viscous losses in the flowing metal while $\gamma_{fl} - \gamma_{fv}$ is a measure of minimum energy required for infiltration to proceed.

In the case of a pure metal, calculation of K can be based on the Blake-Kozeny (130) approximation or on appropriate relationships derived for the particular preform in question. The value of K for continuous fibres and square distribution is given as,

$$K = \frac{0.427 r_{sf}^2}{V_{sf}}\left[1-\sqrt{\frac{2V_{sf}}{\pi}}\right]^4\left[1+0.473\left(\sqrt{\frac{\pi}{2V_{sf}}}-1\right)\right] \tag{2.13}$$

and applicable for flow parallel to the fibre axes, where, r_{sf} is the radius of the solid material and V_{sf} is its volume fraction (132). Equation (2.13) is valid for solid volume fractions ranging from 0.5 to $\pi/4$. The second equation given as,

$$K = \frac{2\sqrt{2}r_{sf}^2}{9V_{sf}}\left[1-\sqrt{\frac{4V_{sf}}{\pi}}\right]^{5/2} \tag{2.14}$$

is for flow perpendicular to the fibre axis. Equation (2.14) is valid for solid volume fractions ranging from 0.2 to $\pi/4$. It is accurate within a factor of 2 (133).

In the case of pure metal, liquid and solid metal can only coexist at the melting point of the metal, if equilibrium is assumed at the solid-liquid interface. If the initial fibre temperature is above the melting point of the metal, no solid metal will form. The problem is then one of uncoupled fluid flow in which the infiltration kinetics can be derived independently to yield, for unidirectional infiltration, the position 'X', of the metal front as a function of time 't' and is given as,

$$X = \frac{L}{\sqrt{t}} \tag{2.15}$$

The infiltration distance 'L' is then given by,

$$L^2 = \int_0^t \frac{2K\Delta p_\mu(t)}{\mu(1-V_f)}dt \tag{2.16}$$

or,

$$L^2 = \frac{2K\Delta p_\mu t}{\mu(1-V_f)}$$

If the initial fibre temperature is below the melting point of the metal, some solid metal forms at the infiltration front due to release of latent heat, to heat the fibres to the melting point of the metal. In the case of pure metal, this solid metal must solidify like a sheath surrounding the fibres as solidification is limited by the heat transfer to the cold fibres. This assumption is substantiated by the measurement of infiltration kinetics predicted as above but with a changed value of permeability in the region close to the infiltration

front that can be predicted by increasing the effective fibre diameter. The solid volume fraction 'V_s' in the metal phase is given by,

$$V_s = \frac{\rho_f C_f V_f \left(T_m - T_f\right)}{\rho_m \Delta H} \tag{2.17}$$

where, ρ_f is the density of fibres, C_f is the specific heat of fibres, T_m is the metal temperature, T_f is the fibre preform temperature, ρ_m is the density of the matrix and ΔH is the latent heat of solidification of the matrix.

When no metal is solidified, K is calculated from Eqns. (2.13) and (2.14) by taking r_{sf} and V_{sf} as equal to r_f and V_f respectively. When metal is solidified around the fibres, the K is calculated from Eqns. (2.13) and (2.14) by taking r_{sf} and V_{sf} as,

$$r_{sf} = r_f \sqrt{\frac{V_{sf}}{V_f}}, \quad \text{and} \quad V_{sf} = V_f + V_s \tag{2.18}$$

Masur et al. (134) have shown that the excess pressure necessary to initiate the infiltration of a dense network is of the order of ten atmosphere (~1MPa). Other workers have also shown that the pressure increment necessary to generate rapid flow for complete infiltration in about a second is not more than ten atmosphere whereas the corresponding velocity and pressure gradient values are about 30mm/s and 40 kPa/mm respectively (22). However, Masur et al. (134) have shown that about 3.5 MPa is sufficient for complete infiltration of the preform without any compression of the fibre preform.

In the practice, the pressure infiltration methods involve the use of pressure ranging from 20 to 100 MPa (38,135). Hence, these pressures appear to greatly exceed the minimum pressure necessary. However, as shown by Girot et al (136) such pressures are needed in order to avoid solidification of the liquid during infiltration when the temperature of the reinforcing network is lower than the melting temperature of the metal matrix.

2.5 FABRICATION OF Al/CF COMPOSITES

Continuous fibre reinforced aluminium/aluminium alloy matrix composites have been fabricated by a number of different techniques. Prominent among these are solid state diffusion bonding, liquid state pressure infiltration, vacuum infiltration and squeeze casting. Also, there are few attempts to fabricate the continuous fibre reinforced aluminium/aluminium alloy matrix composites without the application of external pressure or vacuum.

Pepper and co-workers (34) have fabricated Al-13wt.%Si/CF composites having 28vol.% of fibres. They have developed a process for the complete infiltration of graphite yarn. The composites are fabricated by liquid phase hot pressing of these infiltrated yarns. The literature has not provided any information regarding the infiltration process and hot pressing conditions.

Baker et al. (137) have fabricated the continuous carbon fibre reinforced aluminium composites by hot pressing the carbon fibre tows, which are pre-coated with aluminium by Chemical Vapour Deposition (CVD) process. The CVD process is based on the thermal decomposition of tri-isobutyl aluminium, i.e., $(C_4H_9)_3Al$. Two types of carbon fibres i.e. high modulus and high strength have been used. Composites with fibre volume fractions in the range of 20 to 40% are fabricated by hot pressing the carbon fibre tows in vacuum. Hot pressing conditions used are: a temperature of 550^0C at a pressure of 77.3 MPa for 1h and a temperature of 600^0C at 7.73 MPa for 0.5 h.

Khan et al. (138) have fabricated the graphite fibre reinforced aluminium alloys composites by liquid metal infiltration followed by solid state diffusion bonding. They have used TiB_2 coated graphite fibres for infiltration by 1100, 6061 and 201 aluminium alloys to get the composites with 25 to 30% fibre volume fraction. The solid state diffusion process is accomplished with the pressing of precursor wires at 21 MPa & 575^0C for 40 mins in case of 6061Al alloy and at 21 MPa & 555^0C for 40 mins in case of 201 Al alloy composites.

Imprescia et al. (139) have fabricated the Al/CF composites by liquid metal infiltration followed by vacuum hot pressing. Titanium carbide coating is formed on graphite fibres by chemical vapour deposition in the temperature range of 1192^0C - 1477^0C for 150 secs prior to infiltration with aluminium alloy. Other workers have also fabricated the unidirectional Al/CF composites with different fibre volume fractions, first infiltrating the copper coated carbon fibres by aluminium and subsequently, vacuum hot pressing at 620-650^0C and ~ 2-5 x 10^{-5} torr for 30-120 mins (140).

Towata et al. (37) have successfully incorporated the high modulus carbon fibres in different aluminium alloys by squeeze casting to fabricate the Al/CF composites. Uncoated carbon fibres have been reinforced in pure Al, Al-Mg (2 and 5wt.% Mg), Al-0.6wt.% Ca and Al-4.5wt.% Cu alloys by preheating the carbon fibres in nitrogen gas atmosphere at 757^0C and then squeeze casting at 50 MPa and 757^0C for 60 secs. In another study, Towata et al. (14) have fabricated the hybrid Al/CF composites by incorporating high strength carbon fibres coated with SiC whiskers and particulates in pure Al and Al-5wt.%Mg alloy matrices with fibre volume fractions of 0.52 and 0.70 respectively. The squeeze casting is carried out under a pressure of 90 MPa at 757^0C for a pressing time of 60 secs. They have also fabricated conventional composites having 70% volume fraction of high strength carbon fibres by squeeze casting under the same conditions.

The 201 aluminium/graphite composite having 41% fibre volume is fabricated by liquid metal infiltration followed by solid state diffusion bonding. The TiB_2 coated P-55 graphite fibres are infiltrated by 201-aluminium alloy to produce precursor wires. These precursor wires within two cover foils of 6061 Al alloy are pressed at 21 MPa and 555^0C for 40 mins to consolidate a unidirectional two ply panel of Al/CF composite (105).

Warrier et al. (31) have fabricated Al/CF composites containing low fibre volume fraction by vacuum infiltration. Different types of carbon fibres with silver coating and without coating have been reinforced in 6063 Al alloy matrix. The silver coating is carried out by electroless plating technique. The coated fibres are vacuum infiltrated by 6063 Al alloy under a vacuum of 1.3 x 10^{-7} MPa at different processing

temperatures for different processing time. They have used argon to back fill the reaction tube to reduce the reaction between the fibres and the matrix in all the castings.

RIM (Rapid Infrared Manufacturing) technique has been developed for pressureless liquid infiltration of carbon fibres by aluminium. The Al/CF composites are fabricated in a very short processing time by this process. These composites have shown negligible fibre degradation due to fast heating and cooling rate and precise temperature control (106,107).

Cheng et al. (12) have fabricated Al/CF composites by pressure casting based on hybridization method. They have successfully reinforced the high modulus and high strength carbon fibres in different aluminium alloy matrices by preheating the as received carbon fibres at 375^{0}C in air and infiltrating by aluminium alloy matrices. The fibres are infiltrated by applying a pressure of 49 MPa at 780^{0}C for a pressure holding time of 60 secs. All the composites fabricated are hybridized with 1.0 volume percent of SiC particles.

Wang et al. (88) have also fabricated the Al/CF composites by squeeze casting. The high strength PAN based carbon fibres are coated with SiC by polycarbosilane solution process to reinforce the Al-10wt.%Si alloy matrix. The coated fibres are preheated at 450^{0}C - 550^{0}C and are squeeze casted by applying a pressure of 30 - 80 MPa at a temperature of 740^{0}C - 800^{0}C for a pressure holding time of 30 secs.

2.6 MORPHOLOGY AND INTERFACES IN CAST Al/CF COMPOSITES

Porosity, due to either poor infiltration or shrinkage of the matrix during solidification has often been observed in the cast Al/CF composites (12). The problem of feeding matrix shrinkage during solidification can be solved by applying very high pressure during solidification as observed in squeeze casting (2).

The grain size in a casting is determined by the nucleation rate as well as by the presence of fluid flow during solidification, which results in grain multiplication

(141). The nucleation rate is influenced by the cooling rate and by the presence of heterogeneous nucleation catalysts. Carbon fibres, however, do not act as heterogeneous nucleation catalysts for aluminium base alloys as grain sizes far in excess of the fibre diameter have been observed with carbon fibres (142). Possible exceptions of commercial significance may include hypereutectic Al-Si alloys, as there is some indication that silicon nucleates preferentially on carbon (143).

One method of refining the grain size, specific to FMMC, is that of casting metal into a fibre preform which is held below the melting point (or liquidus) of the metal matrix. Very rapid heat exchange takes place as the matrix encounters the cold fibres. It results in the formation of some solid in the vicinity of the fibres. This leads to a fine grain size on the scale of the fibre diameter. Such grains have been observed by several workers (144,145).

In most of the cases, nucleation is not initially on the reinforcement surface. For an alloy, the solid phase avoid the reinforcement as it grows. The reinforcement acts as a barrier to solute diffusion ahead of the liquid-solid interface (146). Consequently, the last portion of the metal to solidify is located either close to or at the fibre-matrix interface, resulting in the enrichment of the interface with solute and secondary phases (104,147).

Studies on the solidification of Al-4.5wt.%Cu between carbon fibres (148,149) have shown that the fibres influence the secondary dendrite arm coarsening processes which leads to the elimination of all dendrite arms at sufficiently low cooling rates. The resulting microstructure consists of solute-poor primary phase away from the fibres and solute-rich primary phase with secondary phases concentrated at the fibre-matrix interface.

Even at low cooling rates, micro segregation in the matrix can be eliminated by solid state diffusion, resulting in a homogenized matrix in the as cast condition with no concentration gradients and no secondary phases within the limits of solid solubility of the alloy. The kinetics of the processes responsible for the evaluation of these unique microstructures have been modeled (150) and it is both predicted and

verified experimentally that the solidification times involved are only of the order of a minute in cases of commercial interest (151).

The distribution of the fibres, in general, is an important and unresolved issue in FMMC solidification processing. The metal tends to form channels during infiltration due to poor wettability of the fibre reinforcement and to liquid metal viscosity. The fibre reinforcement is therefore concentrated into regions of high fibre volume percent surrounded by channels of unreinforced metal (2). For all practical purposes, one is therefore limited to fabricate a composite in which the reinforcement is packed to maximum density (55 to 60vol.% for fibres) to prevent channeling. This reduces flexibility in tailoring the properties of the composite and also leads to frequent fibre to fibre contact points. These have shown a significant lowering of the transverse strength of continuous carbon fibre reinforced aluminium composites (152). It is due to stress concentration in these areas and poor infiltration of these areas in non-wetting systems (2).

The control of the carbon fibre distribution, in continuous fibre reinforced aluminium, have been achieved to some extent by Towata et al. (14) and Cheng et al. (12) after coating the carbon fibres with fine particles or whiskers of silicon carbide which hold the fibres apart. Low fibre volume fractions have been obtained but most notably fibre to fibre contact points are suppressed. Greatly improved transverse strength of the composites has been observed (153).

After solidification, large stresses can build up in the aluminium matrix due to differences in the coefficient of thermal expansions between the matrix and the carbon fibres (154). These stresses result in higher dislocation densities in the matrix (155,156) and consequently, influence the heat treatment characteristics of the matrix (157,158).

The influence of composite reinforcements on the evolution of age hardening precipitates is observed in aluminium/carbon fibre (Al/CF) composites. Aging produces a high density of Guinier-Preston (GP) zones and during heat treatment, solute segregation at the interface causes a precipitate-free zone (PFZ) to develop at the fibre interface. These PFZs contain several dislocations caused by thermal stresses

that develop during cooling as a result of the different thermal expansion coefficients of the fibre and the matrix (159,160).

The formation of PFZs involves the depletion of solute atoms from the interface during heat treatment. Solute depletion can result from interfacial segregation and from the heterogeneous nucleation of precipitate phase on the fibre-matrix interface. The nucleation of $CuAl_2$ precipitates on the fibre interface has been observed in an artificially aged Al-Cu/CF composite. The $CuAl_2$ precipitate nucleates on the TiB_2 coating of the fibres and consumes excess copper from the matrix as it grows. Heterogeneous nucleation of precipitate phases is also commonly observed in most fibre/metal matrix composite systems (161) and appears to be an almost unavoidable consequence of the large areas of incoherent interface present.

Grain boundary precipitation is commonly observed in aluminium base composites with continuous reinforcements. Depending on the aluminium alloy, different phases precipitate on the grain boundary and grow into the grains, a process of discontinuous precipitation (162,163). In this process, particle growth occurs only at the boundary and is therefore not continuous with time. Nucleation of precipitate laths is facilitated by the grain boundary energy and by the low interface energy between specific lattice planes of the particle and the matrix (161). As the laths thicken, they remain partially coherent on at least one side of the boundary and some times, on both sides depending upon the relative misorientation between adjacent grains. The lower interface boundary exhibits several steps called growth ledges and thickening of the precipitate can occur by the edge wise propagation of ledges along this face. The distribution of the ledges indicates that they form at the centre of the face and migrate towards the ends, a widely reported mechanism of precipitate growth (164,165).

Most grain boundaries in continuous Al/CF composites extend transversely between the fibres as the fibre-matrix interface effectively replaces much of the grain boundary area in longitudinal orientations. Many of these transverse grain boundaries are composed of dislocation arrays and the structure of defect array is locally perturbed at some points by dislocations intruding from the matrix as observed in a

Al/CF composite, artificially aged to increase the matrix yield strength and to prevent plastic flow during cooling (160).

The aging has resulted in PFZs along the sub-boundary and several grain boundary regions. Dislocation glide may occur more easily in PFZ than in the precipitate hardened matrix. The defects that are parallel and straight in the PFZ become tangled away from the boundary where glide is impeded by the precipitates. Transverse grain boundaries in Al/CF composites also provide a growth path for iron bearing constituent particles that nucleate at the fibre interface during casting. The particles extend few microns along the transverse boundaries and some times, span interfibre distances. Because these constituent particles are inherently brittle, their presence can cause premature crack initiation and facilitate crack growth between the fibres.

Most metal matrix composite systems are nonequilibrium systems in the thermodynamic sense; i.e., there exist a chemical potential gradient across the fibre-matrix interface. So, in favourable kinetic conditions, diffusion and/or chemical reactions occur between the constituents. The interface layer(s) formed because of such a reaction generally have characteristics different from those of either one or both the components. Sometimes, a controlled amount of reaction at the interface is desirable for obtaining strong bonding between the fibre and matrix but too thick an interaction zone, however, adversely affects the composite properties (166).

Interface between the fibres and the matrix in FMMCs plays a very vital role in transferring the load from matrix to fibres and acts as a mechanical fuse, a wetting agent and a diffusion barrier. It is very difficult to obtain an optimum interface for a composite because many factors like type of fibres (surface microstructure), coating deposited on the fibres, composition of the matrix alloy, processing condition of the composites etc. affect the nature of the interface. In the ideal case, there should be good wetting without any solubility and reaction between the matrix and the fibres. Reactions between structural matrices and available fibres are quite complex which lead to a wide variety of interfaces.

Broutman and Krock (167) have defined the interface as a region of significantly changed chemical composition that constitutes the bond between the matrix and the reinforcement for transfer of load between these members of the composite structure. They have proposed a general classification for the types of interfaces, based on the nature of chemical reaction occurring between the reinforcement and the matrix. The three classes proposed are,

Class 1: fibre and matrix mutually nonreactive and insoluble in each other.
Class 2: fibre and matrix mutually nonreactive but soluble in each other.
Class 3: fibre and matrix react to form compound(s) at interface

It is very difficult to classify the interfaces into these three categories because most of the composite systems either overlap different classes or have another transient state. They have proposed another subgroup called pseudo class 1 composites alongwith the above classification. In this class, composites appear free of interaction after fabrication by the optimum processing techniques but thermodynamic data indicates that the constituents should react. Aluminium/carbon, aluminium/boron and aluminium/silicon carbide can be considered pseudo class 1 composite systems as they show apparent nonreactivity when fabricated by the optimum processing, in contrast to the time reactivity of the constituents. All class 3 systems may have a transitory existence as pseudo class 1 system until the preexisting films on the surface of matrix and fibre are dissipated.

The above classification of interfaces is based on the physical, chemical and mechanical bonding. Class 1 composite systems are related to mechanical bonding, arises mainly from interlocking of the two components across an interface as well as frictional resistance due to squeezing one component around an inclusion of the other component. Class 2 composite interfaces may be attributed to physical bonding arises mainly from interaction at molecular level between fibres and the matrix due to the elimination of contaminant films present on the surfaces of the constituents. The elimination of contaminant films occurs as a result of wetting and dissolution (without chemical reaction). Physical bonding involves interatomic distances of 3 to 5 Å and is governed by Vander Waal's bonds having bond energies of the order of 0.5 - 10

kcal/g-mole. This leads to a theoretical strength of the order of 0.69 GPa - 6.9 GPa. Chemical bonding is responsible for class 3 interfaces, arises mainly from the formation of new compound at the interface due to reaction between the constituents. Chemical bonding is governed by primary bonds (ionic, covalent and metallic) and involves interatomic distances of 1 to 3 Å. Primary bonds have energies of the order of 30-100 kcal/g-mole, which leads to a theoretical strength of the order of 6.9 GPa - 69 GPa (168).

Breakdown from one type to another results in mixed bonding due to partial transition from pseudo class 1 systems to class 3 systems as observed in aluminium/carbon system. In case of aluminium/carbon system, the liquid aluminium reacts with the oxygen present on the carbon fibre surface and forms an oxide layer. This layer acts as a barrier between the fibre and the matrix and prevents direct contact of the constituents. As soon as this oxide layer is ruptured, aluminium reacts with carbon and forms Al_4C_3 as a reaction product at the interface. Since the solubility of carbon in liquid aluminium (1100^0C) and solid aluminium is 0.35wt.% and 0.015wt.% respectively (97), upon cooling from processing temperature of 1100^0C, essentially all dissolved carbon is precipitated out as Al_4C_3.

Baker and Bonfield (169) have expressed the formation of Al_4C_3 at the interface of the carbon fibre and aluminium as,

$$3C + 4Al \rightarrow Al_4C_3 \qquad (2.19)$$

For this reaction to occur between carbon fibre and aluminium matrix, the free energy of the reaction must favour the reaction to proceed. This condition applies to both dissolution and formation of reaction product (Al_4C_3). Kubaschewski and Alcock (170) have shown that the Gibbs standard free energy of Al_4C_3 formation in the temperature range of 659 - 1727^0C is given as,

$$\Delta G = -266520 + 92.6T \quad \text{kJ/mole} \qquad (2.20)$$

The Gibbs free energy, as given by the above equation, being highly negative suggests that the tendency of forming Al_4C_3 is very strong.

The reaction product is formed as rhombohedral aluminium carbide at the interface, which nucleates heterogeneously from the fibre and grows on to the aluminium matrix as lath like crystals (36). It is further observed that the axis of these aluminium carbide crystals lie parallel to the basal plane of the crystal lattice of the carbon fibres. This has led to the conclusion that carbide nucleates on the defects on the carbon fibre surface such as exposed basal plane edges (171).

Aluminium carbide growth has also occurred with a plate like morphology, with the platelets originating from the fibre surface. Since the activity of both the constituents is unity and the free energy of carbide formation is highly negative, Al_4C_3 crystals nucleate rather uniformly over the entire fibre surface. On an atomic level, in graphitized fibres, a large amount of basal planes lie parallel to the fibre circumference (172). Although the basal planes are relatively inert, nucleation occurs preferentially along the high energy basal edges. Al_4C_3 has shown faceted growth characteristics with growth occurring in a direction parallel to the carbide basal planes.

Interfacial carbides have been observed to be lath like shape only in processes involving the presence of the liquid phase, otherwise they usually develop as thin platelets (173). Yang and Scott (174) have studied the Al/CF interface for Al-7wt.%Si/CF composites, fabricated by liquid metal infiltration. They have observed that the growth of interfacial carbides is controlled by a ledge movement mechanism but they could not explain the occurrence of precipitates as laths instead of platelets.

Diwanji and Hall (175) have found a consistent carbide/matrix and carbon/carbide relationship as (0003) Al_4C_3 // (111) Al, [11$\bar{2}$0] Al_4C_3 // [123] Al and (002) gr // (0003) Al_4C_3 respectively which means that Al_4C_3 basal planes lie parallel to the graphite basal planes. As most of the basal planes lie parallel to fibre circumference in graphite fibres and due to the preferred growth direction of Al_4C_3

crystals, a significant amount of nuclei start to grow nearly tangential to the fibre surface which quickly impinge upon each other and cease to grow any further. The nuclei that do not impinge can continue to grow with a plate like morphology as a result of free energy minimization based on surface energy considerations. So they have interpreted the preferential growth behaviour of carbides in terms of normal interfacial free energy, coherency and elastic stress consideration.

Sanctis et al. (36) have observed a crystallographic relationship in the form of (0001) Al_4C_3 // (001) C with the fibre structure and subsequent fast growth of carbides into the molten aluminium matrix along preferential $[\bar{2}110]$ direction. They have suggested that carbide develops lath like in shape mainly because their thickening at the fibre surface is limited by the different orientation and lower reactivity of adjacent fibres surface regions. On the other hand, Carpenter and Lo (176) and Chen and Hu (177) have found that no orientation relationship exists between the carbides and the matrix material.

Increased contact time between the reinforcement and liquid aluminium, increased melt temperature and increased infiltration length, all lead to the growth of the interfacial carbide phase and bond strength along the fibre matrix interface (178). Lin (101) has studied the extent of interfacial reaction as a function of processing time for Al/CF composites and has observed a linear increase in the thickness of carbide phase with processing time. He has also observed that the thickness of carbide phase corresponding to zero value of processing time is finite which is attributed to the reaction occuring during cooling. Although a linear growth rate reflects a chemical reaction of zeroth order but due to the presence of dense Al_4C_3 layer and the platelets, Lin (101) has suggested that the average growth is controlled by mechanism other than chemical reaction. The rate of growth in thickness of Al_4C_3 is calculated as 1.8 μm/min, which roughly corresponds to the carbon depletion rate of 0.48 μm/min. These high rates have suggested that composites have to be fabricated in a very short time (1 to 2 min) to prevent heavy degradation of carbon fibres. For fibres of 10 μm diameter, a 1 μm reaction zone is developed in about 2 min of processing time, which corresponds to a reaction zone to fibre volume ratio of 0.44. In other words, for 20

vol.% fibre composite, there is roughly 9 vol.% reaction zone in the composite, which is quite significant so as to alter the mechanical behaviour of the composite.

It is observed that heat treatment and higher ageing temperature increase the severity of the interfacial reaction and carbide grain growth (179). As the carbide phase grows, the carbide inclusions increase mainly in size rather than in numbers (180). Baker et al. (169) have observed a mixture of aluminium and aluminium carbide after annealing of aluminium coated carbon fibres at annealing temperature of 475^0C - 550^0C and aluminium carbide alone at annealing temperature of 600^0C - 650^0C at the interface. The carbide formation is observed relatively at lower annealing temperature of 475^0C in case of high strength carbon fibres as compared to 550^0C in case of high modulus carbon fibres. Khan (138) has also observed the formation of Al_4C_3 at the interface of Al/C couple which has a hexagonal structure (a_o=3.32Å, c_o = 24.89 Å) at about 500^0C. Heat treatment of Al/C couple at 600^0C results in the growth of Al_4C_3 in the form of single crystalline platelets having (0001) orientation with the c-axis of the hexagonal carbide lattice perpendicular to the platelets. He has observed that the thickness of carbide phase increases with heat treatment temperature and time and the thickening process is diffusion controlled. He has also observed that thickening 'rate constant' obeys the Arrhenius law, with the calculated activation energy Q required for the formation of Al_4C_3 to be 35.17 kcal/mole, however, he has not observed any appreciable effect of the crystallographic structure of carbon on the interface structure development.

Hashmi et al. (105) have observed the presence of Al_4O_4C and TiB_2 at the interface of as received composites whereas the interface in the heat treated composites consists of Al_4C_3, Al_4O_4C and TiB_2. They have found that the reaction zone thickness increases with heat treatment temperature and time, which is about one magnitude lower than the estimated thickness value when thickening process is diffusion controlled. This difference has been attributed to the TiB_2 coating, which acts as an effective diffusion barrier. Cheng et al. (12) on the other hand, have observed no trace of interfacial reaction in the as cast and heat treated aluminium alloy composites reinforced with high modulus carbon fibres. However, in case of Al/CF composites containing high strength carbon fibres, they have observed the

probable presence of Al_4C_3 at the interface, which grows, with T_6 treatment of the composites.

2.7 MECHANICAL PROPERTIES OF FMMCs

The continuous fibre metal matrix composites are anisotropic due to the presence of fibres, oriented in a particular direction within the matrix. Since the properties of the two phases are different, the composite properties vary with the fibre orientation and are not only defined merely by the type of the constituents and their volume fractions, but also by the distribution of the fibres.

If $E_f > E_m$ and $\sigma_f > \sigma_m$ (where E and σ represent the Young modulus and strength and suffice f and m stand for fibre and matrix respectively), the composite properties in the fibre direction are chiefly dependent on the fibre volume fraction and their properties whereas the composite properties in a transverse direction to the fibres are chiefly dependent on the properties of the matrix (181).

The mechanical properties of a unidirectional continuous fibre composite in fibre direction are predicted accurately by law of mixtures model representing the iso-strain conditions, which is equivalent to that treated by Voigt (182). According to law of mixtures, the modulus and the strength of a composite containing continuous fibres are given as,

$$E_C = V_f E_f + V_m E_m \tag{2.21}$$

and,

$$\sigma_C = V_f \sigma_f + V_m \sigma_m \tag{2.22}$$

where, V represents the volume fraction and suffice c, f and m stand for composite, fibre and matrix respectively.

In transverse direction, the properties of the composite are predicted by law of mixtures model representing the iso-stress condition, which is equivalent to that treated by Reuss (183). The modulus and strain in transverse direction are given as,

$$\frac{1}{E_c} = \frac{V_f}{E_f} + \frac{V_m}{E_m} \tag{2.23}$$

and,

$$\varepsilon_c = \varepsilon_f V_f + \varepsilon_m V_m \tag{2.24}$$

where, ε represent the fracture strain.

A stress-strain curve of a metal matrix composite conveniently represents its basic mechanical behaviour like stiffness, yield, flow and fracture stresses. The stress-strain curve of a typical continuous fibre metal matrix composite consists atmost of four stages (184), which are summarized as follows:

(I) Both the fibres and the matrix deform elastically

(II) The fibres continue to deform elastically, but matrix now deforms plastically

(III) Both the fibres and the matrix deform plastically

(IV) The fibres fracture followed by composite fracture.

Metal matrices are ductile and yield at a very low strain so that stage I constitutes only a small portion of the composite stress-strain curve. Stage II and III constitute the major portion of the composite stress-strain behaviour and therefore, are the prime regions of concern to the engineering aspects of these materials. Most of the multifilament fibres available today are brittle and have a fracture strain greater than the yield strain of the metal matrix. So, stage III is not observed when metal matrices are reinforced with these brittle fibres. Stage IV is difficult to locate precisely but occurs at the point where composite fractures and longitudinal strain in the composite equals to the fracture strain of the fibres. So most of the fibre reinforced metal matrix composites possess the first and second stages.

In Stage I, the composite modulus 'E_c' is predicted accurately by the law of mixtures and is given by Eqn. (2.21). In stage II, matrix deforms plastically and its stress-strain curve is no longer linear, so that the composite modulus is predicted at each strain level as,

$$E_c = E_f V_f + \left(\frac{d\sigma_m}{d\varepsilon_m}\right)_{\varepsilon_f} V_m \tag{2.25}$$

where, $\left(\frac{d\sigma_m}{d\varepsilon_m}\right)_{\varepsilon_f}$ is the slope of the stress-strain curve of the matrix at the fracture strain, ε_f of the fibres.

In stage I, the composite strain $\varepsilon_c < \varepsilon_{my}$, composite strength is given as,

$$\sigma_c = \varepsilon_c [E_f V_f + \varepsilon_m (1-V_f)] \tag{2.26}$$

In stage II, $\varepsilon_{my} < \varepsilon_c \leq \varepsilon_f$, the composite strength is given as,

$$\sigma_c = \varepsilon_c E_f V_f + \sigma_{my} (1-V_f) \tag{2.27}$$

or,

$$\sigma_c = V_f \sigma_f + \sigma_{my} (1-V_f), \qquad \text{when, } \varepsilon_c = \varepsilon_f$$

Equations (2.26) and (2.27), whichever is appropriate, gives the tensile strength for a composite made of high strength brittle fibres when the matrix strength 'σ_m' is substituted for matrix stress 'σ_{my}' corresponding to the fibre fracture strain ε_f.

Kelly and Davies (185) have pointed out that a composite must have a certain minimum fibre volume fraction so that the composite strength is ideally reached at a total strain equal to the fracture strain of the fibres, thus showing real fibre reinforcement. It is given as,

$$V_{min} = \frac{\sigma_m - (\sigma_{my})_{\varepsilon_f}}{\sigma_f + \sigma_m - (\sigma_{my})_{\varepsilon_f}} \tag{2.28}$$

In order to have a composite strength greater than that of the matrix, the fibre volume fraction in the composite must exceed the critical fibre volume fraction given as,

$$V_{crit} = \frac{\sigma_m - (\sigma_{my})_{\epsilon_f}}{\sigma_f - (\sigma_{my})_{\epsilon_f}} \qquad (2.29)$$

where, σ_f, σ_m and $(\sigma_{my})_{\epsilon_f}$ represents ultimate fibre strength, ultimate matrix strength and matrix stress corresponding to the fracture strain of the fibres respectively. Equations. (2.28) and (2.29) are applied for continuous fibres and assume no alteration in the work hardening or stress-strain characteristics of the matrix due to the presence of the fibres. They have been derived after assuming that the fibres are of equal strength and all break in a given cross-section.

The above equations representing the composite are valid only when the fibre volume fraction exceeds a minimum value V_{min}, given by Eqn. (2.28). Normally, V_{crit} is always greater than V_{min}. It is clear from Eqn. (2.29) that V_{crit} increases with increasing UTS of the metal matrix and decreases with increasing UTS of the fibres. In case of light metal matrices and multifilament high strength ceramic fibres, the value of V_{crit} is far lower than the volume fraction of the fibres used normally in the fabrication of FMMCs, hence it is insignificant.

The transverse (tensile) strength, σ_T is known to depend strongly on the strength of the matrix-fibre interface relative to the transverse fibre strength, the matrix strength and also the fibre volume fraction. Thus σ_T is usually much smaller than σ_L of the same metal matrix composite. Prewo and Kreider (186) have predicted the transverse strength on the basis of a simple model by assuming that the fibres are replaced by holes. Thus, the transverse strength is controlled by the matrix fracture strength times the reduced cross sectional area. However, this model is considered to be an over simplification of the actual fracture mode where the fracture path is presumably a mixture of interfacial debonding, fibre splitting and the matrix fracture. In order to simulate the actual fracture mode, one must know the statistical data of the variation of the interfacial bond strength for all the matrix-fibre interfaces in the actual continuous fibre metal matrix composites, the matrix strength and transverse fibre strength.

Kyono et al. (187) have attempted to simulate the transverse tensile stress-strain curve of FMMC by using a model based on Eshelby method. This model assumes that a composite, subjected to transverse loading σ_T, has a mixture of debonded interfaces and completely bonded interfaces where the interfacial bond strength follows a three point Weibull distribution.

The law of mixtures model is sometimes too crude to predict the strength of a composite. Rosen (188) and Zweben (189) have proposed more accurate models for the prediction of σ_L, which are based on the statistical distribution of flaws or imperfections that result in fibre failure under applied stress. As suggested by Coleman (190), the fibre strength 'σ_f' in a statistical manner, is assumed to obey the Weibull distribution as,

$$f(\sigma_f) = \frac{\beta\sigma^{(\beta-1)}}{a^{\beta}} exp\left[-(\sigma/\alpha)^{\beta}\right], \qquad \sigma,\beta,\alpha > 0 \tag{2.30}$$

where, α and β are scale parameter and shape parameter of Weibull distribution respectively. Parameters α and β are related to the fibre length 'l' as,

$$\alpha = (l\delta)^{\frac{-1}{\beta}} \tag{2.31}$$

where, δ is a constant that can be determined from tests on monofilament fibres. The corresponding cumulative distribution function is given as,

$$F(\sigma_f) = \int_0^{\sigma_f} f(\sigma_f)d\sigma_f = 1 - \exp\left[-(\sigma/\alpha)^{\beta}\right] \tag{2.32}$$

The mean value of the fibre strength '$\bar{\sigma}_f$' is then given by,

$$\bar{\sigma}_f = \alpha\Gamma\left(1+\frac{1}{\beta}\right) \tag{2.33}$$

where, Γ is the gamma function. Parameters α and β in Eqns. (2.31) and (2.33) are also related to the standard deviation 'S_d' and coefficient of variation 'C_v' as,

$$S_d = (\alpha)^{-1/\beta}\left\{\Gamma(1+2/\beta) - \Gamma^2(1+1/\beta)\right\}^{1/2} \tag{2.34}$$

and,

$$C_v = \frac{S_d}{\sigma_f} = \frac{\left\{\Gamma(1+2/\beta) - \Gamma(1+1/\beta)\right\}^{1/2}}{\Gamma(1+1/\beta)} \tag{2.35}$$

2.8 MECHANICAL PROPERTIES OF Al/CF COMPOSITES

From the mechanical property point of view, Dicarlo (191) has summarized the requirements for strong and tough metal matrix composites. Generally, FMMC consists of a ductile matrix containing strong brittle fibres. For maximum strength in a given direction, continuous fibres (high aspect ratio) must be strongly bonded to the metal matrix for efficient load transfer. However, fibre matrix reaction at the interface either during fabrication or in service and thermal stresses due to expansion mismatch between fibre and matrix are the main factors responsible for inefficient load transfer from matrix to the fibres. For a tough MMC, fibres with a high in situ strength and a low density of critical flaws are required together with maximum interfibre spacing for a given fibre volume fraction. The later requirement exploits the crack blunting characteristics of tough metals and can be achieved for a given fibre volume fraction by using fibres with as large a diameter as possible.

Initially, Al/CF composites have been fabricated by solid state diffusion bonding process. The carbon fibres are infiltrated by liquid metal infiltration or coated with aluminium by different coating techniques to produce precursor wires. Davis and Sullivan (192) have examined various graphite fibre/aluminium precursor wires up to 45% fibre volume fraction. They have reported a very high modulus of about 152 GPa for the graphite/aluminium composites in wire form. Table-2.1 shows the average tensile strength of Al/CF composites in precursor wire form (91).

Table-2.1

Average tensile strength of Al/CF composites in precursor wire form

S. No.	Aluminium alloy	Precursor fibre type	Commercial designation	Volume fraction (%)	Average tensile strength (MPa)
1.	201	Rayon	Thornel 50 (8 end)	30	870
2.	202	Rayon	Thornel 50 (8 end)	28.7	795
3.	201	Rayon	Thornel 50 (1 strand)	41	1045
4.	202	Rayon	Thornel 75	27	810
5.	202	PAN	Thornel 300	29	245
6.	201	PAN	Thornel 300	45	350
7.	201	PAN	Stackpole Panex	23	125
8.	201	PAN	Hercules Type A	37	240
9.	201	PAN	Hercules HM-S	24	785

The Al/CF composites are highly anisotropic as the strength and modulus values differ largely in the longitudinal and transverse directions. The properties of these composites are found to increase with increase in fibre volume fraction (193,194). The mechanical properties of these composites as summarized by Rubin (9) are shown in Table (2.2).

Table-2.2

Mechanical properties of Al/CF composites

Fibre direction	Matrix alloy	Fibre volume fraction (%)	Density gm/cm^3	Tensile strength (MPa)		Tensile modulus (GPa)	
				L	T	L	T
0°	201Al	30	2.38	620	48	165	35
0°	201Al	34	2.38	655	31	207	35
0°	201Al	30	2.44	550	69	158	41
0°	6061Al	41	2.44	620	103	324	48
0°	6061Al	50	2.49	1375	138	235	158
0°	Pure Al	42	-	950	-	120	-
0°	Pure Al	70	-	1450	-	250	-
0°	Pure Al	38	-	350	-	60	-

The mechanical behaviour of Al/CF composites has been investigated by several workers. Imprescia et al. (139) have reported the strength of these composites as high as 90% of the law of mixtures values. Generally, the strength values are less than that estimated by the law of mixtures but Pepper et al. (34) have observed the

strength of Al-13wt.%Si/CF composite having a fibre volume fraction of 28% greater than the theoretical strength based on law of mixtures. They have reported an average uniaxial tensile strength of 730 MPa, however, several values between 900 MPa to 1000 MPa are also obtained. They have not observed any change in the tensile properties of the composites when thermally cycled between -193^0C to $+20^0$C and between -193^0C to $+500^0$C twenty times. Khan (138), on the other hand, has observed 18% degradation of composite strength when thermally cycled between 20^0C to 500^0C for 10 times and this degradation remains constant. He has observed a maximum tensile strength of 552 MPa and elastic modulus of about 142 GPa for Al/CF composites having a fibre volume fraction of 0.25 to 0.30. He has also observed that the strength of the composites remains unaffected when exposed to high temperature of 500^0C and afterwards decreases drastically. However, elastic modulus remains unaffected to high temperature exposure.

Towata et al. (37) have fabricated Al/CF composites by reinforcing high modulus carbon fibres in pure Al and Al-2wt.% Mg alloy matrices with 60% fibre volume fraction. They have observed the tensile strength of the composites very well in agreement with the law of mixtures strength whereas the tensile modulus is found greater than that predicted by law of mixtures. They have also observed that the flexural strength is larger than the tensile strength while flexural modulus is lower than the tensile modulus for both the composites. These results are very well in agreement with those observed for other composite systems (195).

They have observed the axial compressive shear strength of the Al-2wt.%Mg matrix composites about two and half times as large as that of pure aluminium matrix composites. They have observed the dependence of composite strength on the annealing temperature and the alloying addition to the aluminium matrix. They have also observed that flexural strength of pure Al matrix composite decreases slightly while shear strength increases slightly above 500^0C. Further, they have observed that flexural strength increases two times whereas shear strength decreases to half of the original value at 600^0C, in case of Al-2 wt.%Mg matrix composite. They have observed a decrease in the flexural strength of Al-5 wt.%Mg, Al-0.6 wt.%Ca and Al-4.5 wt.%Cu matrix composites after annealing at 500^0C whereas the shear strength of these composites have increased after annealing at 500^0C. The Al-0.6 wt.%Ca matrix

composite has shown lowest decrease in flexural strength after annealing at 500^{0}C while Al-5 wt.%Mg matrix composite has shown the highest increase in shear strength after annealing at 500^{0}C.

Towata et al. (14) in another study, have observed a 50% increase in the longitudinal flexural strength of hybrid composites, where hybridization is accomplished with the addition of SiC particles and whiskers to the high strength carbon fibres, over conventional Al/CF composites even when the fibre volume fraction in hybrid composite is significantly lower than that of conventional composites. However, the longitudinal flexural modulus is found to be lower for hybrid composites than conventional composites but same for both the hybrid composites containing pure Al and Al-5wt. %Mg as matrices. The transverse flexural strength is found nearly same in hybrid and conventional composites having pure Al as the matrix whereas it is observed quite different in case of the composites containing Al-5wt. % Mg matrix as conventional composite has lower flexural strength than that of hybrid composites.

Hashmi et al. (105) have studied the mechanical behaviour of Al/CF composite in as cast and heat treated conditions. They have observed the law of mixtures values very well in agreement with the tensile strength and elastic modulus of the composite. The tensile strength is decreased significantly with heat treatment temperature whereas elastic modulus is found virtually constant after high temperature treatment. The transverse tensile strength is observed to be much lower than the longitudinal tensile strength. They have also observed a lower strength and modulus measured in compression than those measured in tension.

The strength of the composites has also been found to depend upon the degree of graphitization of carbon fibres. Warrier et al. (31) have observed the strength of Al/CF composites as 65%, 62% and 58% of the theoretical strength values (calculated by law of mixtures) for aluminium matrix reinforced with silver coated CVD annealed graphite fibres, pitch base fibres and PAN base fibres respectively. They have also observed the composite strength as 47% and 59% of the theoretical strength with uncoated CVD annealed and pitch base graphite fibres respectively.

In case of high strength carbon fibres, fibre coating prior to solidification processing of Al/CF composites has been proved beneficial in improving the mechanical properties. Wang et al. (88) have observed an increase of 189% in the strength of the composites fabricated by squeeze casting the SiC coated carbon fibres with aluminium over those fabricated by squeeze casting the uncoated carbon fibres with aluminium. Vessel (20) has also mentioned that the coating of pyrolytic carbon on high strength carbon fibres (T800) results in the high strength of Al/CF composites, which is very close to that predicted by law of mixtures. He has also observed a very high modulus of about 410 GPa for Al/CF composites having 55% fibre volume fraction of high modulus graphite fibres in Al-7wt.%Si-0.6wt.%Mg alloy matrix. He has also pointed out that high modulus carbon fibres result in lower transverse strength of Al/CF composites than that with high strength carbon fibres.

The creep behaviour of FMMCs has been investigated by a number of workers. Kelly and Street (196) have found that fibre aspect ratio and the matrix stress exponent in the power law creep relationship are important parameters. Lilholt (197) has expressed power law creep in terms of an effective rather than an applied stress. Mclean (198) has discussed the modelling of creep behaviour in FMMCs. In FMMCs consisting of continuous ceramic fibres in a metal, for example Al/CF, the operating homologous temperatures for fibre and matrix may be 0.1-0.3 and 0.4-0.7 respectively as the differences in the melting points of the matrix and fibres is large. Mclean (198) has pointed out that in such composites the matrix is subjected to creep rates in order of magnitude greater than those of the fibres, leading to a situation for having elastically deformed fibres in a creeping matrix. Thus it is difficult to observe a steady state creep rate in such composites. Instead, the creep rate progressively decreases and asymptotically approaches zero as the strain attains an equilibrium value.

Relatively less attention has been paid to the fatigue behaviour of FMMCs because it has not been regarded as important a problem as, say, high temperature strength by the users of the composites. Baker et al. (137) have carried out reversed bending fatigue studies on Al/CF composites containing high modulus and high strength carbon fibres. They have observed that high strength carbon fibre composites show lower fatigue properties than the composites containing high modulus carbon fibres, even after having less number of broken fibres and more alignment of fibres in

high strength carbon fibre composites. They have also observed that the high modulus carbon fibre composites, pressed at low temperatures, show poorer fatigue properties than composites pressed at high temperatures due to increase in aluminium carbide formation with pressing temperature.

Amateau and Hanna (199) have reported the effect of fabrication process on the fatigue strength of graphite fibre reinforced aluminium composites. They have observed that the composites produced by LMI exhibit a fatigue strength 50% greater than those produced by hot pressing. They have explained the fatigue failure in these composites by a process of crack initiation in the matrix at the points of cavities and inclusions, leading to crack propagation along the previously broken fibres. Thus, fatigue properties are controlled by initiation and propagation of cracks within the matrix. Similar conclusions have been derived by Shimnin and Toth (200) and Christian (201).

It has been shown that the fatigue process in FMMCs is strictly matrix controlled. However, interface may have significant effects on fatigue life of composites. If the interface could be weakened enough to permit debonding, the sharp cracks would be blunted at the interface, resulting in higher fatigue strength. Cyclic loading results in a uniform distribution of dislocations in the metal matrix resulted due to mismatch in the thermal expansions of the constituent phases. Rosenkranz et al. (202) have found that the variations in the matrix and fibre strength and the interfacial bond strength have significant influence on the fatigue damage and failure.

Hashmi et al. (105) have observed the effect of heat treatment and nature of the fatigue testing on the fatigue strength of the Al/CF composites. They have shown that fatigue strength of aluminium alloy is increased when reinforced with carbon fibres, however, in other systems the composites have lower fatigue strength than unreinforced matrix. They have also observed that the strength of the composites continuously decreases with heat treatment temperature and time in tension/tension fatigue whereas the fatigue strength initially decreases with heat treatment temperature and again increases to reach the as cast composite fatigue strength at 545^0C in compression/compression fatigue. They have reported that the mechanism of failure in tension/tension fatigue is due to the initiation of cracks at the interface and

their subsequent propagation in the matrix. The reaction zone is the controlling factor in tension/tension fatigue whereas compression/compression fatigue is matrix dependant.

Toughness and ductility are the other important properties in respect to FMMCs. Although they are different, but related to each other in the sense that composites having low toughness also show lower ductility and vice a versa. The toughness and ductility of FMMCs containing high strength brittle fibres generally depend on the fracture strain of the fibres but Crowe et al. (203) have pointed out the negative effect of fibre orientation, nonuniform fibre distribution, second phase particles and inhomogeneous internal stress on the fracture toughness of the composites. Wang et al. (88) have pointed out the importance of interfacial bonding in this regard. They have shown that an intermediate strong interface in Al/CF composites results in improved toughness and ductility by enabling the fibres to pullout during loading whereas strong interface in these composite results in inferior toughness and ductility due to negligible fibre pull out.

Another important property, which is considered for use of FMMCs in aerospace and military applications, is the coefficient of thermal expansion (CTE). Al/CF composites show very low thermal expansion, which continuously decreases with increasing fibre volume fraction due to the almost zero longitudinal expansion coefficient of carbon fibre (104). The thermal expansion of these composites is larger in transverse direction than in axial direction as carbon fibres have axial coefficient of thermal expansion nearly equal to zero while radial coefficient of thermal expansion has a value of $8x10^{-6}\ K^{-1}$ (166).

Among the greatest profits with continuous fibre reinforced aluminium matrix composites are their superior high temperature properties as compared to unreinforced metal matrix and polymer composites. These composites have been considered for applications at temperatures below 400^0C (5). Davis and Sullivan (192) have studied the tensile strength of Al/CF composites at high temperatures (250^0C to 350^0C). They have observed that longitudinal tensile strength of the composites is approximately 10% lower than the tensile strength of the same composites at room temperature.

Elastic modulus and tensile strength of FMMCs have been found to decrease with increase in temperature, in most of the composite systems. It has been shown that modulus values of fibre reinforced aluminium matrix composites are retained above that of unreinforced matrix up to 400^0C (204) whereas strength values are found to be superior to that of unreinforced matrix up to 350^0C (205). Vessel (20) has mentioned that Al/CF MMCs possess better specific strength than that of Ti based MMCs up to 350^0C. The fatigue strength of Al based FMMCs is also found to decrease with temperature (206). However, the decrease is relatively gradual with high fibre volume fraction whereas it is quite sharp in composites having low fibre volume fraction.

2.9 INTERFACIAL PROPERTIES OF Al/CF COMPOSITES

The fibre-matrix interfacial mechanical properties, especially the interfacial shear strain, a root cause for interfacial shear strength and fracture toughness, influences the macroscopic properties of composite materials and they have attracted much attention in recent years. Simple approach to evaluate the interfacial shear strength and fracture toughness has been studied by several workers (207). In 1993, a round-robin program (208) was undertaken to investigate the testing methods for measuring the interfacial shear strength. Four commonly used methods are: single fibre pullout, microdebonding, fragmentation, and micro-indentation tests. There are several test methods for evaluating the interfacial fracture toughness of the bi-material interface (209). To evaluate the interfacial fracture properties of the fibre-matrix interface, the most pertinent method is the single fibre pullout test of the concentrated axisymmetric model (210). This method is simple in principle but due to small diameter of the fibre, many factors affect the accuracy of the results. The embedded length and the free length of the fibre are difficult to measure exactly, so the results show a large scatter (211).

On the basis of microscopical analysis of the fibre distribution in unidirectional fibre composites, the relation between average and maximum interfacial strain can be obtained with the help of microstructure. Assuming the fibres are distributed hexagonally, through a simple geometrical analysis (207), the interspacing between two fibres is obtained as,

$$s = 2\left[\left(\frac{\pi}{2\sqrt{3}V_f}\right)^{1/2} - 1\right]r_f \tag{2.36}$$

where, V_f is the volume fraction of the fibre, s is the distance between two fibres, and r_f is fibre radius. For square distribution of the fibres, Eqn. (2.36) is expressed as,

$$s = 2\left[\left(\frac{\pi}{2\sqrt{4}V_f}\right)^{1/2} - 1\right]r_f \tag{2.37}$$

and the distance between the centers of two fibres is given as,

$$S = 2r_f + s \tag{2.38}$$

When the composite undergoes a longitudinal shear deformation, the fibre modulus can be assumed to be large as compared to the matrix and hence, the shear deformation is all caused by the matrix. Thus, the average shear strain is given as,

$$\nu_{av} = \frac{\Delta u}{2r_f + s} \tag{2.39}$$

where, Δu is the difference between the longitudinal displacement of the centers of the two adjacent fibres in the through-thickness direction, i.e., $\Delta u = u_2 - u_1$ as shown in Fig.2.5. In the matrix, the maximum shear strain takes place at the location where the separation distance of the two fibres is minimum. Thus the maximum shear strain in the matrix is given as,

$$\nu_{max} = \frac{\Delta u}{s} \tag{2.40}$$

Consequently, the relationship between the average shear strain of the composite and the maximum strain in matrix is derived as,

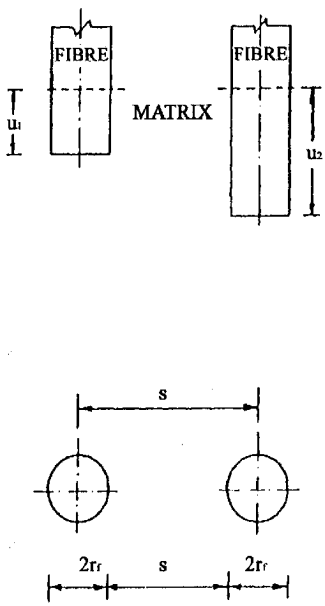

Fig. 2.5 Schematic diagram showing the longitudinal displacement of the centres of two adjacent fibres.

$$\frac{v_{av}}{v_{max}} = \frac{s}{2r_f + s} \tag{2.41}$$

From the compressive performance of carbon fibres, Vin Con et al. (212) have analyzed that the high strength fibres present a very high failure strain (greater than 1.7% for T300) as compared to high modulus fibres (about 1%). They have concluded that compressive failure strain is higher than tensile failure strain. The 'single fibre composite' (SFC) test originally proposed by Kelly and Tyson (213) for MMCs provides abundant statistical information from only a few specimens having different interfacial failure modes and 'interfacial shear strength', (IFSS). On the basis of an equilibrium condition in an axial fibre stress and matrix shear stress, they have shown that the IFSS 'τ' is given by,

$$\tau = \frac{\sigma_f r_f}{l_c} \tag{2.42}$$

where, σ_f is fibre fracture strength, r_f is the fibre radius and l_c is the average critical fragment length. Since the actual fragment length and the strength are not constant but are strongly dependent on the gauge length, Eqn. (2.42) can be modified as,

$$\tau = \frac{\sigma_f r_f}{l_c} K \tag{2.43}$$

where, σ_f is the fibre tensile strength at a gauge length equal to the mean fragment length and K is a coefficient, which depends on the variation of the fragment length. If the fragment length varies between $l_c/2$ and l_c, $K = 0.75$ can be taken as a mean value.

EXPERIMENTAL WORK

This chapter describes the experimental procedures followed in the present investigation to carry out wettability studies, solidification processing, microstructural characterization and properties determination of the different composites investigated.

3.1 WETTABILITY STUDIES

3.1.1 Synthesis of the Alloys

Master alloys of Al-15wt.%Zr and Al-2.3wt.%Li have been received from BARC, Bombay and DMRL, Hyderabad respectively. These alloys are diluted by adding pure aluminium to get three Al-Li alloys and three Al-Zr alloys each having different concentration of primary alloying elements in following steps: Small pieces of master alloy and of pure aluminium are taken in proportion of weights to get the required concentration of alloying element and are sealed in a silica quartz tube of 15 mm dia at a vacuum of 10^{-4} mm of Hg. The quartz tube is heated in a furnace to a temperature above the liquidus of the master alloy and kept for some time at this temperature for homogenization. The silica quartz tube is taken out of the furnace and air cooled to the room temperature. Al-Cu alloy has also been prepared following the same procedure by melting pure Al and pure Cu. Table 3.1 lists the various aluminium alloys investigated for wettability with vitreous carbon in the present study.

Table-3.1

Aluminium alloys investigated for wettability in the present study

S.No.	Alloy	S.No.	Alloy
1.	Al-4.5 wt. % Cu	5.	Al-2.1 wt. % Zr
2.	Al-1.1 wt. % Li	6.	Al-3.4 wt. % Zr
3.	Al-1.6 wt. % Li	7.	Al-5.2 wt. % Zr
4.	Al-2.3 wt. % Li		

3.1.2 Experimental Apparatus and Procedure

Sessile drop experiments are carried out in the setup shown in Fig.3.1. The schematic diagram of sessile drop apparatus, shown in Fig. 3.2, consists of a high frequency induction coil rated at 10 kW and 400 kHz, surrounded by molybdenum radiation shields. It is located in a stainless-steel chamber having two windows, enabling the sessile drop on the substrate to be illuminated and photographed. The stainless-steel chamber is connected to argon gas (oxygen free grade) supply. All the experiments are carried out under argon atmosphere at a gas flow rate of 1.0 litre/min. The temperature is measured by a Pt-Rh thermocouple, attached just below the carbon substrate and is kept constant by controlling the current to induction coil.

The experimental procedure involves placing a piece of aluminium alloy on the carbon substrate just below the induction coil and heating rapidly to the desired temperature so as to provide minimum time for diffusion to occur at the interface. The drop is kept for 10 minutes at a constant temperature after complete melting of the alloy piece. The drop is observed through the window and the optical axis of the camera is made to coincide with the upper surface edge of the carbon substrate. The photograph of the drop is taken on 35 mm film that is enlarged to measure the contact angle.

The geometrical process to obtain the contact angle from the photographed silhouette of a drop is shown in Fig. 3.3. The angle θ between line BC and the tangent line at B of the silhouette is taken as the contact angle. By drawing a circle through B and C with centre O and the line AB perpendicular to the line OB, the angle θ is measured using a protractor. Takahashi et al. (48) have successfully used this process with an accuracy of $\pm 2^{\circ}$.

In order to determine the surface tension 'γ_{lv}' from the photographic enlargements, it is necessary to determine the shape factor 'β' of the drop and the radius of curvature at the origin 'b' as shown in Fig. 2.2. The parameters β and b are related to γ_{lv} according to Eqn. (2.5) and are calculated using the method discussed

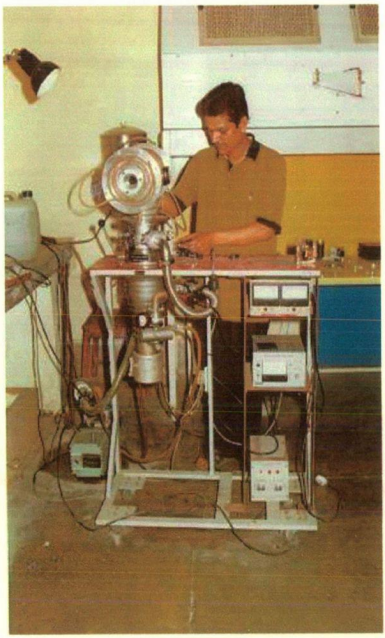

Fig. 3.1 Sessile drop setup used in the present study.

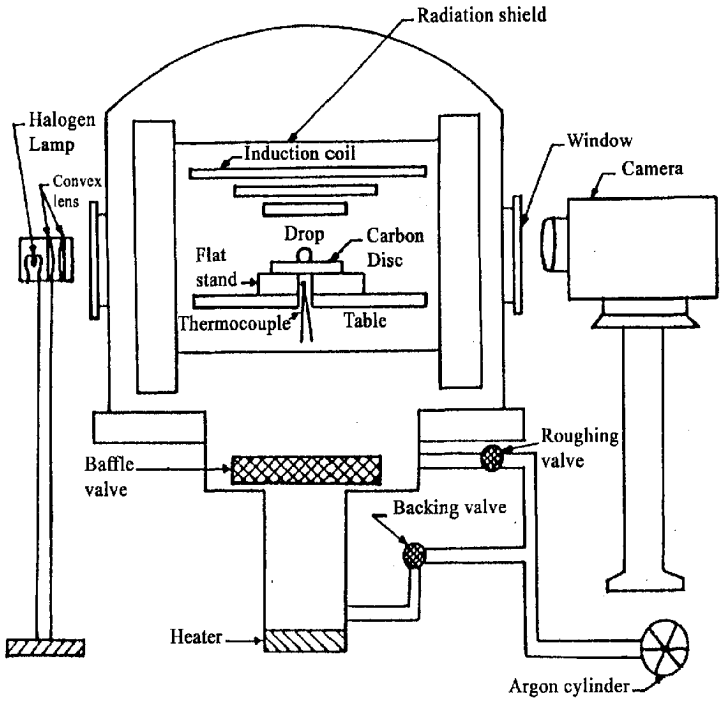

Fig. 3.2 Schematic drawing of the sessile drop setup.

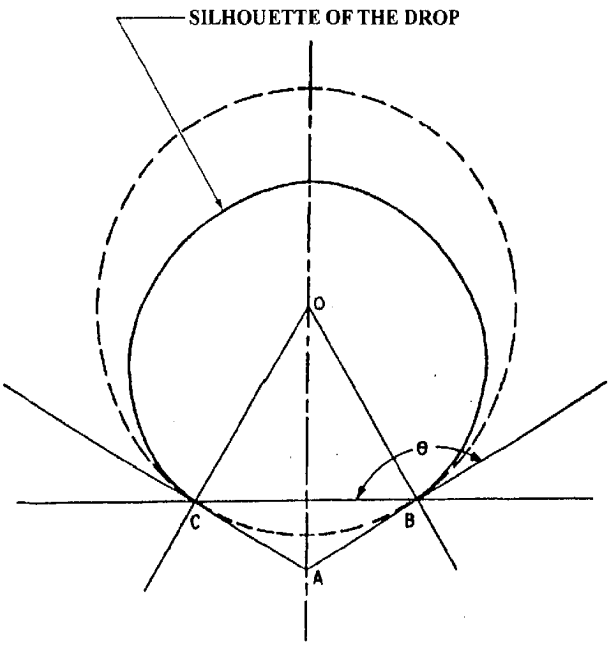

Fig. 3.3 Geometrical process to obtain the contact angle from drop profile.

in section 2.2 of chapter 2. The density of various alloys used for calculating the surface tension at various temperatures, are those given by Lucas (212) for pure aluminium as,

$$\rho = 2.369 - 3.11 X 10^{-4} (T - T_m) \ gm/cm^3 \qquad (3.1)$$

where, ρ is the density, T is the test temperature and T_m is the melting point of the aluminium alloys. Although, the density of the alloys is different but the difference at high temperatures is negligible and hence, density of aluminum can be used for that of alloys.

After the experiments, interfacial reactivity is characterized for the specimens, sectioned and detached from the substrates after cooling, by scanning electron microscopy (SEM), electron probe micro-analysis (EPMA) and X-ray diffraction analysis (XRD).

3.2 SOLIDIFICATION PROCESSING OF COMPOSITES

3.2.1 Matrix Selection

In spite of being expensive, continuous fibre reinforced MMCs are widely used in aerospace and military industries as 'weight saving' is of great importance and material price is less as compared to development cost. Weight saving, which can be achieved, depends mainly upon the matrix material of the composite. So, low density metals like Al, Mg and Ti are preferred over other metals to reinforce continuous fibres. Due to problems of oxidation/burning associated with the melting of magnesium/magnesium alloys and problems associated with the high melting point of titanium/titanium alloys, they are not used as matrices for reinforcing the continuous fibres by liquid phase fabrication methods. Further, magnesium and its alloys do not wet most of the fibre reinforcements available today.

Aluminium, having a low density (2.7 gm/cm^3) and ease of fabrication due to low melting point (660^{0}C), is the cheapest metal matrix to reinforce the continuous

fibres by liquid phase fabrication methods. It has a unique combination of good corrosion resistance, low electrical resistance and excellent mechanical properties. Since aluminium also does not wet most of the fibre reinforcements, aluminium alloys are used as the matrices for good bonding and strength in the composite. Alloying addition of Li and Zr improve wettability and interfacial bonding of aluminium with most of the fibre reinforcements, by disrupting the oxide layer on molten aluminium and promoting the reaction between reinforcement and molten aluminium respectively. Addition of Cu to aluminium, besides improving its strength, also reduces the thermal expansion coefficient of metal matrix and thus, helps in minimizing the stresses, developed after solidification due to difference in thermal expansion coefficients of both the constituents. So, aluminium and its alloys exhibit high potential for their selection as metal matrices in the solidification processing of continuous fibre reinforced metal matrix composites. Table 3.2 shows the composition of different aluminium alloys selected as matrices for reinforcing the carbon fibres.in the present study.

Table-3.2

Chemical composition of the matrix alloys

S. No.	Matrix alloy	Li (wt.%)	Cu (wt.%)	Fe (wt.%)	Si (wt.%)	Mg (wt.%)	Zr (wt.%)	Al (wt.%)
1.	Al-Cu	-	4.49	.09	1.7	1.26	-	Balance
2.	Al-Li	2.34	2.15	-	-	1.59	0.14	Balance
3.	Al-Zr	-	2.76	0.72	-	-	5.32	Balance

3.2.2 Reinforcement Selection

The selection of continuous fibre reinforcement largely depends upon its density and mechanical properties and marginally on its cost and availability. Carbon fibre (T300) is the cheapest (except Al_2O_3 fibre) reinforcement having good mechanical properties and lowest density (~1.76 gm/cm^3) so as to fulfill the prime motive of weight saving which, to a large extent, depends upon the density of the reinforcement.

The solubility of carbon in molten aluminium is 0.10 wt. % - 0.14wt. % in the temperature range of 800^0C - 1000^0C and 0.015wt.% in solid aluminium, which is beneficial in preventing the degradation of carbon fibres due to dissolution. Though, aluminium does not wet carbon in this temperature range but reacts with a high degree to form aluminium carbide at the interface in this temperature range. The alloying additions of Li and Zr to aluminium improve its wettability with carbon. The degradation of carbon fibres due to the reaction at the interface can be controlled in solidification processing of Al/CF composites by squeeze casting in the temperature range of 700^0C to 850^0C.

The choice of carbon fibre as the reinforcement in aluminium and its alloys is made in the context of the reaction at the interface so as to produce necessary bonding required for good mechanical properties. Table 3.3 shows the characteristics of the carbon fibres used in the present study.

Table-3.3

Characteristics of the carbon fibres used in the present study

Make	Trade name	Fibre type	Filament count	Mean diameter	Tensile strength	Tensile modulus	Fracture strain
Toray Japan	Torayla (PAN)	HS T300	12000	7.0 μm	3.5 GPa	230 GPa	1.7%

3.2.3 Design of Die and Plunger

The die and plunger used in this study to forge the molten metal into the fibre preform are made up of hot die steel material having a composition as 0.4% carbon, 1.0% silicon, 0.4% manganese, 5.0% chromium 1.5% molybdenum and 1.0% vanadium.

The die mainly consists of a mould made up of hot die steel material and having the dimensions as shown in Fig. 3.4. It is fabricated by drilling a hole of 75 mm in a block of hot die steel having dimensions 220 x 180 x 200 mm^3. After

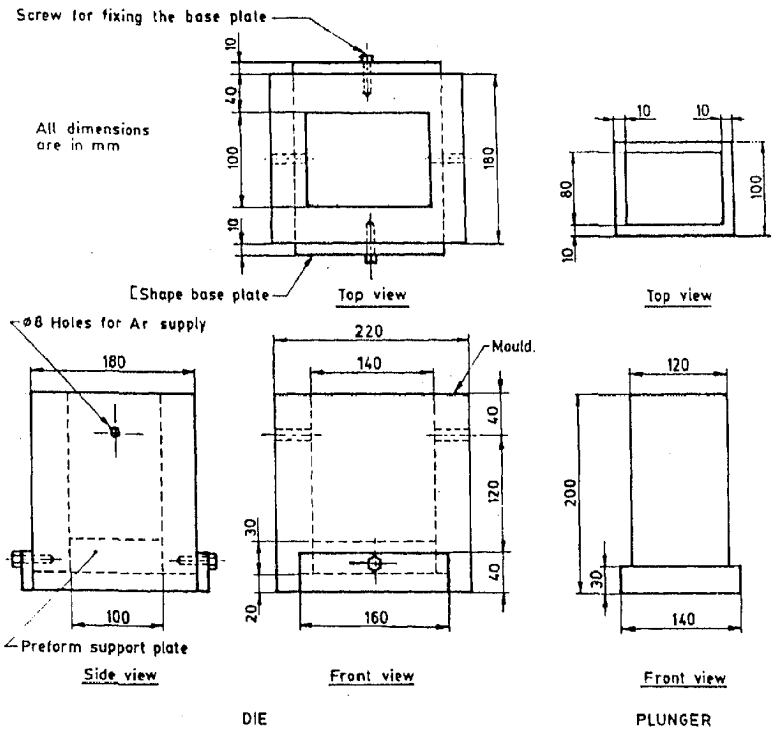

Fig. 3.4 Detailed drawing of the die and plunger used for squeeze casting in the present study

drilling, the hole is machined under a vertical slotter to produce inner dimensions as 136 x 96 mm^2, i.e., 2.0 mm off the required dimensions. After rough machining, it is stress relieved as removal of large amounts of material induces stresses, which may cause distortion or warpage during heat treatment. Stress relieving is carried out by heating the die between 600^0C - 700^0C for two hours followed by air-cooling to the room temperature. The tolerance of 2.0 mm over finished size is provided to accommodate any distortion resulting from the release of stresses. Final machining of the die is carried out on a horizontal shaper machine to produce the final dimensions of inner cavity as 140 x 100 mm^2.

For hardening treatment, the die is preheated in stages in a furnace to a temperature of approx. 850^0C, just below the austenitic transformation region. The dilatometric curve in Fig.3.5 shows the volume changes, which occur during the full heat-treatment cycle of die steel. Following a controlled preheating cycle, the die is heated to 1000^0C into the austenitic region to take carbon and other alloying additions into the solid solution. It is then quenched in water to cool down up to 50^0C. Tempering treatment is given by heating the die from 50^0C to 600^0C and keeping it for half an hour at this temperature. Finally, the die is air cooled to the room temperature to acquire a hardness of 500 BHN.

After the hardening treatment, the inner sides of the die cavity are polished with silicon carbide rods of triangular cross section to produce smooth surfaces. Plunger is fabricated from a block of same material having dimensions 150 x 110 x 200 mm^3, by removing the excess material on a shaper machine to get the final dimensions as shown in Fig. 3.4. It is also given the same hardening treatment that is given to the mould.

The last component of the die is mild steel base plate, which is fixed with the mould by two screws, one on each side of the mould, as shown in Fig.3.4. The purpose of this plate is to keep the supporting plate inside the mould during lifting of the die up to the platform of the hydraulic press and obviously to close the bottom of the die.

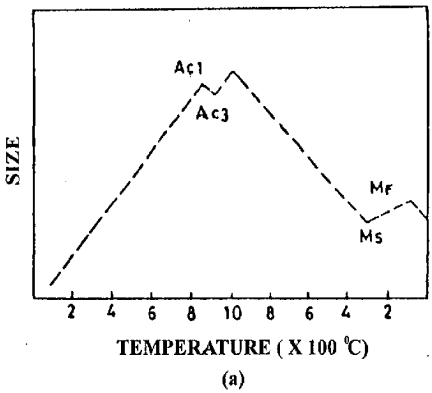

(a)

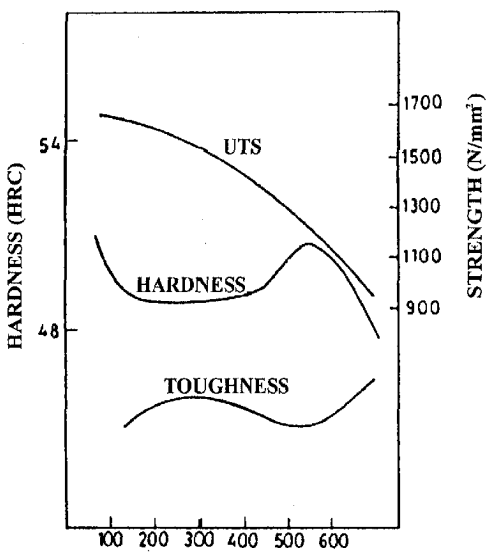

(b)

Fig. 3.5 Hardening and Tempering treatment of the die and plunger (a) schematic diagram showing size changes during hardening (b) variation of mechanical properties with tempering temperature.

3.2.4 Preform Preparation

Carbon fibres without coating and without any binder have been used in preform fabrication. Figure 3.6 (a) shows various steps involved in preform fabrication. Carbon fibre tows containing 12,000 individual fibres are passed through a bath of ethyl alcohol. The fibres are cut to 65.0 mm length and are longitudinally inserted into a rectangular steel pipe, open at both ends and having an inner cross-section of 70 x 10 mm^2 as shown in Fig. 3.6 (b). The rectangular steel pipe has a cut of 5.0 mm width on its upper side so as to insert the fibre tows easily.

3.2.5 Solidification Processing

In the present study, continuous carbon fibre reinforced aluminium metal matrix composites are processed by solidification synthesis. Three different aluminium alloys are used as metal matrices and each of these is reinforced with three different volume fraction of carbon fibre reinforcement. Table 3.4 shows the different composite systems with processing routes for their synthesis.

Table-3.4

Composite systems and their processing routes

S.No.	Composite system	Processing route
1.	Al-Cu/CF composite	Squeeze casting
2.	Al-Li/CF composite	Squeeze casting
3.	Al-Zr/CF composite	Squeeze casting

3.2.6 Experimental Setup and Procedure

Squeeze casting is carried out using the set up shown in Fig.3.7. It mainly consists of two resistance wound vertical muffle furnaces (one for melting the aluminium alloy and other for preheating the die and fibre preform), die containing the fibre preform, a hydraulic press for applying the desired pressure and an argon cylinder. The schematic diagram of the squeeze casting process is shown in Fig. 3.8.

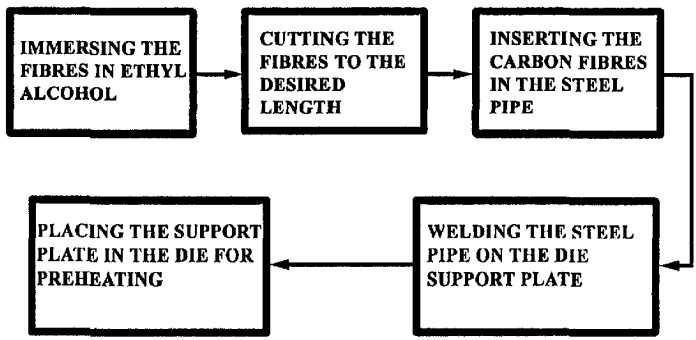

(a)

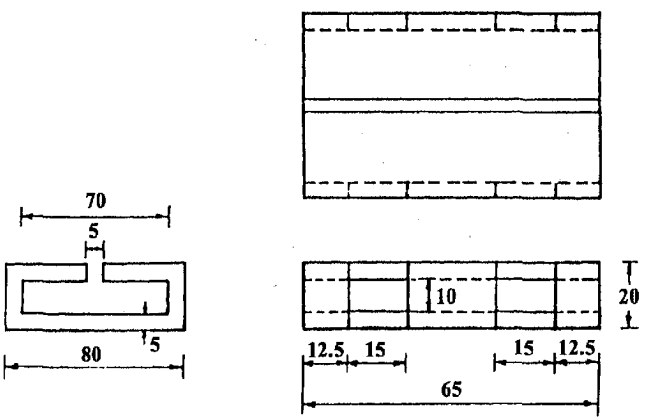

(b)

Fig. 3.6 Preform preparation (a) various steps involved in preform preparation (b) details of rectangular steel pipe used for making fibre preform

Fig. 3.7 Squeeze casting setup used in the present study.

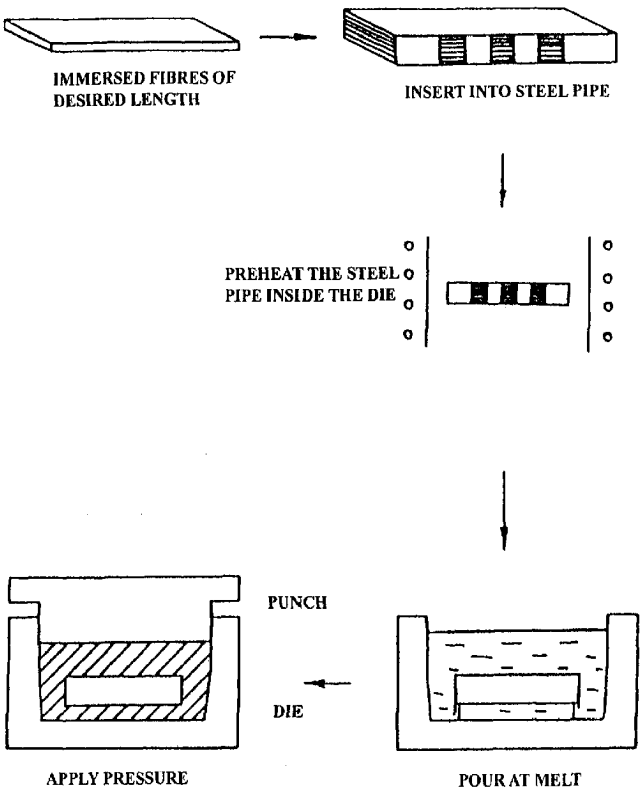

Fig. 3.8 Schematic diagram of composite fabrication by squeeze casting.

A thoroughly cleaned graphite crucible is placed inside the melting furnace and a Pt-Rh thermocouple, attached to a digital temperature controller is placed in the centre of the crucible at a sufficient depth. Another Pt-Rh thermocouple, coupled with a second temperature controller is placed in the centre of the preheating furnace at an appropriate depth and both the furnaces are switched on. The temperature of the melting furnace is set at 800^0C, 750^0C, and 850^0C for Al-Cu, Al-Li, and Al-Zr alloys respectively while that of preheating furnace is set at 650^0C in all the castings. These temperatures have been selected by hit and trial method, based on the complete infiltration and minimum degradation of the fibres.

The inner cavity of the die and sides of the plunger are sprayed with graphite powder dispersed in water and both are left for air-drying. It is necessary because graphite is a good solid lubricant and it provides sufficient lubrication between the contacting surfaces of the die cavity and plunger. The rectangular steel pipe containing fibres is welded to preform support plate to restrict its horizontal movement. This whole assembly is inserted in the die cavity from the bottom. The base plate is then fixed up with the die, to close the die cavity, by tightening the screws. Two cylindrical steel pipes of 8.0 mm diameter are inserted into the holes provided at the upper side of the die. These pipes are connected to the argon supply.

As the desired temperature is reached in the melting furnaces, about 1.0 kg of the aluminium alloy in the form of small pieces is placed inside the graphite crucible. The top of the furnace is covered by an asbestos sheet. As the required temperature is reached in the preheating furnace, the die is placed inside the muffle. Argon gas supply is started at a constant flow rate of 1.0 lit/min. The open end of the die cavity is covered by a steel plate, specially fabricated for this purpose. Preheating is carried out for half an hour at this temperature to remove the sizing resin.

The graphite crucible is taken out with the help of a tong after confirming the complete melting of the alloy. At the same time, argon gas supply is closed and the die cavity cover is removed. After skimming the melt with the help of a heated mild steel rod having spoon end, the molten metal is poured in the die cavity. Precaution is taken to keep the surface level of the molten metal in the die cavity at least 20mm below the

holes provided for argon gas supply. The temperature range of 725^0C to 775^0C and 800^0C to 850^0C is used as the pouring temperature of the molten metal in case of Al-Cu/CF and Al-Zr/CF composites respectively. In case of Al-Li/CF composite casting, the alloy is melted inside the die itself at a temperature of 675^0C to 725^0C under argon atmosphere. A mixture of LiCl and LiF is added time to time during melting of the alloy to provide a cover on the surface of the molten alloy for reducing the loss of lithium due to oxidation.

The plunger is inserted into the die cavity up to a sufficient depth and the whole unit is centrally placed on the platform plates of the hydraulic press, just below the ram. The press is then switched on and a pressure of 75 MPa is applied for about 60 secs, by lowering the ram. The ram speed is recorded as 5 mm/sec.

3.2.7 Determination of Chemical Composition of Matrix Alloys

The chemical composition of the matrix alloys in the composites is determined by inductively coupled plasma (ICP). The solutions of matrix alloys are prepared by dissolving 1.0 gm of the powder, obtained by filing the unreinforced alloys, in HCl and HNO_3. Distilled water is added to make 1.0 litre solution of each alloy. The standard solution of copper is prepared by dissolving 1.0 gm of electrolytic copper while those of Li and Zr are prepared by dissolving 1.0 gm powder of their respective master alloys. The wt. % of Cu is determined by dividing the reading of alloy solution to that of standard solution multiplied by 100. The wt. % of Li and Zr is calculated by dividing the readings of alloy solutions to that of their respective standard solutions and multiplied by the Li and Zr wt. % in their master alloys.

3.2.8 Optical Microscopy and Estimation of Fibre Volume Fraction

The cast composites are examined under optical microscope after preparing the specimens by standard procedure. The specimens are polished up to 4/0 grade emery paper. These specimens are cloth polished by using polishing grade alumina suspension. After polishing, the specimens are thoroughly cleaned with water. After drying, they are etched for 20 to 30 secs with Keller's reagent followed by washing

and drying again. Etched and polished specimens are examined under optical microscope (model MEF 3) for observing the distribution of fibres in aluminium alloy matrices. The specimens are viewed at different locations and micrographs are taken at different magnifications.

The fibre volume fraction in the composites is determined by quantitative metallography, i.e., by point counting technique. The magnification in the microscope is so adjusted that a maximum resolution could be obtained and at the same time, the condition of not more than one grid point falling on one dark spot is satisfied because fibres present in the composites are observed as dark spots under optical microscope. For each sample, 10 such observations are made at random locations. The fibre volume fraction of dark spots is calculated by dividing the average value of the number of grid points in dark spots to the total number of grid points. In order to cross check, the number of dark spots is counted in an area of 72 x 48 mm^2 at a magnification of 1000 X. The fibre volume fraction is then calculated by dividing the area occupied by dark spots to the total area.

3.3 CHARACTERIZATION OF COMPOSITES

3.3.1 Scanning Electron Microscopy

All the continuous fibre reinforced metal matrix composites in as cast condition are examined under scanning electron microscope (model LEO 435VP) to observe the distribution of carbon fibres in different aluminium matrices. The etched specimens of these composites, which were used for optical microscopy earlier, are also used for SEM study. These specimens are mounted on specimen holders with the help of adhesive. A silver paint coating is applied on the side surface of the specimens from top to bottom, in order to provide better electrical conduction. The distribution patterns of the composites are viewed on the screen and micrographs are taken at different locations and at different magnifications.

3.3.2 Energy Dispersive Spectroscopy (EDS) and Electron Probe MicroAnalysis (EPMA)

After scanning electron microscopy, same specimens are examined for energy dispersive spectroscopy and electron probe micro analysis (model JXA 8600M), to observe the distribution of alloying elements in various composites. The composite specimens are mounted on specimen holders by using adhesive and carbon coating is applied on the specimen surface for better conduction, before introducing the specimens in the electron beam chamber. An acceleration voltage of 20 kV is employed for these studies.

EDS and EPMA micrographs are taken, for Al-Cu/CF and Al-Li/CF composites, to observe the distribution of alloying elements in the alloy matrix of the composites. EDS point analysis and line analysis of selected regions are carried out for Al-Cu/CF composite having 66% fibre volume fraction. EPMA Line analysis across the interfibre region is carried out for Al-Zr/CF composite to observe the distribution of alloying elements in the composite and to find out the presence of the elements at the interface.

3.3.3 Transmission Electron Microscopy

TEM studies are also carried out to characterize the microstructure of the cast composites by analysing the interface regions as macroscopic behaviour often depends upon the structure at the interface. TEM study of Al-Cu/CF composite is carried out.

(a) **Specimen preparation:** A thin sheet of approx. 10 x 15 x 0.1 mm^3 size is cut from Al-Cu/CF composite plate using a diamond cutter (model Isomet 1000). The thin foil is subjected to ion thinning for electron transparency. Ion beam thinning enables electron transparent foils of the composite materials to be prepared reproducibly. A beam of 5 kV ions is directed to the specimen, which causes ejection of atoms or molecules from the specimen at the point of ion impingement. In order to get high thinning rate, argon gas is used as the bombarding specie as it is the heaviest inert atom.

The specimen is mounted on a special holder and is rotated in such a way that two beams impinge on opposite sides of the specimen at a low angle of approx. 30° initially and approx. at 15° in the later stage of thinning. The rate of thinning is calculated to be 0.10 μm/h as it takes 12 h to get an electron transparent thickness of about 10 μm. A short period of about half an hour of ion beam thinning is used to clean oxide from the surface of the specimen.

(b) **Structural measurements:** TEM study of the Al-Cu/CF composite having 66% fibre volume fraction is carried out on transmission electron microscope (model Philips EM 400T/ST), to identify the phases present at the interface. The specimens are mounted on the specimen holders and are placed inside the electron beam chamber. Different regions are viewed on the screen and TEM micrographs are taken alongwith the selected area diffraction patterns (SAD) using different camera constants.

(B) **Indexing of diffraction patterns:** Two types of SAD patterns, i.e., spot patterns and ring patterns are obtained for Al-Cu/CF composite specimens when examined by selected area electron diffraction.

(i) ***Camera constant method:*** If the camera constant '$L\lambda$' is known accurately after calibrating with the gold/silver specimen, d values are calculated by measuring R_1, R_2 and R_3 values and by substituting for R in $Rd=L\lambda$, where, λ is the wavelength of the electron beam and L is the distance between the specimen and the screen. The d values are checked with the likely ASTM data cards and the angles between the reflecting planes are checked for equality, to provide a cross check. The beam direction B, i.e., approximately zonal axis (u v w) of the planes (h_1 k_1 l_1) and (h_2 k_2 l_2) is given as $u = k_1 l_2 - k_2 l_1$, $v = l_1 h_2 - l_2 h_1$ and $w = h_1 k_2 - k_1 h_2$.

(ii) ***Indexing spot patterns:*** The distances R_1, R_2, R_3 are the distances of the diffracted spots of the transmitted beam, measured from the centre spot (000) as shown in Fig.5.11 (b) of Chapter-5. The parameter R is the characteristic of

interplanar spacing 'd_{hkl}' of the reflecting plane and the magnification due to the lens settings, i.e., camera constant. The d values are calculated by substituting R_1, R_2 and R_3 for R in $Rd=L\lambda$.

From Fig.5.11, R_1, R_2 and R_3 are measured as 3.46 mm, 8.61 mm and 9.67 mm respectively. The $d_1.d_2$ and d_3 values are calculated as 2.338, 0.929 and 0.827 Å respectively. These values correspond to the d values of Al-FCC. The reflecting planes corresponding to these d values are $(2\bar{2}4)$, (111) and $(\bar{1}3\bar{3})$. The angles between R_2 and R_1 and between R_2 and R_3 are 53° and 81° respectively. The calculated ϕ_1 and ϕ_2 values as 53° and 81° further confirm the indexing. The beam direction is found to be $[3\bar{1}\bar{2}]$.

(iii) ***Indexing ring patterns:*** The radius of each ring, as shown in Fig.5.12 (b) of Chapter-5, is characteristic of the spacing of the reflecting planes in the crystal and setting of microscope lenses. This is calibrated using silver specimen in the present study.

The diameter of rings R_1, R_2 and R_3 are measured. These distances are converted into interplanar spacings using the camera constant as $d_n=\frac{L\lambda}{R}$. From the ASTM data cards, starting with the most likely phase present on the basis of the known constituents of the composite, the phases present in the interface near the fibre and near the alloy matrix are identified.

The R_1, R_2, and R_3 are measured in Fig.5.12 (b) as 3.65 mm, 6.84 mm and 9.36 mm respectively. The corresponding d values obtained are 2.19, 1.17 and 0.686 Å. From the ASTM data card, it is observed that these d values correspond to the planes (100), $(20\bar{3})$ and $(\bar{1}03)$ for amorphous carbon.

3.3.4 X-ray Diffraction Analysis of Cast Composites

The X-ray diffraction analysis of cast composites has been conducted to identify the various phases and reaction products (due to chemical interaction between carbon fibres and matrix during squeeze casting) present in the composites.

The powder samples of the cast composites are taken by filing the composite surfaces with hard jeweller's file. The specimens for X-ray diffraction analysis are prepared by placing these powder samples on a glass plate for making the slides. The X-ray diffraction study is carried out for the specimens under an automatically scanned Phillips X-ray diffractometer (model PW1140/90) in the angle range between 5° - 120° using a copper target and nickel filter with a current of 20 mA at 35 kV.

The intensity of diffracted beam against 2θ is plotted on a graphical chart at a chart speed of 1 cm/min and at the goniometer speed of 1°/cm. For all the intensity peaks and their corresponding values of 2θ, the inter planner spacing d is calculated using Bragg's law,

$$\lambda = 2d\sin\theta \tag{3.2}$$

where , λ is the wave length of CuK_{α} radiation used for diffraction and is taken as 1.5405 $\mathring{A}$, in the present work. From the calculated d values, the different phases present in the composites are identified with the help of ASTM X-ray diffraction data card.

3.4 PROPERTIES OF CAST COMPOSITES

3.4.1 Density of Cast Composites

The density of the composites has been determined by weight loss method. Three specimens of each composite, which were used for microstructural analysis earlier, have also been used for the determination of the density of cast composites.

According to weight loss method, if w_1 is the weight of the specimen in air and w_2 is the weight in liquid, the density of the specimen is given as,

$$\rho_c = \frac{w_1 \times \rho_l}{w_1 - w_2} \tag{3.3}$$

where, ρ_l is the density of the liquid.

In the present study, pure methanol has been used for measuring the weight loss because it is inert to the interfacial carbides, formed due to chemical interaction between carbon fibres and aluminium matrix during squeeze casting of the composites. The density, ρ_l, of pure methanol is taken as 0.790 gm/cm^3 at 25^{0}C. A very thin stainless steel fibre having a diameter of approx. 0.080 mm is used to hang the composite specimen while dipping in absolute methanol.

Three specimens of each unreinforced alloy (one specimen is taken from each unreinforced alloy plate obtained during squeeze casting of composites having same matrix but different volume fraction of carbon fibres) are prepared with final dimensions as 15 x 7.5 x 7.5 mm^3, by polishing all the surfaces of the specimens up to 4/0 grade emery paper. The density of each specimen is determined by using the same procedure as for composite specimens. The density of each composite and each unreinforced alloy is determined by taking the average of three density values.

Density of the composites have also been calculated by 'Law of Mixtures' as,

$$\rho_c = \rho_f V_f + (1-V_f)\rho_m \tag{3.4}$$

Where, ρ_c, ρ_f and ρ_m are the density of composite, fibre and matrix respectively and V_f is the fibre volume fraction in the composite. The fiber density ρ_f is taken as 1.76 gm/cm^3 whereas the experimentally determined density of unreinforced alloys (by weight loss method) is used for matrix density ρ_m.

3.4.2 Mechanical Properties of Cast Composites and Unreinforced Alloys

(a) **Hardness:** In metal matrix composites, bulk hardness is generally preferred over micro hardness because bulk hardness measurement utilizes large size indentor so as to take the contribution of all the constituents proportionally at a particular location. In micro-hardness measurements due to small size of the indentor, the values obtained show large scattering depending upon the location of the indentation.

The Brinell test is a simple indentation test for determining the hardness of a wide variety of materials and is particularly preferred for composites. The same three specimens of each composite, which were used for density determination earlier, are also used for Brinell hardness testing. Both the faces (perpendicular to the fibre axis) of each specimen have been used for the measurement of hardness. So in total six hardness values (one on each face) are obtained for each composite and for each unreinforced alloy. The reported Brinell hardness value is calculated by taking the average of six hardness values.

The Brinell hardness measurements have been carried out on a Brinell cum Vickers hardness tester (WPM) made in the German Democratic Republic. The test consists of applying a load of 62.5 kg for a specified time of 30 secs using a 2.5 mm diameter hardened steel ball indentor on thoroughly cleaned and polished surface of the specimen. Time for the application of load is selected so as to ensure that the plastic flow of the metal matrix composite in the indentation area is ceased. The load is removed slowly to allow elastic recovery. The diameter of the circular impression is measured in millimeters nearest to 0.01 mm by using a low power microscope attached with the testing machine. To eliminate any error in the measurements due to deviation from sphericity, measurements are taken along two mutually perpendicular diameters. The average value of these diameters is used as the diameter of the indentation. The Brinell hardness is calculated as,

$$HB = \frac{4P}{\pi D_i \sqrt{D^2 - D_i^2}} kg/mm^2 \qquad (3.4)$$

where, P is the applied load and D and D_i are the diameters of the indentor and indentation respectively.

(b) **Tensile properties:** The round specimens for unreinforced alloys are prepared after cutting the rectangular bars of dimensions 10 x 10 x 50 mm^3 from unreinforced alloy plates. These bars are machined on the lathe machine to remove excess material for getting the final dimensions to confirm ASTM specifications as shown in Fig. 3.9 (a).

Dog bone shaped specimens have been used for tensile testing of composites. Composite strips having dimensions 65 x 20 x 4 mm^3 are taken by cutting the composite plates on a diamond cutter (model Isomet 1000). These strips are machined on a milling machine in the dog bone shape, approx. 1mm off the final dimensions. These strips are polished on emery papers up to 4/0 grade for getting the final dimensions of the polished specimen to confirm ASTM specifications as shown in Fig.3.9 (b).

Three specimens of each composite have been prepared from a composite plate whereas three specimens of each unreinforced alloy have been prepared from three different unreinforced alloy plates, obtained during squeeze casting of three composites having same aluminium alloy matrix but different volume fractions of carbon fibres.

The tensile tests have been carried out at ambient temperature for as cast composites and for as cast unreinforced alloys. These tensile tests are performed on a pneumatically operated Hounsfield Tensile Testing Machine equipped with a computer for printing out the load vs. extension curves. All the tests are carried out on a load scale of 0-10,000 N and at a speed of 1mm/min, i.e., 16.6 μm/sec. The gauge thickness, gauge diameter and gauge

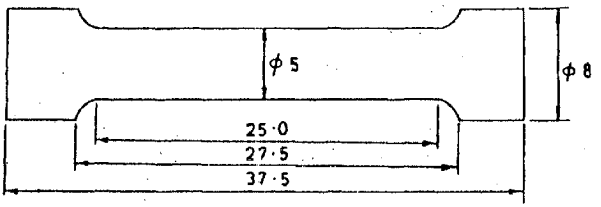

(a)

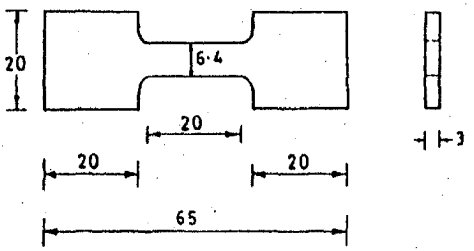

ALL DIMENSIONS ARE IN mm.

(b)

Fig. 3.9 Dimensions of the tensile specimens (a) unreinforced alloy (b) composite.

length of dog bone shaped and round specimens are measured with the help of a Vernier Callipers before and after the test.

The ultimate tensile strength (UTS) of the composite specimens is evaluated by dividing the maximum force to the initial cross sectional area of the specimens in units of MN/m^2 or MPa. The engineering fracture strain is calculated by dividing the extension at the fracture to the initial gauge length. As there are three specimens of each composite and unreinforced alloy, three values of UTS and three values of engineering fracture strain are obtained. The values of UTS and fracture strain reported here are obtained by taking the average of these three values evaluated for three specimens of each composite and unreinforced alloy.

The law of mixtures predictions for ultimate tensile strength of composites 'σ_c' are made as,

$$\sigma_c = V_f \sigma_f + (1-V_f)\ \sigma_m \tag{3.5}$$

where, σ and V stands for strength and volume fraction respectively and subscripts c, f and m correspond to composite, fibre and matrix respectively. The values of σ_m used for these predictions are those evaluated experimentally for unreinforced alloys whereas the value of σ_f is taken as 3.5 GPa.

3.4.3 Single Fibre Tensile Test

Single fibre tensile tests have been carried out for preheated and extracted (from composites) fibres. The extraction of carbon fibres from Al/CF composites is accomplished with dipping the composite pieces in a 10wt.% NaOH aqueous solution, in order to dissolve the matrix alloy, followed by a gentle removal of the separated fibres. The preheated fibres are already separated. Adhesive tape is used to remove a single fibre from the fibre tows.

Single fibre is stretched slightly and is stuck to a sheet of paper by using epoxy adhesive as shown in Fig.3.10. The paper sheet is then clamped in the grips of a Instron make mini universal testing machine (model 4411) having a load cell of 5.0 mg. The paper support is cut at the middle after clamping in the grips. Total 50 fibres of gauge length of 25 mm are tested for each composite at a crosshead speed of 8.3 μm/sec to obtain Weibull distribution of fibre strength. Single fibre diameter is not measured and the nominal value is used to calculate the fibre strength.

The most appropriately used estimator of F(σ) is $\frac{i-.375}{n+.25}$, where, i is the serial number of the fibre and n is the total number of fibres. The mechanics of the process is simple. On the special Weibull paper, σ_f is plotted on the logarithmic x-axis and F(σ), i.e., $\frac{i-.375}{n+.25}$ x 100 is plotted on the y-axis (often labelled as % failure).

The degree to which the plotted data fall on a straight line determines the conformance of the data to a Weibull distribution. If the data reasonably plot as a straight line, the Weibull distribution is a reasonable fit, and the shape parameter 'β' and the scale parameter 'α' can be obtained. If a line is drawn parallel to the plotted straight line from the center of a small circle ⊕ (in the TEAM paper called ORIGIN) until it crosses the SMALL BETA ESTIMATOR on the TEAM paper, the value of β is obtained. To find α, draw a line from the 63.2 (0.0 level at the right vertical line of the TEAM paper) until it intersects with the fitted straight line. From this intersection, draw a vertical line until it intersects with the x-axis, and read off the x-axis value at this intersection. This value represents the scale parameter α. The average fibre strength can be calculated from Eqn. (2.33).

3.4.4 Fractography and Interfacial Properties

In order to have an understanding about the mode of fracture and measuring the fibre pull out lengths, fractured surfaces of tensile specimens have been examined under a scanning electron microscope (model LEO 435 VP). Small samples from the fractured side of the broken tensile specimens are cut out of their lengths without any

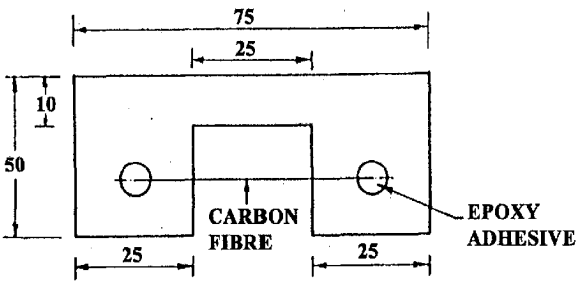

ALL DIMENSIONS ARE IN mm

Fig. 3.10 Drawing showing the dimensions of tensile test specimen for single fibre.

damage to the fractured surface. These samples are then fixed by quickfix carefully on the specimen holder of the SEM. In order to improve the electric conduction, silver paint is applied on the side surface of the specimen. The SEM micrographs of the fracture surfaces of each composite are photographed at different magnifications.

The interfacial properties of cast composites are calculated by using Eqns. (2.40) and (2.43) as given in chapter 2. For calculating the interfacial properties, the fibre pullout length is measured experimentally and is taken equal to longitudinal displacement between two adjacent fibres and average fragment length respectively.

RESULTS AND DISCUSSION: WETTABILITY STUDIES

This chapter describes the results of wettability studies carried out for different aluminium alloys on vitreous carbon substrate. The results have been discussed to develop a coherent understanding of the phenomena involved for the observed improvement in the wettability. Finally, these results have been compared with the results of other workers to sort out the reasons responsible for the observed discrepancy.

4.1 RESULTS

The wettability characteristics of aluminium on a ceramic substrate are very much dependent on the presence of oxygen during experiments. It has been reported by several workers that the oxygen present in the atmosphere reacts with molten aluminium to form an oxide layer, which prevents the actual contact with the ceramic substrate, and hence, alter the wettability of the aluminium with that substrate. So, it is necessary to examine the deoxidation of molten aluminium before conducting the wettability studies. It has also been observed by several investigators, that deoxidation of aluminium is a kinetic issue which depends upon time and temperature.

In the present investigation, the deoxidation of aluminium is verified by conducting two separate sessile drop experiments on Al/Al_2O_3 system, as it is non-reactive at low temperatures i.e. < 900^0C and solubility of oxygen is very low in aluminium i.e. $<10^{-5}$ at.% at 927^0C (51). These test experiments are conducted in argon atmosphere at 850^0C, which lies in between the investigated temperature range for Al/C system in the present study. Figure 4.1 shows the contact angle kinetics obtained at 850^0C for Al/C system in two different experiments. It is observed from Fig. 4.1 that contact angle is initially very large, i.e., more than 160^0 and decreases rapidly to 110^0 in about 400 secs. Afterwards, it decreases slowly up to 100^0 in about 600 secs. So in both the experiments only small changes in contact angle are observed after 400 secs.

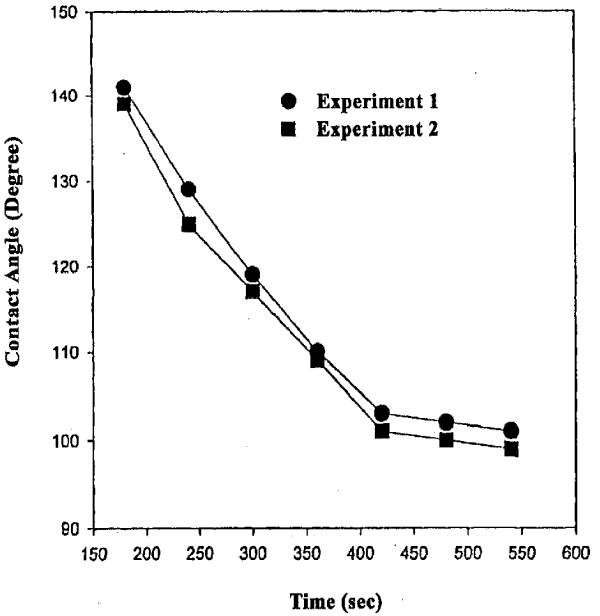

Fig. 4.1 The variation of contact angle with time for Al/Al_2O_3 system in two different experiments.

These two separate experiments confirm the deoxidation of aluminium after 400 secs as contact angle becomes steady after this time. The two separate experiments form the basis for reproducibility of contact angle within $\pm 5^{\circ}$ in the investigated temperature range selected for the wettability study of Al-X/C_v system. These experiments also explain the basis to select a contact angle reported time of about 10 mins after the melting of the aluminium alloy, in the present study.

4.1.1 Contact Angle and Work of Adhesion

The contact angle and work of adhesion for different Al alloys are given in Table-4.1 and Table A4 in Appendix A respectively.

Table-4.1

Contact angle of aluminium alloys on vitreous carbon at different temperatures

S. No.	Aluminium Alloy	Contact angle (Degree)					
		700^{0}C	775^{0}C	850^{0}C	925^{0}C	1000^{0}C	1075^{0}C
1.	Al-4.5 wt.% Cu	154	147	135	115	105	86
2.	Al-1.1 wt.% Li	147	136	120	93	82	78
3.	Al-1.6 wt.% Li	132	124	111	90	79	76
4.	Al-2.3 wt.% Li	118	112	100	81	75	72
5.	Al-2.1 wt.% Zr	160	143	128	109	94	84
6.	Al-3.4 wt.% Zr	161	145	125	103	82	69
7.	Al-5.2 wt.% Zr	163	149	121	99	72	55

(a) **Al-4.5wt%Cu alloy:** Figure 4.2 shows the variation of contact angle with temperature for Al-4.5wt.%Cu/C_v system. The same effect is depicted by change in sessile drop profile with temperature as shown in Fig. 4.3. This system features three regions in which the wetting differs significantly.

The first temperature region ranging from 700^{0}C to 850^{0}C shows very large contact angles of 155° to 135°. Above 850^{0}C, the contact angle reduces rather rapidly and approaches about 115° at 925^{0}C. Further, a very little change

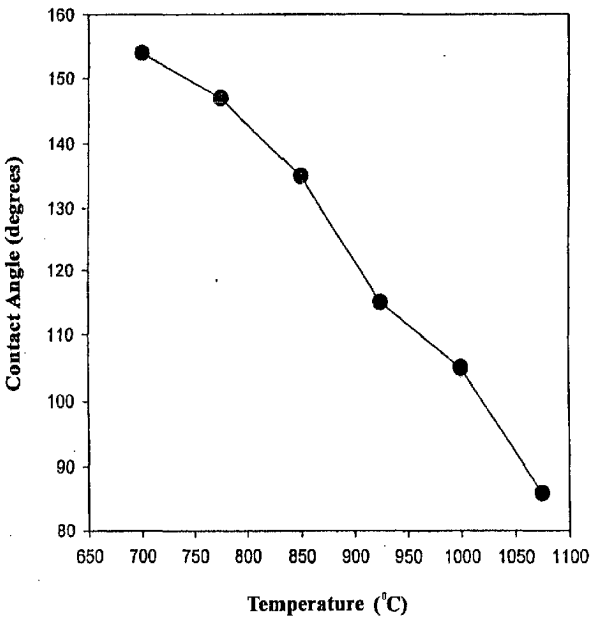

Fig. 4.2 The variation of contact angle with temperature for Al-4.5wt.%Cu alloy.

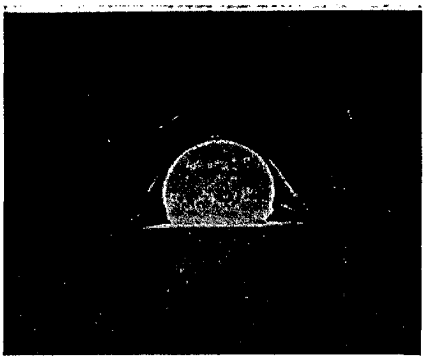

(a)

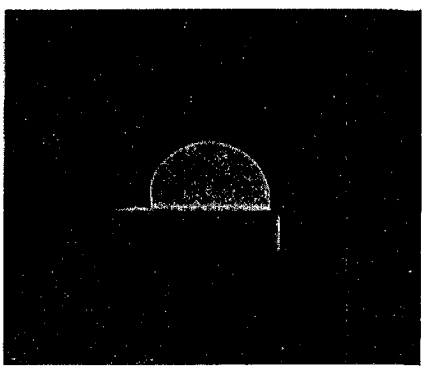

(b)

Fig. 4.3 The change in sessile drop profile with temperature for Al-4.5wt.%Cu/C. system (a) 775°C (b) 1075°C.

is observed for contact angle up to 1000^0C. Above 1000^0C, the alloy wets the carbon substrate as the contact angle attains a value ~ 86° at 1075^0C.

Figure 4.4 illustrates the variation of work of adhesion with temperature for Al-4.5 wt.%Cu/C_v system. It is observed from the figure that the work of adhesion, increases slowly in the temperature range of 775^0C to 925^0C and rapidly afterwards, to obtain a value by almost one order of magnitude higher at 1075^0C than the value at 775^0C.

(b) **Al-Li alloys:** Figure 4.5 illustrates the variation of contact angle with temperature for different Al-Li alloys on vitreous carbon substrate. The same effect is depicted through a series of photographs in Fig. 4.6, which shows the drop profiles at different temperatures for Al-2.3wt.% Li alloy. It is observed from Fig.4.5 that all the curves show a sharp decrease in the contact angle at low temperatures (700^0C to 850^0C) above which, the contact angle decreases rather slowly up to 925^0C. Although, the contact angle lies in the non-wetting range at low temperatures, there is a very significant decrease in the contact angle at low temperatures depending upon the concentration of Li in the alloys. This difference in the contact angle of different aluminium-lithium alloys at a particular temperature reduces as one proceeds from low temperatures to high temperatures. Finally, no significant reduction in the contact angle is observed for different Al-Li alloys at a high temperature of 1075^0C though, all the alloys wet carbon substrate at this temperature by attaining a contact angle in between 72° to 78°.

The variation of work of adhesion with alloying concentration of lithium at different temperatures has been shown in Fig. 4.7. It is observed from this figure that work of adhesion increases rapidly with lithium concentration at low temperatures whereas it increases slowly with lithium concentration at high temperatures.

(c) **Al-Zr alloys:** Figure 4.8 shows the variation of contact angle with temperature for different aluminium-zirconium alloys. The same effect is depicted through

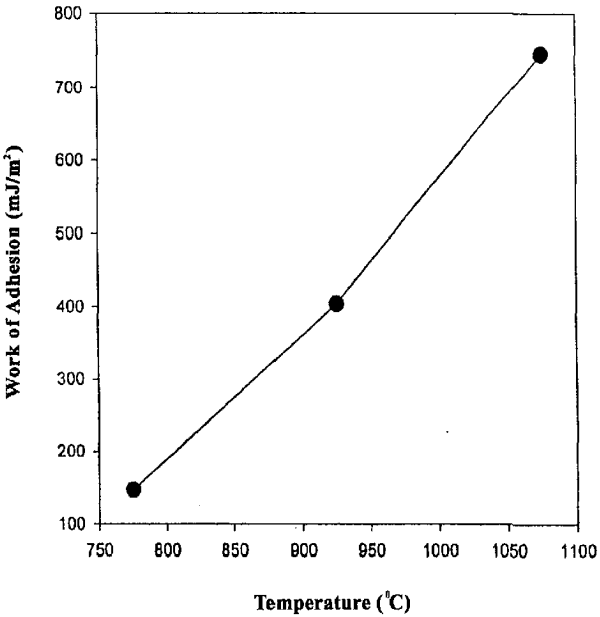

Fig. 4.4 The variation of contact angle with temperature for Al-4.5wt.%Cu/C_v system.

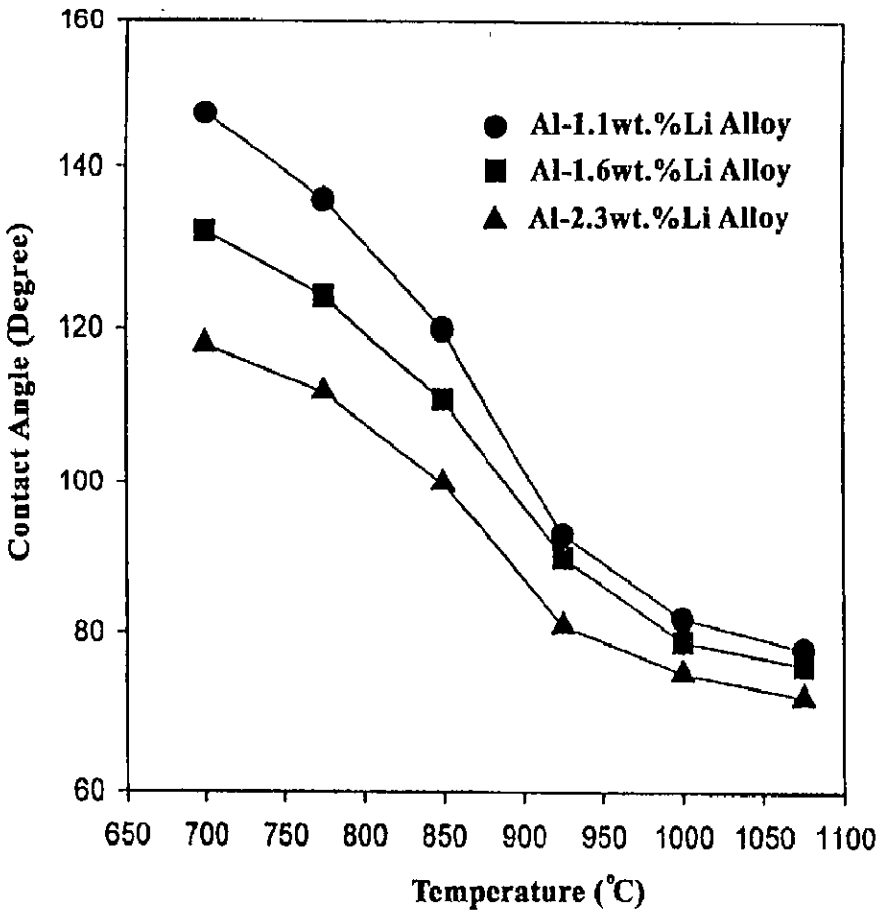

Fig. 4.5 The variation of contact angle with temperature for different alloys.

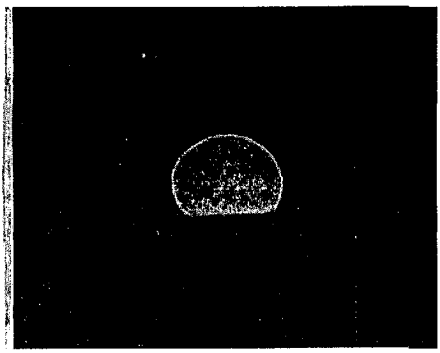

(a)

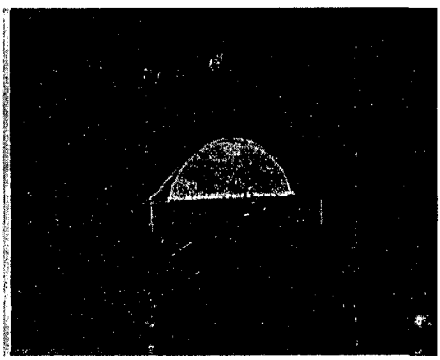

(b)

Fig. 4.6 The change in sessile drop profile with temperature for Al-2.3wt.%Li/C_v system (a) 775 C (b) 1075 C.

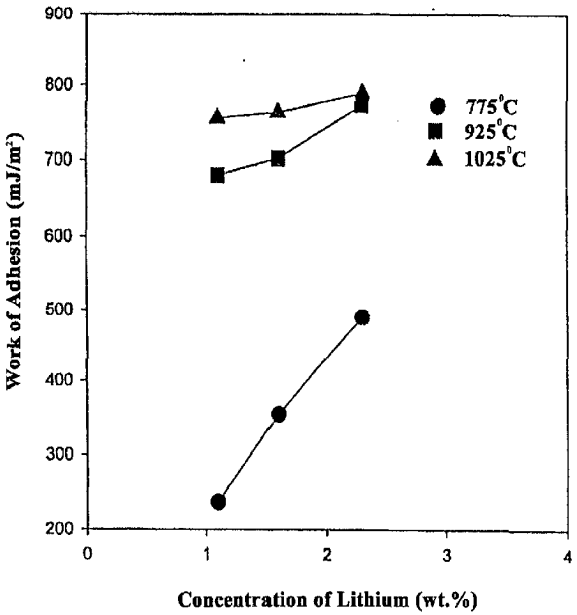

Fig. 4.7 The variation of work of adhesion with lithium content for different Al-Li alloys.

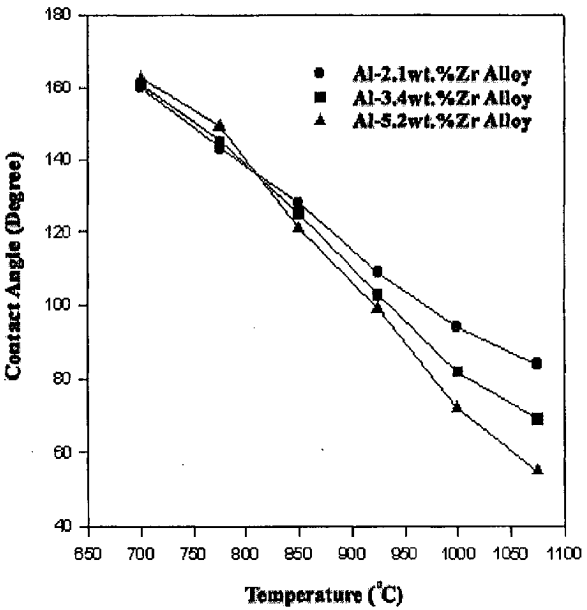

Fig. 4.8 The variation of contact angle with temperature for different Al-Zr alloys.

a series of photographs in Fig. 4.9, which shows the drop profiles at different temperatures. It is observed from Fig. 4.8 that all the curves, which correspond to different alloys, follow the same trend in lower temperature range of 700^{0}C to 850^{0}C and are associated with large contact angles of the order of 160° to 125°. Above 850^{0}C, a sharp decrease in contact angle is observed for all the alloys as the contact angles approaches to nonwetting to wetting transition range for all the alloys at about 1000^{0}C. All the alloys then wet the carbon substrate by showing a contact angle of less than 90° at about 1075^{0}C.

Figure 4.10 shows the variation of work of adhesion with the concentration of zirconium in the aluminium-zirconium alloy, measured at different temperatures. It has been observed that the work of adhesion remains nearly constant with increase in zirconium content at lower temperatures i.e. from 775^{0}C to 925^{0}C. Above 925^{0}C, the work of adhesion increases with zirconium content in the alloy to attain the highest value at 1075^{0}C, for Al-5.2wt.%Zr/C_v system.

4.1.2 SEM and EPMA Studies

SEM and EPMA studies have been conducted on the sessile drops of different aluminium alloys to investigate the various phases present at the interface. At low temperatures, it is observed that there is no reaction at the interface as sessile drops are easily detached from the substrate. However, at high temperatures, interfacial reaction might have taken place as it becomes very difficult to detach the drops from the substrate. The detachment is associated with a large fragment of carbon substrate, which comes out alongwith the drop specimens.

Figures 4.11 to 4.13 show the SEM micrographs of the interface between carbon substrate and different aluminium alloys at high temperature. These micrographs also show the surface of the alloy drops investigated at low temperature It is clearly visible from these SEM micrographs that a reaction layer is present at the interface of Al-Cu/C_v and Al-Zr/C_v systems whereas there is no sign of reaction layer

(a)

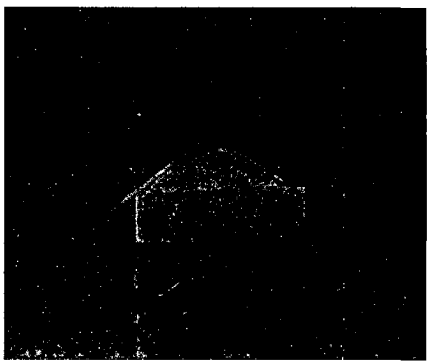

(b)

Fig. 4.9 The change in sessile drop profile with temperature for Al-5.2wt.%Zr/C_v system (a)775°C (b)1075°C.

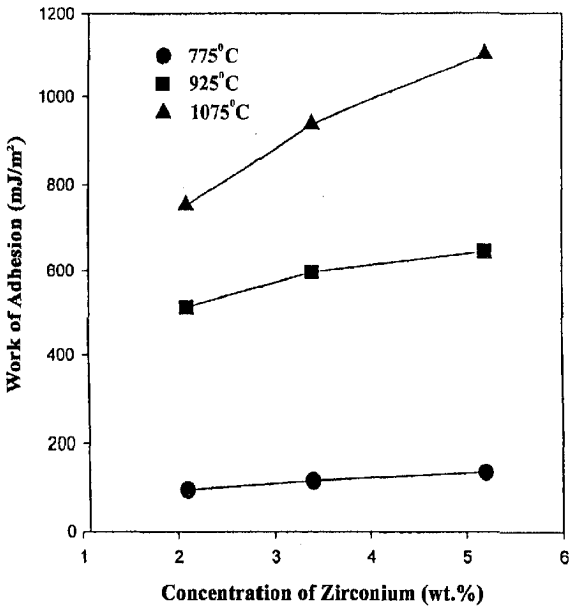

Fig. 4.10 The variation of work of adhesion with zirconium content for different Al-Zr alloys.

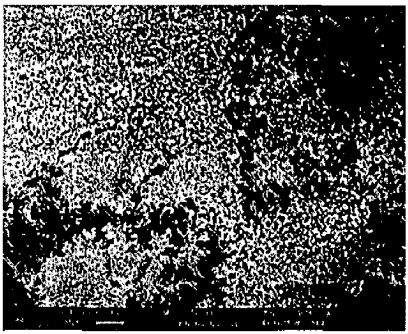

(a)

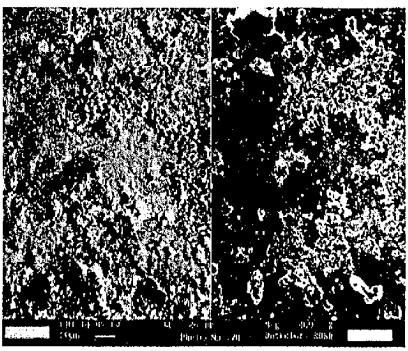

(b)

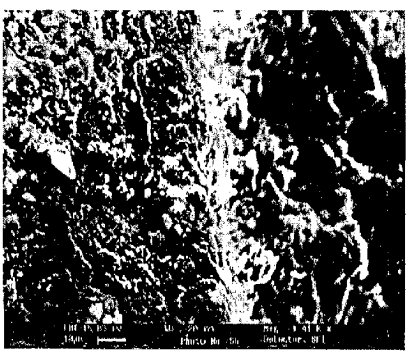

(c)

Fig. 4.11 SEM micrographs showing the interface in Al-4.5wt.%Cu/C system (a) drop surface at 850°C (b)back scattered image (c) interface at1075°C.

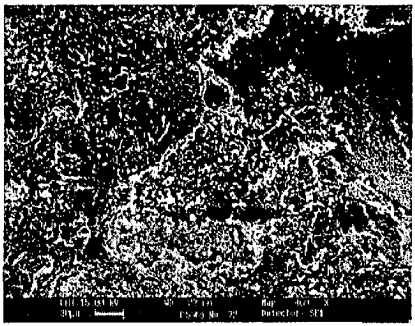

(a)

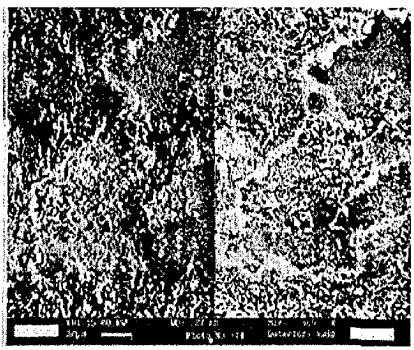

(b)

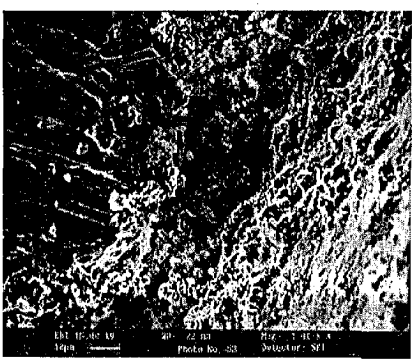

(c)

Fig. 4.12 SEM micrographs showing the interface in Al-2.3wt.%Li/C. system (a) drop surface at 850°C (b) back scaattered image (c) interface at 1075°C.

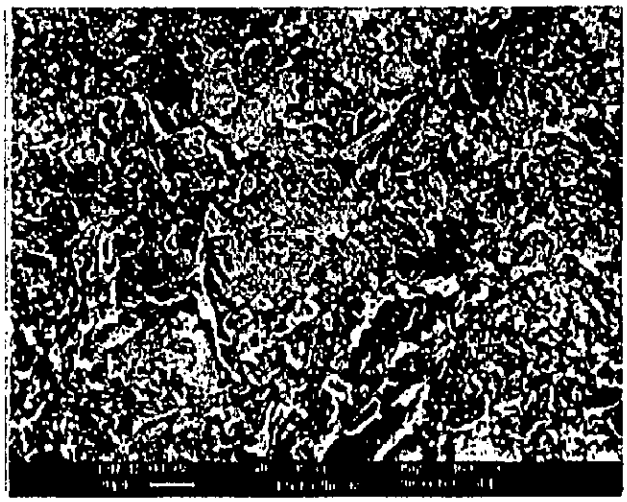

(a)

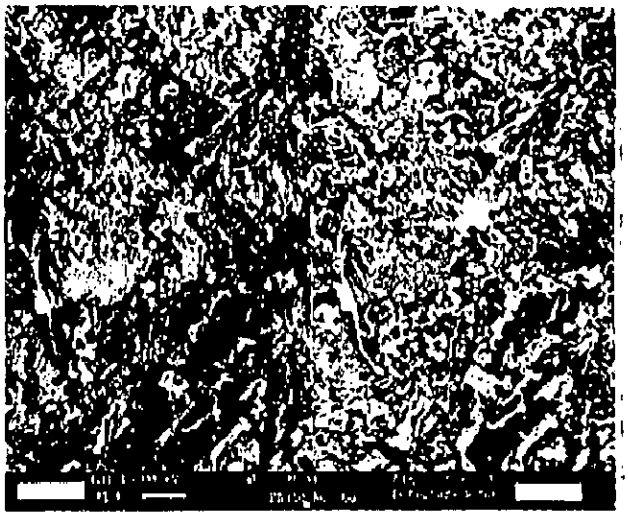

(b)

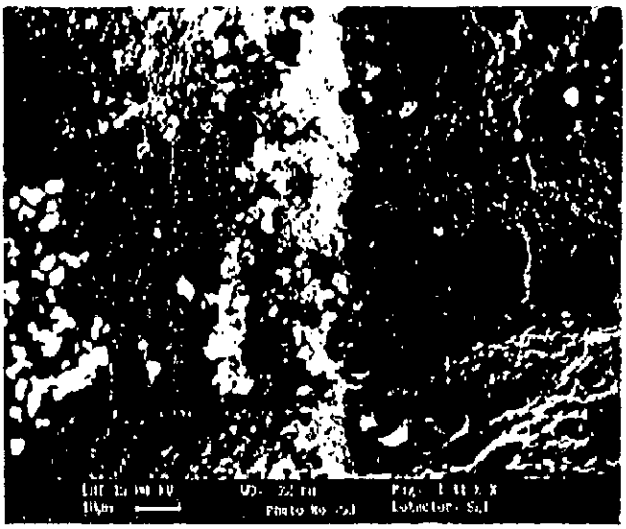

(c)

Fig. 4.13 SEM micrographs showing the interface in Al-5.2wt.% Zr system (a) drop surface at 850°C (b) back scattered image interface at 1075°C.

at the interface of Al-Li/C_v system. In case of Al-Cu/C_v system, the interface between alloy and substrate mainly consists of a single layer, as shown in Fig. 4.11 (c) whereas in case of Al-Zr/C_v system, it consists of two different layers, as shown in Fig.4.13 (c). The EPMA line analysis, as shown in Figs. 4.14 and 4.15, reveals the presence of aluminium and zirconium at the interface of Al-Cu/C_v and Al-Zr/C_v systems respectively.

4.1.3 X-ray Diffraction Analysis

The X-ray diffraction analysis of interface region shows the presence of Al_2O_3 in all the samples, investigated at low temperatures. Besides Al_2O_3, the presence of LiO_2 is also observed at the interface of Al-Li/C_v system, investigated at low temperatures. The X-ray analysis of all the specimens tested at higher temperature reveals the presence of Al_4C_3 at the interface whereas at the interface of Al-Zr/C_v system, ZrC phase is also detected. Table 4.2 shows the various phases identified at the interface of different aluminium alloys and vitreous carbon.

Table-4.2

X-ray diffraction analysis of interface of different systems

Composite system	2θ (degree)	Sinθ	I/I_o	I/I_o ASTM	d (Å)	hkl	Phase(s)
Al-Cu/C_v	21	0.179	16	100	4.30	100	$CuAl_2$
	32	0.275	13	60	2.80	012	Al_4C_3
	38	0.328	10	100	2.36	111,110	Al, Al_2O_3
	44	0.374	28	100	2.06	002	C
	55	0.464	36	100	1.66	110	Al_4C_3
Al-Li/C_v	25	0.212	16	100	3.63	-	LiC_{16}
	34	0.289	30	100	2.66	-	Li_2O
	38	0.328	10	100	2.36	111,110	Al, Al_2O_3
	40	0.341	23	100	2.26	220	AlLi
	44	0.374	20	100	2.06	002	C
Al-Zr/C_v	33	0.284	21	100	2.71	111	ZrC
	38	0.328	10	100	2.36	111,110,114	Al,Al_2O_3,Al_3Zr
	44	0.374	23	100	2.06	002	C
	55	0.464	12	50	1.66	220	ZrC
	58	0.481	26	80	1.60	116	Al_2O_3

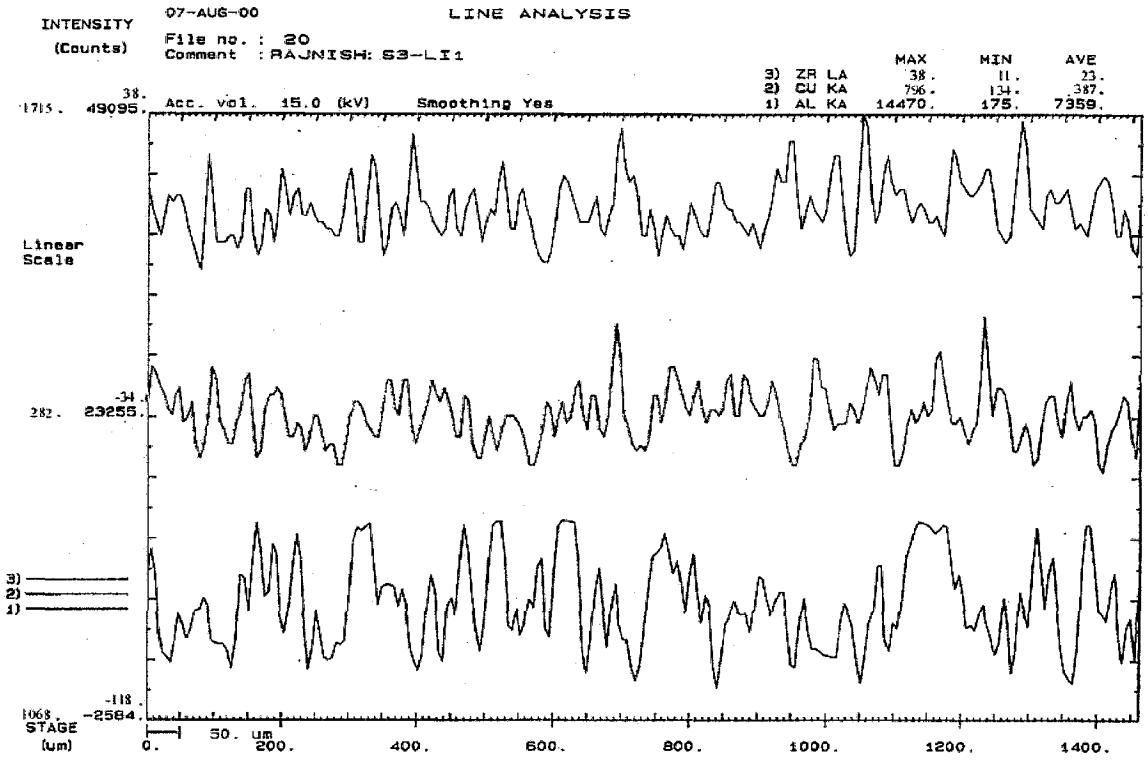

Fig. 4.14 EPMA line scan across the interface in Al-4.5wt.%Cu/C$_f$ system.

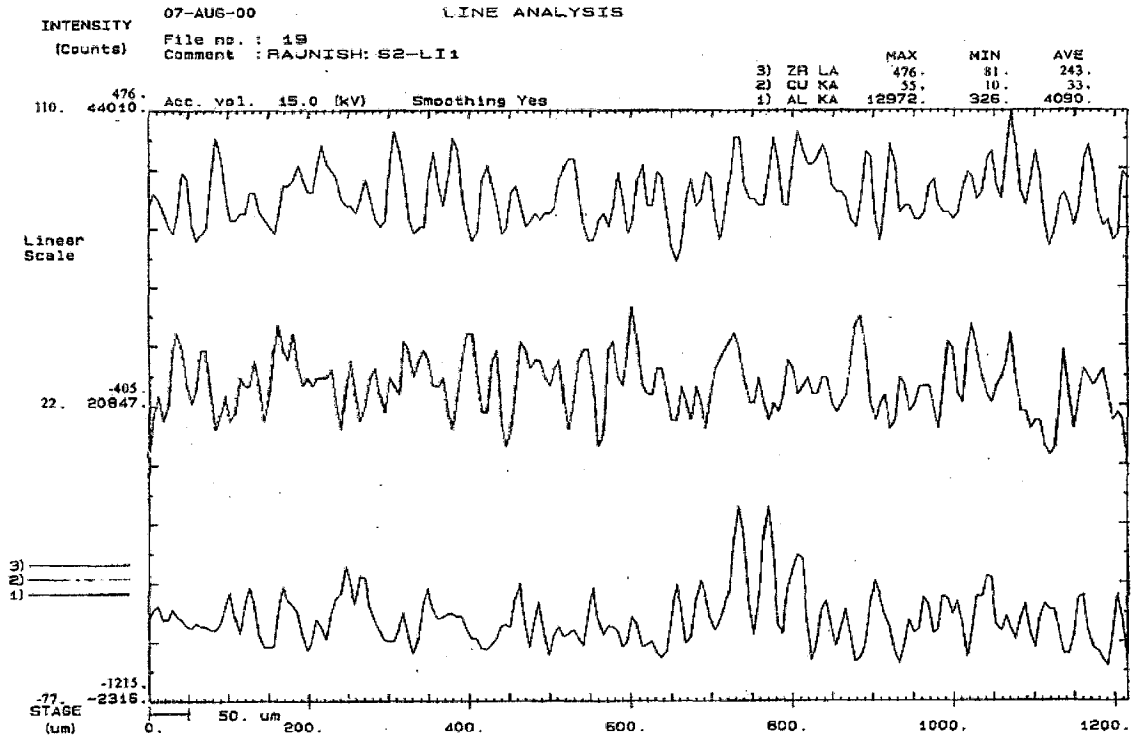

Fig. 4.15 EPMA line scan across the interface in Al-5.2wt.%Zr/C$_f$ system.

4.2 DISCUSSION

The deoxidation of aluminium has been verified by examining the contact angle kinetics of aluminium on α-Al_2O_3. The steady contact angle obtained in this system is in good agreement with the contact angles of same system measured under those experimental conditions which generally suppress the influence of the oxide layer on wetting (51). This clearly shows that in the present investigation, the deoxidation of aluminium is achieved in about 10 mins after melting at 850^0C. Although the deoxidation of aluminium, in the present study, is achieved in a longer time duration after melting but can be attributed to different experimental conditions. Deoxidation is mainly produced due to reduction of the oxide layer by liquid aluminium with production of gaseous suboxide (51).

The contact angle of Al-Cu/C_v, Al-Li/C_v and Al-Zr/C_v systems shows large values at low temperatures, i.e., from 700^0C to 850^0C. Though there is a significant decrease in contact angle for Al-Li/C_v system as compared to other systems, they are still greater than 100^0. The work of adhesion of Al-Cu/C_v, Al-Li/C_v and Al-Zr/C_v systems is about 150 mJ/m^2, 250 mJ/m^2 and 100 mJ/m^2 respectively at 775^0C, which is equivalent to 10 to 20% of the work of cohesion of aluminium alloys. This shows that the Al alloy/C_v interface is energetically weak and the same effect is realized from the fact that no force is required to detach the drop specimens from the carbon substrate.

These values of contact angle and work of adhesion are comparable with those measured in nonreactive metal/carbon systems like Cu/C_v (98,99) or Ag/graphite (19) in which, adhesion has been attributed to Vander Waal's interaction (19). These values of contact angle are greater than the values of contact angle measured for Al/Al_2O_3 system, in the presented study, at 850^0C. This difference may be attributed to the fact that either the additions of Cu and Zr increase the surface tension of aluminium alloy or the deoxidation of Al-Cu alloy drop and Al-Zr alloy drop is not achieved in 10 mins of holding time as deoxidation also depends on the testing temperature. So in the present study, large contact angles are observed in the low temperature range of 700^0C to 850^0C.

The second factor, related to the deoxidation of alloy drop, is more relevant as SEM study shows the presence of oxide at the surface of the alloy specimens tested at these temperatures as shown in Figs. 4.11 (a), 4.12 (a) and 4.13 (a). At the same time, the XRD analysis also shows the presence of Al_2O_3 at the interface between vitreous carbon substrate and these alloys at low temperatures as given in Table 4.2. The temperature dependence of the deoxidation of aluminium have been observed by Landry et al. (19) who shows experimentally that the deoxidation of aluminium is achieved in less time depending upon the temperature, as it takes about 8000 secs at 750^0C against 800 secs at 977^0C to obtain the deoxidation conditions. Eustathopoulos (29) has also pointed out that the rate of establishment of equilibrium is determined by temperature itself as it takes 60 mins at 850^0C to obtain a constant (steady) contact angle as against 30 mins at 900^0C.

In case of Al-Li/C_v system, despite of decrease in surface tension, the large contact angles and low work of adhesion are observed because the lithium present in the alloy probably substitute for aluminium in the oxide layer as it is more electropositive than aluminium and brings about weakening of the oxide layer. But at the same time, it seems that the concentration of lithium is not sufficient to reduce the surface tension considerably or to react with the carbon substrate so as to form a compound wettable by aluminium. The SEM study does not show the presence of interface between the substrates and Al-Li alloys, however, X-ray analysis shows the presence of Li_2O at the interface which confirms that complete deoxidation of alloy drop is not achieved. Although the formation of Li_2C_2 crystals has been reported at 700^0C in argon atmosphere by Secrist and Winsyl (213) but no Li_2C_2 has been observed in the X-ray analysis. This may be either due to very less formation of Li_2C_2 or due to insufficient amount of lithium addition in the alloy, incapable of forming the lithium carbide besides replacing the aluminium in the oxide layer at the surface of the molten alloy.

The exact process of decreasing the contact angle in the present study is not clear at low temperatures but these results confirms the predictions made by Manning et al.(18) who have reported that wetting is not significantly affected by the addition of small quantities (2 to 3wt.%) of surface active elements.

At high temperatures, all the alloys show wettability with vitreous carbon substrate as the observed contact angle is less than 90° for Al-Cu/C_v and Al-Zr/C_v systems above 1000°C whereas Al-Li/C_v system shows a contact angle of less than 90° at 925°C for high Li content alloy. It is also observed from Fig.4.8 that at high temperatures, there is large difference in contact angles for Al-Zr/C_v system depending upon the Zr content in the alloy. High Zr containing alloy shows contact angle of 55° while low Zr containing alloy shows contact angle of 84° at 1075°C which is close to that observed for Al-4.5wt.%Cu alloy at this temperature. It is therefore concluded that addition of small amount of reactive elements does not improve wettability of aluminium with carbon. These results are in good agreement to that observed by other workers (18).

On the other hand, the contact angles of Al-Li alloys on vitreous carbon substrates at high temperatures are very close to each other. The low lithium content alloy shows contact angle of 78° whereas high lithium content alloy shows contact angle of about 72°. Lithium addition to aluminium improves the wettability as the contact angles of Al-4.5wt.%Cu/C_v and Al-2.3wt.% Li/C_v systems at 850°C are around 135° and 100° respectively. It may be concluded that further addition of lithium to aluminium does not produce a remarkable difference on the wettability of carbon at high temperatures. The same effect has been observed by Eustathopolous et al. (29) who observed a constant contact angle of 29° at all temperatures during the wetting of vitreous carbon substrate by Al-6.0wt.% Li alloy.

The work of adhesion measured for these systems at high temperatures is nearly one magnitude higher than the measured at low temperatures. The work of adhesion of the interface is very high and equals, depending upon the temperature and system, ~60% to 75% of the work of cohesion of the alloys. The interface is thus energetically strong and adhesion can not be interpreted in terms of weak Vander Waal's interactions but in terms of chemical interactions.

It is well known that the deoxidation of aluminium depends upon time and temperature. The holding time of 10 mins is sufficient to deoxidize the aluminium alloys at 850°C, i.e., without any reaction between aluminium and Al_2O_3. So in view

of the above fact, it is possible that at high temperatures, the deoxidation of aluminium alloys might have been achieved in less than 10 mins and there might be sufficient time for reaction to occur between the substrate and the liquid alloy.

The SEM analysis of Al-4.5wt.%Cu/C_v system at 1075^{0}C, reveals the presence of a reaction layer having a uniform thickness throughout as shown in Fig. 4.11 (c). The EPMA line analysis of this reaction layer shows the presence of aluminium in it as shown in Fig.4.14. The SEM analysis of the interface between different Al-Zr alloys and C_v substrate shows the presence of two different layers at the interface as shown in Fig. 4.13 (c). The EPMA analysis reveals the presence of aluminium in the layer near to substrate whereas layer near to the alloy shows the presence of zirconium as shown in Fig.4.15. The SEM analysis of the interface between Al-Li alloys and vitreous carbon substrate does not reveal the presence of any reaction layer at the interface, for high lithium content alloys at about 1075^{0}C, as shown in Fig. 4.12 (c). The EPMA analysis of the interface in Al-Li/C_v system is not carried out by JEOL 8600M, as it is unable to detect the Li element.

The X-ray diffraction analysis of the samples taken from the interface region of Al-4.5wt.%Cu/C_v system shows the presence of $CuAl_2$ and Al_4C_3 which formed during reaction between aluminium copper alloy and the vitreous carbon substrate. The X-ray analysis of the samples taken from the interface region of Al-Zr alloy/C_v system shows the presence of Al_4C_3, ZrC and Al_3Zr at the interface. But as the EPMA results suggest the presence of Al in the layer near the substrate and Zr in the layer near the alloy drop, it may be concluded that these layers are of Al_4C_3 and ZrC respectively. The X-ray analysis of the interface of Al-Li/C_v system reveals the presence of Li_2O, LiC_{16} and AlLi as given in Table 4.2

The solubility of carbon in molten aluminium is very low i.e. 0.14wt.% at 1100^{0}C (57) whereas the solubility of carbon in solid is estimated to be around 0.015wt.%, so upon cooling from the testing temperature, essentially all dissolved carbon is precipitated out as Al_4C_3. In case of Al-4.5wt%Cu/C_v system, the aluminium reacts with carbon substrate to form aluminium carbide after the deoxidation of the alloy drop. The copper addition does not play any role, as it is inert to carbon. This

reaction between aluminium and carbon substrate depends upon temperature and time of contact. Landry et al. (19), in a detailed analysis on the reactive wetting kinetics of the Al/C system, have mentioned that the reaction between Al and C is strictly localized at the triple line and takes place by a nearly two-dimensional mechanism. They have also pointed out that at the triple line, liquid aluminium has a direct access to the solid carbon substrate and the reaction occurs rapidly without any need of diffusion of carbon (or aluminium) atoms through the solid reaction product layer of Al_4C_3. The reaction rate observed at this particular point is two orders of magnitude higher than the reaction rate at the interface far from the triple line where the reaction occurs by slow diffusion through the solid carbide layer.

In another study, Landry et al. (99) have also pointed out that the reaction rate at the triple line increases with temperature according to the Arrhenius law. The activation energy is about 230 kJ/mole. This value is higher by an order of magnitude than typical activation energies for diffusion in liquids but is of the same order of magnitude as those for diffusion in solids. At the triple line it occurs without any need of solid state diffusion. Therefore, while the thickening process is diffusion controlled, lateral growth process is quite different. The activation energy of lateral growth is also of the same order of magnitude as the cohesion energy of graphite per atom (214), therefore, the formation of Al_4C_3 is controlled by the rupturing of C-C bonds at the substrate surface.

After the deoxidation of the aluminium alloy, the reaction between alloy and substrate takes place and the substrate, at the solid/liquid interface, is covered by a continuous layer of Al_4C_3 which extends also on the substrate free surface near the triple line. Consequently, the contact angle at high temperatures corresponds to the wetting of aluminium carbide by aluminium alloy. Thus the contact angle and work of adhesion measured for Al-4.5wt.%Cu/C_v system in the present study, are in fact related to Al/Al_4C_3 system at higher temperature.

The work of adhesion of the interface at high temperatures is very large (~70% of the work of cohesion of liquid aluminium alloy). It is interesting to note that the results obtained in the Al/Al_4C_3 system in the present study are comparable to those of

Landry et al. (19) in Al/Al_4C_3 system at 977^{0}C and those of Dervet et al. (216) in the Si/SiC system at 1417^{0}C. They both interpreted adhesion at the interface in terms of covalent bonds, similar to the bonds in SiC and Al_4C_3 substrates, established between interfacial atoms of the substrate and atoms of the liquids. So the adhesion at the Al/Al_4C_3 interface in the present study may also be attributed to covalent bonds.

In case of Al-Zr/C_v system, the zirconium is a strong carbide-forming element. The liquidus temperature of all the aluminium zirconium alloys, investigated in the present study, lies between 800^{0}C to 900^{0}C hence they show semi-liquid state at low temperatures. It may be thus possible that the Al_3Zr crystals remain undissolved in the liquid alloy at low temperatures. As a result, zirconium could not react with carbon to form a metal like carbide, which is more wettable than Al_4C_3 by aluminium. Also, the surface tension of liquid alloy increases with increasing amount of zirconium. These factors may be responsible for the large contact angle for Al-Zr/C_v system, measured at low temperatures. Jarfor's et al. (217) have also pointed out that Al_3Ti crystals remain undissolved at 800^{0}C, however, they observed a thin layer of Al_4C_3 at this temperature at the interface. The SEM examination of the interface in the present study does not reveal the presence of any reaction layer at low temperatures whereas the X-ray analysis shows the presence of Al_3Zr verifying the fact that these crystals remain undissolved at low temperatures. The work of adhesion for this system shows higher values in absolute terms as compared to Al-Cu/C_v system at low temperatures. It may be attributed to the higher surface tension of Al-Zr alloys as compared to Al-Cu alloy at these temperatures, however, this work of adhesion is also equal to 20% of the work of cohesion of liquid Al-Zr alloys. So the interface of this system is also energetically weak at low temperatures.

At high temperatures, zirconium strongly reacts with carbon substrate to form zirconium carbide freely in liquid. In low zirconium containing alloys, aluminium carbide is formed at the interface instead of ZrC initially. The depletion of Zr is compensated by the dissolution of Al_3Zr crystals to the extent that their total volume becomes smaller than the volume as per Al-Zr equilibrium phase diagram. The zirconium then forms ZrC by reacting with the initially formed Al_4C_3.

So, the lower zirconium content alloys show a double layer at the interface at high temperatures, one of Al_4C_3 near to the substrate and one of ZrC near to the alloy as observed in SEM and XRD analysis. The same behaviour has been observed by Landry et al. (19) for Al-Ti/C_v system at high temperatures. Sobczak et al. (64) have observed the TiC phase inside the drop in the form of fine particles whose content increases with temperature and time of contact. These particles may form freely in the liquid due to dissolution of the carbon substrate at the very start of the reaction, however, they have suggested the formation of these TiC particles due to solution reprecipitation process.

In case of high zirconium content alloy, the depletion of zirconium in the alloy drop never occurs. It results in the formation of a continuous layer of ZrC on the substrate. It may be possible that Al_4C_3 forms at the places where ZrC layer is discontinuous but due to high zirconium content, it is also converted to ZrC by reacting with Zr. So a continuous layer of ZrC is observed at the interface between high zirconium containing aluminium alloy and vitreous carbon substrate as shown in Fig.4.13(c) and detected by X-ray analysis. Sobczak et al. (64) have also observed a TiC layer at the interface between Al-6wt.%Ti alloy and graphite substrate at high temperatures.

The contact angle of low zirconium content alloy is nearly equal to the contact angle of Al-4.5wt.%Cu/C_v system at high temperatures as the difference of 2° is too small to assert the effect of zirconium addition. It may be due to the fact that formation of ZrC indeed occurs but Al_4C_3 also forms at the same time, hence ZrC does not play any role in the wetting process. On the other hand, as the enthalpy of Zr-C bond is quite large than the enthalpy of Al-C bond, the formation of ZrC at the interface results in a considerable decrease in the contact angle for high zirconium containing alloys at high temperatures. Sobczak et al. (64) have also observed a contact angle of less than 90° for high titanium content alloys at the same temperatures.

The work of adhesion in this system is quite high and is equal to 60 to 80% of the work of cohesion of liquid alloy at high temperatures, depending upon the amount

of zirconium in the alloy. Neglecting the effect of the reaction product roughness, the other parameters determining work of adhesion are the surface tension of the liquid, and the contact angle of the alloy on the substrate. The surface tension increases with increase in zirconium content of the alloy at a temperature and contact angle also decreases with increase in zirconium content as the enthalpy of the Al-C bond in Al_4C_3 layer is lower than the enthalpy of the Zr-C bond in ZrC layer at the interface (19). As a result, work of adhesion increases with increase in zirconium content at high temperatures. The work of adhesion, measured for low zirconium content alloys at high temperature, is equal to 70% to the work of cohesion of liquid aluminium alloy whereas it is equal to 85% of the work of cohesion of the alloy for high zirconium content alloys. The Al-Zr/ZrC interface is thus energetically strong and can be attributed to the formation of metallic bonding across the interface as pointed out by Naidich et al. (59) in an extensive review.

It has been reported that alkali metals like lithium react with graphite to form intercalation compounds where positive ions of the metal are inserted between the basal layers (59). The intercalation is achieved due to the diffusion of lithium between the basal planes of the vitreous carbon substrate. At the same time, it reacts with carbon substrate to form crystals of lithium carbide at about 700^0C in argon atmosphere (213). At low temperatures, the lithium present in the alloy replaces the aluminium in the oxide layer to bring about a weakening of the oxide film. The lithium addition thus leads to rapid dislocation of the oxide layer on the drop and reacts strongly with the carbon substrate to bring about wetting (29).

In the present study, it may happen that instead of Al_2O_3, lithium oxide(s) (Li_2O_2 or Li_2O) are formed at the drop surface initially, which most probably have high permeability than Al_2O_3 layer. It is then possible that the aluminium-lithium alloys, which have relatively lower surface tension than aluminium, penetrate through this oxide layer. So, the fast deoxidation of the drops may be achieved and the lithium present in the alloy reacts with the substrate subsequently.

In case of Li-Al/C_v system the disruptive effect of lithium on the oxide layer is clearly observed at low temperatures as the contact angle is remarkably reduced in comparison to that of Al-Cu/C_v system. It may be attributed to the fast deoxidation of

the alloy drop due to lithium and some extent of chemical interaction between alloy and the substrate. But despite of a remarkable decrease in the contact angle, they are still in non-wetting range. Therefore, it seems that the amount of lithium in the alloys is not sufficient to disrupt the oxide layer as well as to react with the substrate at lower temperatures. The observed contact angles for different Al-Li alloys on C_v substrate are in good agreement with the results of Manning and Gurganus (18) who have reported that the wetting is not significantly affected by the addition of small quantities of surface active elements. From this discussion it appears that a possible beneficial effect of lithium on wetting at low temperatures can not be excluded and indeed, it has been observed by Eustathopoulos et al. (29) with high lithium containing aluminium alloy.

The work of adhesion of Al-Li/C_v system interface, calculated by Eqn. (2.2), is 250 mJ/m^2 to 775 mJ/m^2 depending upon the temperature and amount of lithium in the alloy. It is equal to only 20% to 45% of the work of cohesion of the liquid alloy. This shows that the Al-Li/C_v interface is energetically weak though, stronger than Al-Cu/C_v system interface at the same temperature. It also shows some amount of chemical interaction between the alloy and the substrate. Although, SEM studies do not reveal the presence of any reaction layer but XRD analysis shows the presence of LiC_{16}. The LiC_{16} is formed due to intercalation reaction in which positive ions of lithium are inserted between the basal layers of carbon substrate.

At high temperatures, besides the effect of lithium, the deoxidation of the alloy drop is also accelerated by the effect of temperature. As a result, sufficient amount of lithium is available to react with the substrate after deoxidation of the drop at high temperatures. The lithium then probably reacts with the substrate and diffuses in bulk into the carbon substrate to form the intercalation compounds. Although it has been reported (59) that the enthalpy of the intercalation is not high, the observed wettability may be attributed to the low surface tension of aluminium-lithium alloys.

4.3 COMPARISON OF RESULTS

The observed contact angle of 86° at 1075°Cis very high as compared to 55°,

measured for Al on sintered Al_4C_3 by Ferro and Derby (71) at 1100^0C, slightly higher thanthat used in the present study whereas it is considerably less than the contact angle of 104° of Al over Al_4C_3 substrate measured by Belyaev and Zhemchungina (215) at 1000^0C in vacuum. Eustathopolous et al. (29) have pointed out that the observed contact angle is a dynamic angle in these circumstances hence depends upon the rate of reaction. So apart from the experimental conditions, the high contact angle observed for Al-Cu/C_v system in the present study, with respect of Ferro and Derby (71), may be attributed to the low temperature and less contact time whereas with respect to Belyaev et al. (215), it may be attributed to the long contact time between molten alloy drop and the substrate at a particular temperature.

The observed contact angle of Al-Li/C_v system is higher than that observed by Eustathopoulos et al. (29) for the same system. This difference may be attributed to the high concentration of lithium in the alloy, long holding time and different experimental atmosphere used by them. The observed contact angle of Al-Zr/C_v system is higher than that observed by Sobczek et al. (64) for Al-6wt.%Ti/graphite system in relatively short holding time. The difference may be attributed to the fact that Ti is a stronger carbide forming element than Zr (68). The other reason may be the use of high vacuum during sessile drop experiments as it has been reported that the oxidation of alloy drops is favoured by high vacuum (19).

RESULTS AND DISCUSSION: SOLIDIFICATION PROCESSING AND MICROSTRUCTURAL CHARACTERIZATION OF CAST COMPOSITES

This chapter describes the results on solidification processing and microstructrual characterization of carbon fibre reinforced aluminium alloy matrix composites. In the end, the results have been discussed to develop a better understanding of the phenomenon involved in the observed microstructure of the composites.

5.1 RESULTS

5.1.1 Solidification Processing of the Composites

(a) Casting details: The casting details of composite fabrication are given in Table 5.1.

Table-5.1

Casting Details

Alloy	Volume fraction	Pressure (Mpa)	Casting temp.(^{0}C)	Holdin gtime	Preheating temp. (^{0}C)	Remarks
Al-4.5Cu	24 %	75	750	1 min.	650	Good
Al-4.5Cu	41 %	75	750	1 min.	650	Good
Al-4.5Cu	66 %	75	750	1 min.	650	Fair
Al-2.3 Li	24 %	75	700	1 min.	650	Good
Al-2.3 Li	41 %	75	700	1 min.	650	Good
Al-2.3 Li	66 %	75	700	1 min.	650	Good
Al-5.2 Zr	24 %	75	825	1 min.	650	Good
Al-5.2 Zr	41 %	75	825	1 min.	650	Good
Al-5.2 Zr	66 %	75	825	1 min.	650	Fair

The thickness measured in all castings, lies in the range of 35.0 mm to 40.0 mm. Each casting contains about 15 mm to 20 mm thickness of unreinforced alloy at the upper portion but the lower portion of 20.0 mm thickness contains fibre reinforced composites of 10.0 mm thickness inside the rectangular steel pipe. The rectangular pipe is taken out from the cast ingot by cutting the unreinforced alloy from its top and sides with the help of a saw cutting machine. The surfaces of the rectangular pipe are then removed by the same cutting operation to get the fibre reinforced composite plate. The thickness of different composite plates is measured and lies in the range of 7.0 mm to 8.0 mm while the width lies in the range of 66.0 mm to 68.0 mm.

(b) **Chemical composition of matrix alloys:** The chemical composition of various matrix alloys in different composites is given in Table 5.2.

Table-5.2

Chemical composition of the matrix alloys

S. No.	Matrix alloy	Li (wt.%)	Cu (wt.%)	Fe (wt.%)	Si (wt.%)	Mg (wt.%)	Zr (wt.%)	Al (wt.%)
1.	Al-Cu	-	4.47	1.07	1.53	0.46	-	Balance
2.	Al-Li	2.13	2.09	-	-	0.80	0.14	Balance
3.	Al-Zr	-	2.71	0.32	-	-	5.22	Balance

It is clear from Table 3.1 and Table 5.2 that the concentration of major alloying additions remains nearly unchanged in Al-Cu and Al-Zr matrix alloys whereas it decreases considerably in Al-Li matrix alloy.

(c) **Optical microscopy and fibre volume fraction of composites:** Figures 5.1 to 5.3 show the optical micrographs of Al-Cu/CF, Al-Li/CF and Al-Zr/CF composites respectively. It is revealed from Figs.5.1 (a) to (c) that carbon fibres are uniformly distributed in Al-4.5wt.%Cu matrix alloy, however, distribution varies with fibre volume fraction. Same behaviour is also observed for Al-Li/CF and Al-Zr/CF composites having different fibre volume fraction as shown in Figs.5.2 and 5.3 respectively. The fibre volume fraction

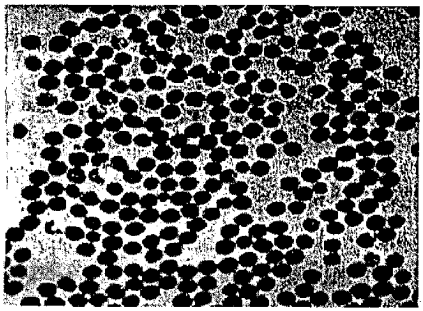

(a)

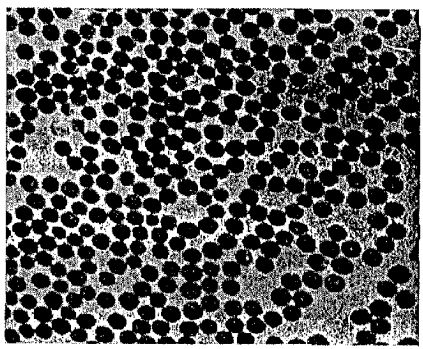

(b)

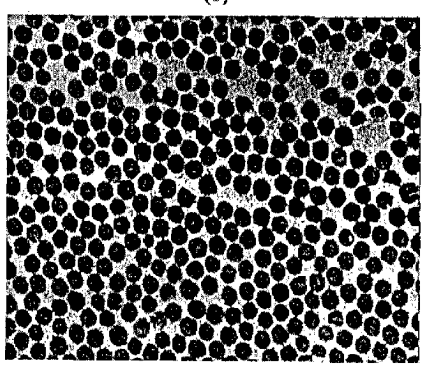

(c)

Fig. 5.1 Optical micrographs showing the fibre distribution in different Al-Cu/CF composites (a) 24% fibre volume fraction (b) 41% fibre volume fraction (c) 66% fibre volume fraction; X400.

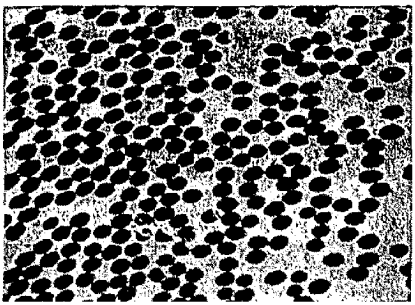

(a)

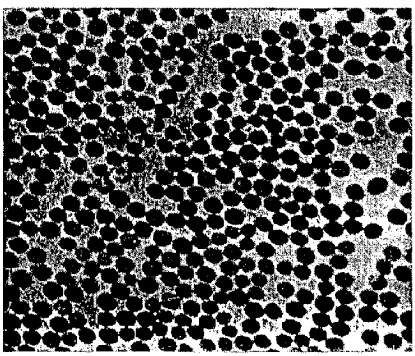

(b)

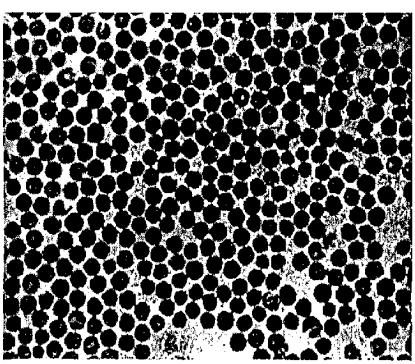

(c)

Fig. 5.2 Optical micrographs showing the fibre distribution in different Al-Li/CF composites (a) 24 % fibre volume fraction (b) 41 % fibre volume fraction (c) 66 % fibre volume fraction; X400.

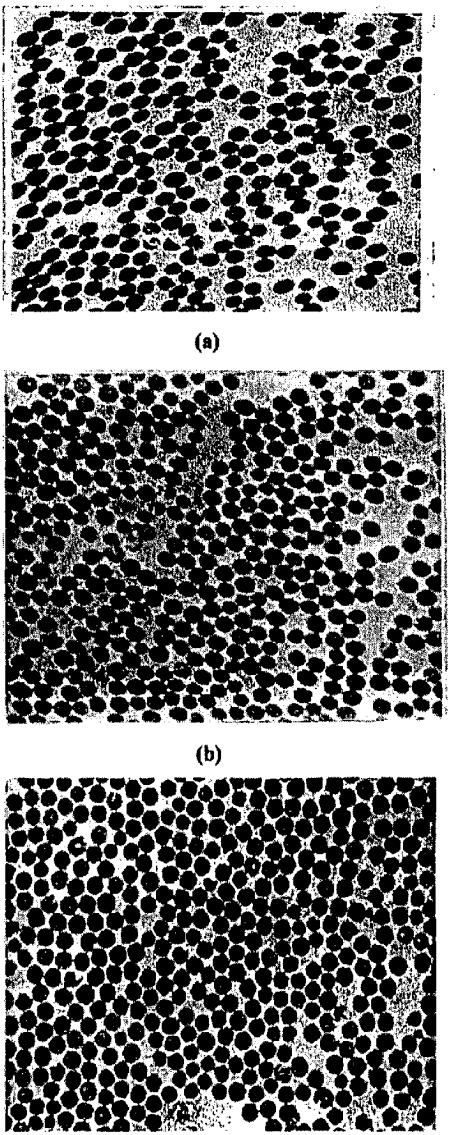

(a)

(b)

(c)

Fig. 5.3 Optical micrographs showing the fibre distribution in different Al-Zr/CF composites (a) 24 % fibre volume fraction (b) 41 % fibre volume fraction (c) 66 % fibre volume fraction; X400.

in different composites as determined by quantitative metallography is reported in Table 5.3.

Table-5.3

Fibre volume fraction in the composites

S. No.	Composite	No. of fibres falling on grid points	No. of fibres in an area of 72x48 mm^2 at 1000 X	Fibre volume fraction(%)
1.	Al-4.5 wt.% Cu/CF	66	337	66
2.	Al-4.5 wt.% Cu/CF	41	209	41
3.	Al-4.5 wt.% Cu/CF	24	125	24
4.	Al-2.3 wt.% Li/CF	66	340	66
5.	Al-2.3 wt.% Li/CF	41	210	41
6.	Al-2.3 wt.% Li/CF	24	124	24
7.	Al-5.2 wt.% Zr/CF	66	339	66
8.	Al-5.2 wt.% Zr/CF	41	211	41
9.	Al-5.2 wt.% Zr/CF	24	126	24

5.1.2 Microstructural Characterization of Cast Composites

(a) Scanning electron microscopy: Figure 5.4 shows the SEM micrographs of the cross-sections of Al-Cu/CF, Al-Zr/CF and Al-Li/CF composites each having 66% fibre volume fraction. It is apparent from these micrographs that satisfactory infiltration of aluminium alloy matrices into the carbon fibres has been achieved. Negligible porosity and few unwetted regions can be observed in Al-Cu/CF and Al-Zr/CF composites.

Figure 5.5 shows the SEM micrographs of the reaction interface in Al-Cu/CF, Al-Li/CF and Al-Zr/CF composites having 66% fibre volume fraction respectively. It is clear from these micrographs that a thick reaction interface is present in Al-Cu/CF and Al-Zr/CF composites while there is no trace of reaction interface in Al-Li/CF composite.

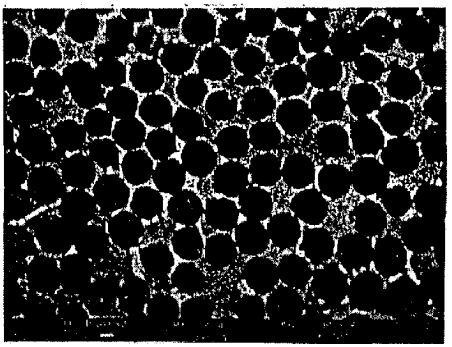

(a)

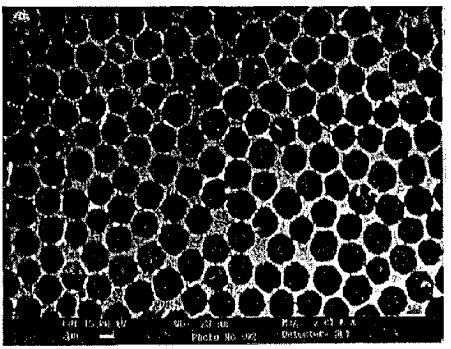

(b)

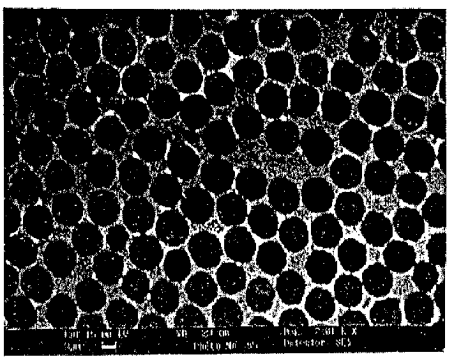

(c)

Fig.5.4 SEM micrographs showing the fibre distribution in different composite containing 66% fibre volume fraction (a) Al-Cu/CF composite (b) Al-Li/CF composite (c) Al-Zr/CF composite.

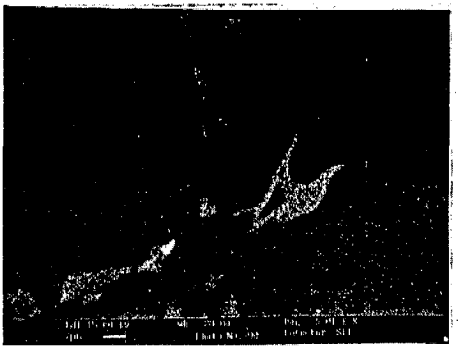

(a)

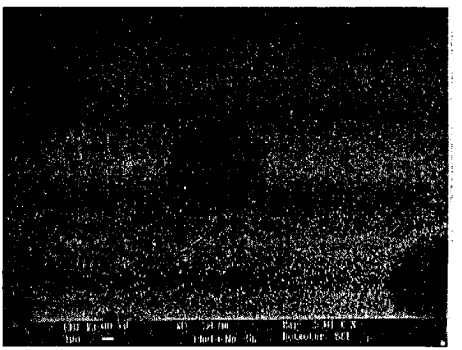

(b)

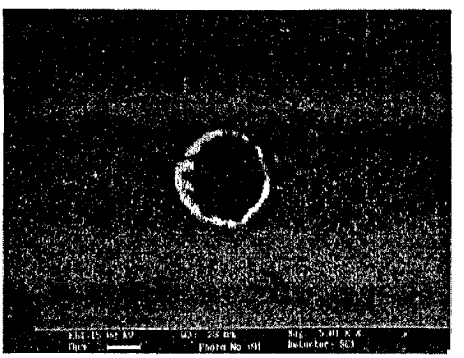

(c)

Fig. 5.5 SEM micrographs showing the interface between carbon fibre and aluminium alloy in different composites (a) Al-Cu/CF composite (b) Al-Li/CF composite (c) Al-Zr/CF composite.

(b) **EDS and EPMA analysis:** Energy dispersive spectroscopic (EDS) point analysis of Al-Cu/CF composite, in the region shown in Fig.5.6, is given in Table A5, in Appendix A. It is apparent from Fig.5.6 and Table A5 that the concentration of Cu is high near the fibre surface and decreases towards the matrix. Oxygen is also present near the fibre surface whereas nitrogen is detected inside the fibres. The carbon concentration is found to increase continuously from the interface towards matrix. The EDS line analysis across a big particle existing between the two fibres is shown in Fig.5.7. It is observed from the point analysis of this particle, as given in Table 5.4, that sufficient amount of Al, Cu, O and C is present in this particle.

Table-5.4

EDS point analysis of big particle in Al-Cu/CF composite

C K (ED)	N K (ED)	O K (ED)	Al K (ED)	Cu K (ED)	Zr L (ED)	Total
14(28)	6.3(10)	15.3(21.7)	35.2(29.7)	28.3(10.1)	-0.07(-0.02)*	100

*<2 sigma

Figures 5.8 (a) to (c) show the EDS micrographs of Al-Cu/CF composites having 66% fibre volume fraction. These micrographs show the distribution of oxygen, copper and aluminium present in the composite. It is observed from Fig.5.8 (a) that there is very little oxygen present in the composite due to oxidation of aluminium. It is also revealed from these micrographs that oxygen and copper are uniformly distributed in the composite.

Figs.5.9 (a) to (c) shows the EPMA micrographs of the Al-Li/CF composite having 66% fibre volume fraction. These micrographs show the distribution of various alloying additions in the matrix of the composite. It is revealed from these micrographs that the alloying additions are homogeneously distributed in the composite. Figure 5.9 (a) shows the presence of copper in the interfibre region of the composite. It is observed that copper concentration is substantial in the interfibre region. The presence of

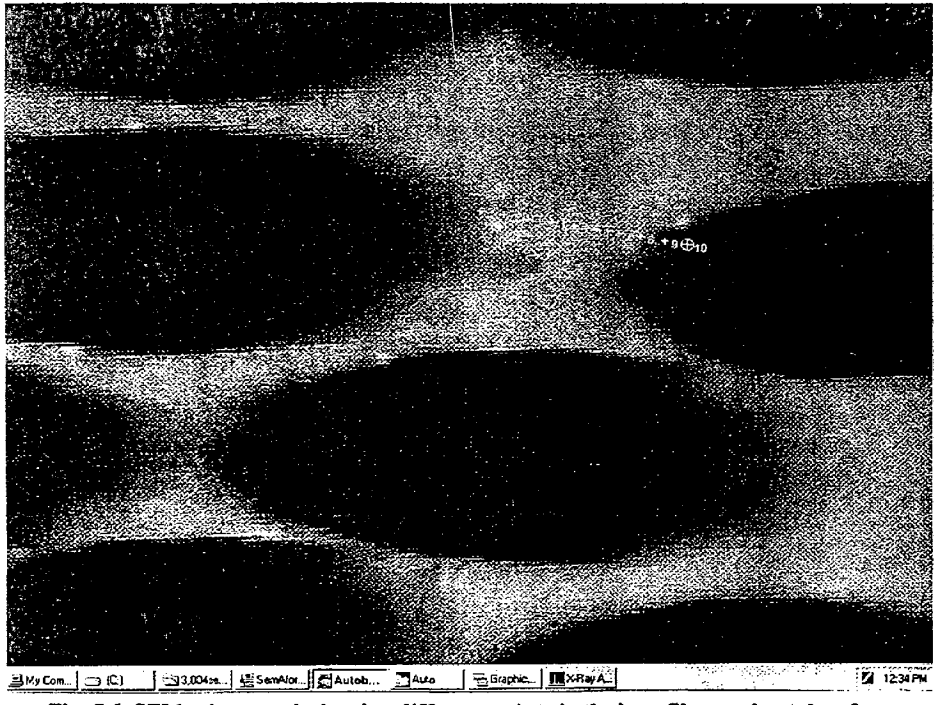

Fig. 5.6 SEM micrograph showing different points in the interfibre region taken for EDS point analysis

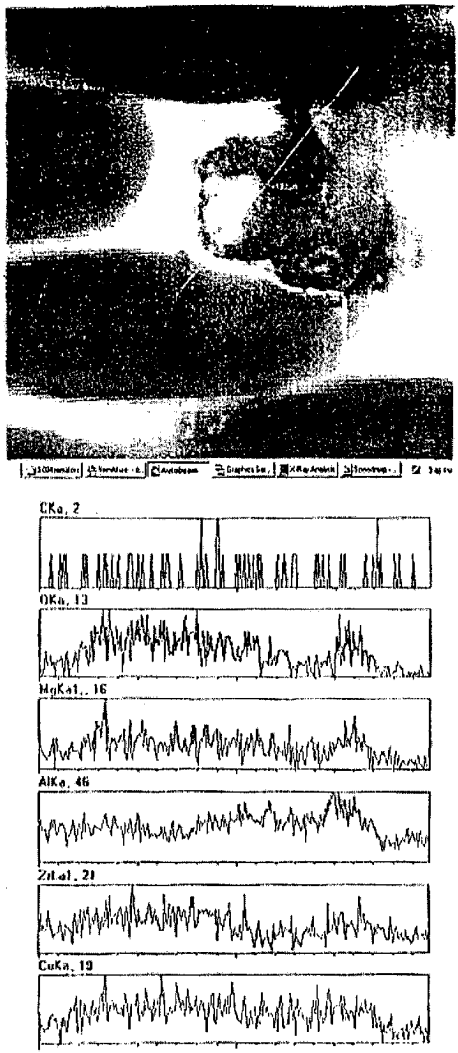

Fig. 5.7 EDS line analysis across a big particle in the inter-fibre region of Al-Cu/CF composite (a) micrograph showing the particle between the fibres (b) line analysis across the particle.

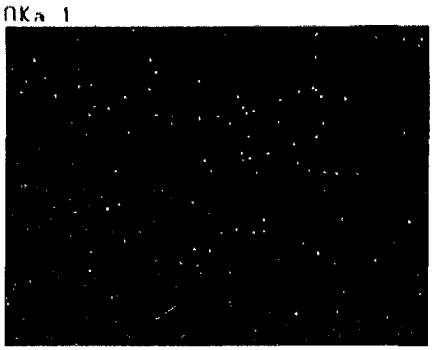

(a)

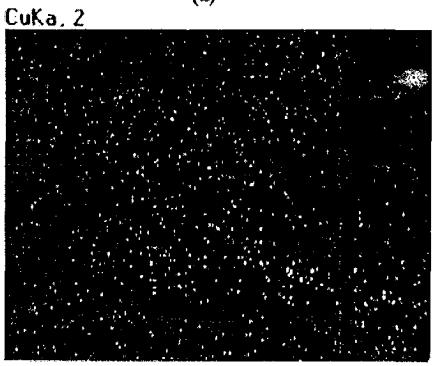

(b)

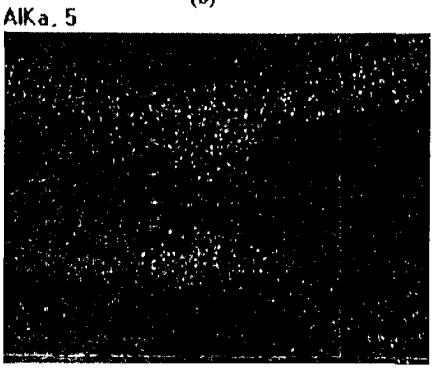

(c)

Fig. 5.8 EDS micrographs showing the distribution of alloying elements in Al-Cu/CF composite (a) oxygen (b) copper (c) aluminium.

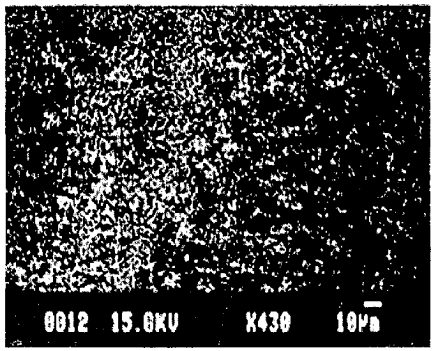

(a)

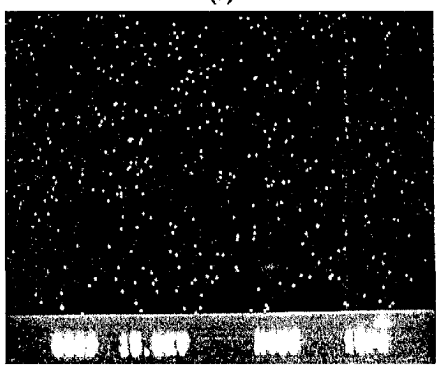

(b)

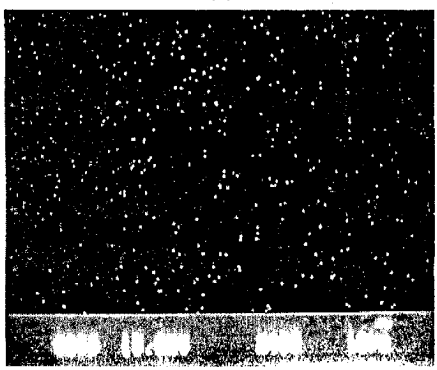

(c)

Fig. 5.9 EPMA micrographs showing the distribution of alloying elements in Al-Li/CF composite (a) copper (b) magnesium (c) zirconium.

Cu, Mg and Zr is also observed at the interface, as shown in Figs.5.9 (a) to (c) respectively. It is also observed from these micrographs that inspite of some segregation of these elements towards the interface, they are distributed uniformly in the inter-fibre region and hence, in the composite.

Figure 5.10 shows the EPMA line scan for different alloying additions in the interfibre region of Al-Zr/CF composite having 66% fibre volume fraction. It is apparent from the line scan that all the alloying additions are homogeneously distributed in the composite. However, this line analysis shows that zirconium content is higher near the carbon fibre surface as compared to matrix.

(c) **Transmission electron microscopy:** Figures 5.11 to 5.15 show the TEM micrographs alongwith SAD patterns, taken at different locations, for Al-Cu/CF composite having 66% fibre volume fraction. The various phases, identified after indexing these SAD patterns, are listed in Table-A6 in Appendix A. It is obvious from Table-A6 that Al_4C_3 crystals are present at the interface of Al-Cu/CF composite. It is also clear from Table-A6 that $CuAl_2$ is also present as a precipitate at the interface of this composite. Other phases like AlFeSi, etc. are also present in the matrix of the composite.

(d) **X-ray diffraction analysis:** The X-ray diffraction analysis of Al-Cu/CF, Al-Zr/CF and Al-Li/CF composites having the same fibre volume fraction is carried out to identify the various phases present at the interface and in the inter-fibre region of the composites.

The X-ray diffraction analysis, carried out for 2θ values ranging from 5° to 120°, of Al-Cu/CF composite having 66% volume fraction of carbon fibres is given in Table 5.5. All the peaks with I/I_0 values of 10 % and higher have been considered to identify the various phases present in the composite. The various phases, identified in Al-Cu/CF composite, are also listed in Table 5.5. It is observed that apart from the primary phase $CuAl_2$, some other phases like Al_4C_3, $FeSiAl_5$, etc. are also present in the composite.

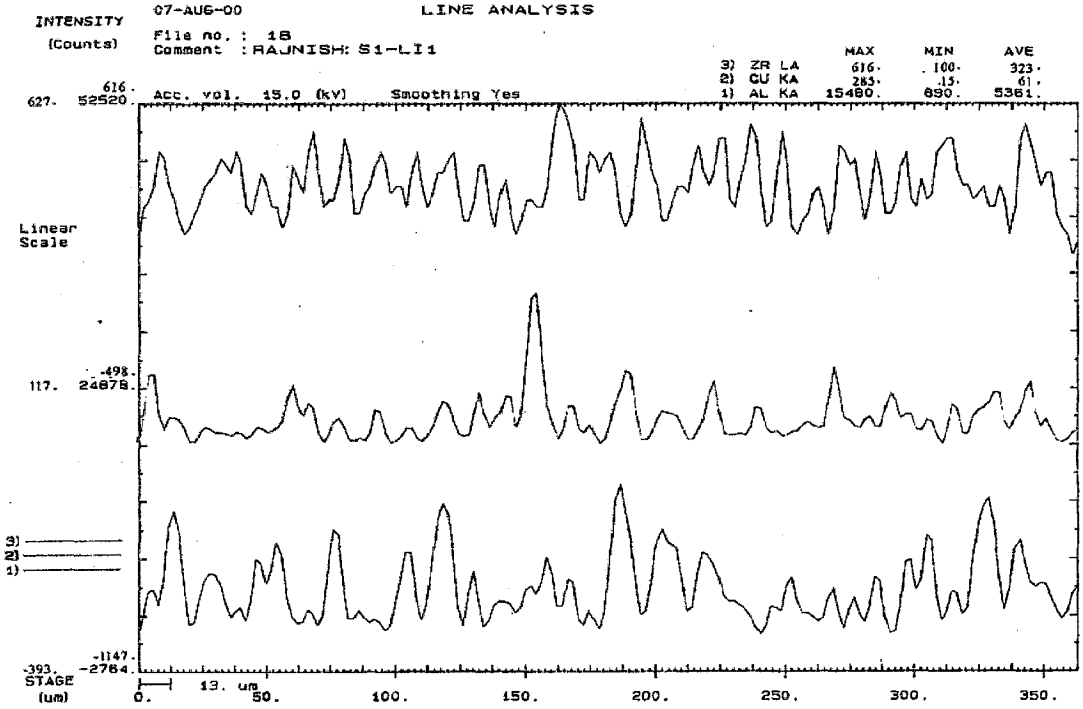

Fig. 5.10 EPMA line scan of the interfibre region in Al-Zr/CF composit having 66% fibre volume fraction.

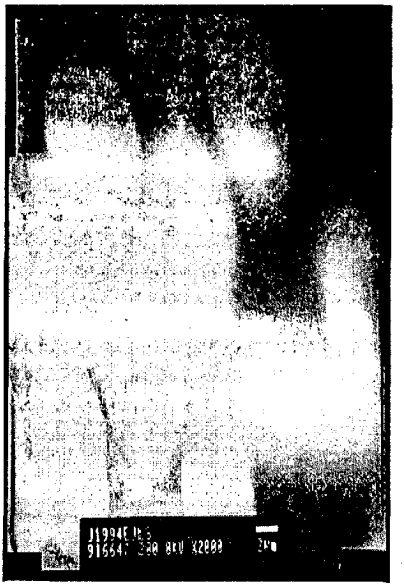

(a)

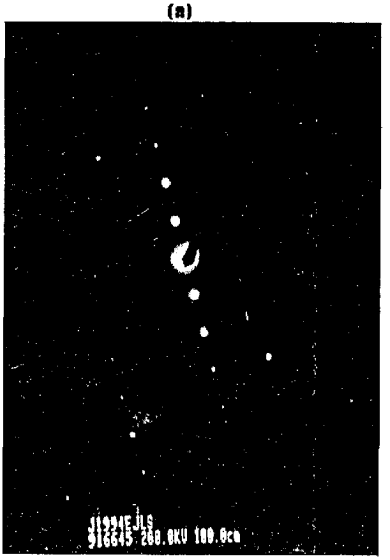

(b)

Fig. 5.11 TEM micrographs and SAD pattern of Al-Cu/CF composite showing (a) micrograph containing dark and white regions (b) SAD pattern of dark region showing base alloy of aluminium.

(a)

(b)

Fig. 5.12 TEM micrograph and SAD pattern of Al-Cu/CF composite showing (a) micrograph containing dark and white regions (b) SAD pattern of white region showing carbon present in the fibres.

(a)

(b)

Fig. 5.13 TEM micrograph and SAD pattern of Al-Cu/CF composite showing (a) micrograph containing interfacial reaction product (b) SAD pattern of dark crystal showing aluminium carbide present at the interface.

(a)

(b)

Fig. 5.14 TEM micrograph and SAD pattern of Al-Cu/CF composite showing (a) micrograph containing interfacial precipitate (b) SAD pattern of dark precipitate showing $CuAl_2$ present at the interface.

(a)

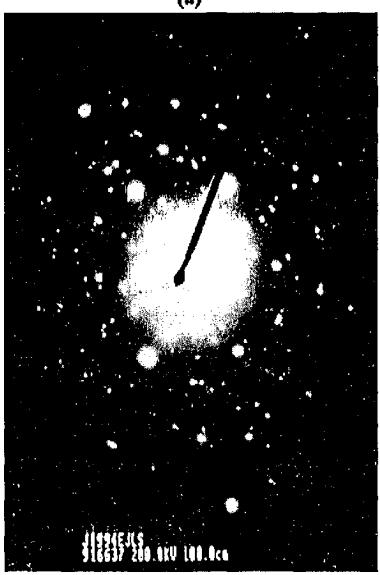

(b)

Fig. 5.15 TEM micrograph and SAD pattern of Al-Cu/CF composite showing(a) micrograph containing white and dark regions alongwith dislocation network (b) SAD pattern of white region showing AlFeSi and other microcrystalline phases.

Table-5.5

X-ray diffraction analysis of Al-Cu/CF composite

Composite	2θ	Sin θ	I/I_o	I/I_o ASTM	d (Å)	hkl	Phase
Al-Cu/CF	21	0.179	16	100	4.30	100	$CuAl_2$
	32	0.275	13	60	2.80	012	Al_4C_3
	38	0.328	100	100	2.36	111,110	Al, Al_2O_3
	44	0.374	25	100	2.06	002	C
	52	0443	30	45	1.74	024	Al_2O_3
	55	0.464	36	100	1.66	110	Al_4C_3
	58	0.481	42	80	1.60	116	Al_2O_3
	62	0.514	10	25	1.50	102	C
	65	0.539	10	22	1.43	220	Al
	73	0.598	10	21	1.29	402	$CuAl_2$
	94	0.730	12	25	1.06	201	C

The X-ray diffraction analysis carried out for Al-Li/CF composites having 66% fibre volume fraction.reveals that besides the primary phase, i.e., LiAl, other phases like Li_2C_2, LiC_{16}, Al_4C_3, and Li_2O are also present in the composite. Table 5.6 shows the various phases present in the composite.

Table-5.6

X-ray diffraction analysis of Al-Li/CF composite

Composite	2θ	Sin θ	I/I_o	I/I_o ASTM	d (Å)	hkl	Phase
Al-Li/CF	24	0.208	14	75	3.70	111	AlLi
	25	0.216	13	100	3.60		LiC_{16}
	33	0.284	29	100	2.71	023	Li_2C_2
	34	0.289	40	100	2.66		Li_2O
	38	0.328	100	100	2.36	111,110	Al, Al_2O_3
	40	0.341	33	100	2.26	220	AlLi
	44	0.374	40	100	2.06	002	C
	52	0.440	11	40	1.75	420	Li_2C_2
	58	0.481	17	80	1.60	116	Al_2O_3
	65	0.539	10	22	1.43	402	Al
	94	0.730	10	25	1.06	201	C

The X-ray diffraction analysis of Al-Zr/CF composite having 66% fibre volume fraction have been carried out for 2θ values ranging from 5° to 120°. The various phases are identified from the diffraction pattern by calculating the d values and comparing these d values to that given in the ASTM data card for diffraction patterns of various compounds. It is observed that besides the primary phase Al_3Zr, other phases like ZrC, Al_4C_3 and Al_2O_3 are also present in the composite. Table 5.7 lists the various phases present in Al-Zr/CF composite having 66% fibre volume fraction.

Table-5.7

X-ray diffraction analysis of Al-Zr/CF composite

Composite	2θ	Sin θ	I/I_0	I/I_0 ASTM	d (Å)	hkl	Phase
Al-Zr/CF	23	0.198	20	60	3.90	101	Al_3Zr
	32	0.275	10	60	2.80	200	ZrC
	33	0.284	27	100	2.71	111	Al_4C_3
	38	0.328	100	100	2.36	111,110 200	Al, Al_2O_3ZrC
	40	0.341	36	100	2.06	002	C
	45	0.385	27	100	2.00	200	Al_3Zr
	58	0.481	37	80	1.60	116	Al_2O_3
	65	0.539	12	22	1.43	220	Al
	94	0.730	10	25	1.06	201	C

5.2 DISCUSSION

The infiltration of fibre preform is expected to divide the molten aluminium alloy stream pushed under high pressure. In absence of fibre preform, a single stream is pushed in the rectangular steel pipe and the solidification takes place dendritically, similar to that in normal castings. But in case of composites having low fibre volume fraction, this forced stream has pushed the loose fibres away from its path leading to inhomogeneous distribution of the fibres. In case of high volume fraction, the fibres are tightly packed in the steel pipe and hence, could not be pushed away by the forced

stream of aluminium alloy. Thus, fibre rich and fibre deficient zones are observed in the composites having low fibre volume fraction whereas the carbon fibres are uniformly distributed in high volume fraction composites.

The few unwetted regions and small porosity as observed in Al-Cu/CF and AlZr/CF composites (Figs.5.1 and 5.3) may be due to the fact that the pressure drop at the infiltration front during penetration is more in these composites (due to high surface tension) as compared to Al-Li/CF composites according to Eqn. (2.9). Thus infiltration front proceeds under relatively higher pressure in Al-Li/CF composites than Al-Cu/CF and Al-Zr/CF composites, which subsequently results in porosity free casting in case of Al-Li/CF composite and porosity containing casting in case of Al-Cu/CF and Al-Zr/CF composites. The presence of unwetted regions as observed in Al-Zr/CF composite (Fig.5.3) may be due to the fact that no superheat has been given during melting of Al-Zr alloy as the melting point/liquidus temperature of the alloy is ~850^{0}C. Thus it is possible that the crystals of Al_3Zr are not dissolved completely and have blocked the interfibre region at few places consequently, have restricted the alloy stream to proceed further. Jarfors et al. (217) have also observed the same behaviour during infiltration of carbon fibres by Al-Ti alloy at the same temperature.

The results of X-ray diffraction clearly show that in all the composites there is a reaction between the carbon fibres and molten aluminium alloys during processing. Jarfors et al. (217) have proposed the following reactions between carbon fibres and Al-Ti alloy as,

$$4Al\ (l) + 3C\ (s) \rightarrow Al_4C_3\ (s) \qquad (5.1)$$

$$Ti\ (l) + C\ (s) \rightarrow TiC\ (s) \qquad (5.2)$$

and,

$$Al_4C_3\ (s) + 3Ti\ (l) \rightarrow 4Al\ (l) + 3TiC\ (s) \qquad (5.3)$$

All these reactions are peritectic and thermodynamically possible. Since Zr is also a reactive carbide forming element like Ti, the same three reactions may also

occur during processing of Al-Zr/CF composites. The chemical reactions proposed for the inferfacial bonding in Al-Li/CF composites are given as,

$$4Li + O_2 \rightarrow 2Li_2O \quad (5.4)$$

and,

$$2Li + 2C \rightarrow Li_2C_2 \quad (5.5)$$

These two reactions are also possible thermodynamically. The presence of intercalation compound LiC_{16} can also be explained on the basis of chemical reaction as it has been reported that alkali metals react with carbon to form intercalation compound where positive ions of the metals are inserted between the basal layers. However, the reaction responsible for the formation of intercalation compound can not be suggested in this study, as it requires a separate thorough investigation. Although in carbon fibres the basal layers are relatively less parallel to the axis, but sufficient enough to form some intercalation compound. The SEM micrographs shown in Fig. 5.5(b) also confirm the absence of any interface in Al-Li/CF composite whereas the interface is quite visible in case of Al-Cu/CF and Al-Zr/CF composite. The EPMA line scan (Fig.5.10) across the interfibre region of Al-Zr/CF composite, too, confirm the presence of zirconium at the interface. Thus it may be concluded that the interface consists of ZrC or ternary carbide of Al and Zr and LiC_{16} in Al-Zr/CF and Al-Li/CF composites respectively.

The TEM micrograph and the SAD pattern, shown in Fig.5.14, reveal the presence of oblong shaped $CuAl_2$ particle near the fibre surface. The EDS point analysis of the interfibre region, given in Table 5.4, also confirms the presence of Cu near the fibre surface, as the concentration of Cu is quite high near the fibre as compare to that away from the fibre surface. It may be therefore concluded that the interface is rich in copper whereas the interfibre region is deficient in copper in Al-Cu/CF composites. Tsai et al. (25) have also observed the same behaviour for Al/CF composites having Al-Cu alloy matrix. Mortenson et al. (2) have pointed out that the reinforcement acts as a barrier to solute diffusion ahead of the liquid/solid interface and the growing solid phase avoids the reinforcement in much the same way that two growing dendrites avoid one another. Consequently, the last portion of the metal to solidify is located either close to or at the fibre/matrix interface. So, in the fibre

reinforced metal matrix composites, the fibre/matrix interface is enriched in solute and in secondary phases.

The TEM micrograph and SAD pattern, shown in Fig.5.13, reveals the presence of Al_4C_3 at the interface. Sanctis et al. (36) have also observed the same behaviour in Al/CF composites. It is clear from this figure that this carbide is in acicular form, which may have an orientation relationship with the matrix and the reinforcement. But in the present study, orientation relationship could not be obtained due the limitation of the TEM equipment for tilting the specimen.

The TEM micrograph shown in Fig.5.15 reveals the presence of dislocation network near the interface and of a precipitate free zone (PFZ) away from the interface. The low dislocation density in this composite may be due to addition of copper in aluminium as it has been reported that the alloying addition of Cu in aluminium lowers the thermal expansion coefficient of the matrix (25). PFZs in Al/CF composites are generally the result of the localized depletion of solute atoms and/or vacancies through their migration to the incoherent fibre interface. An excess vacancy concentration is normally frozen into the matrix during processing at high temperatures. These excess vacancies enhance the homogeneous nucleation of precipitate phases by facilitating the diffusion of solute during processing (160).

RESULTS AND DISCUSSION: PROPERTIES OF SQUEEZE CAST Al/CF COMPOSITES

This chapter describes the results on the properties of different as cast Al/CF composites at ambient temperature. The results on single fibre tensile test are also included in this chapter. The results on the interfacial properties as determined from SEM fractography are also outlined. In the end, the results have been discussed to develop a coherent understanding of these composites in terms of their properties as have emerged from this study. Finally, the strength of the composites has been compared with the reported strength of Al/CF composites by other investigators and reasons responsible for the discrepancy are pointed out.

6.1 RESULTS

6.1.1 Density

Figures 6.1 to 6.3 show the variation of density with fibre volume fraction for different composites. It is clear from these figures that density of the composites decreases with increase in fibre volume fraction. It is also clear that for the same fibre volume fraction, Al-Li/CF composites have lower density as compared to Al-Cu/CF and Al-Zr/CF composites.

It is clear from Figs. 6.1 to 6.3 that in all the composite systems, the density values are more close to law of mixtures values for high fibre volume fraction composites as compared to that for low fibre volume fraction composites.

The density of different as cast Al/CF composites having different volume fraction of carbon fibres is given in the Table-6.1. The calculated values of density for these composites by "Law of Mixtures" are also given in the Table-6.1.

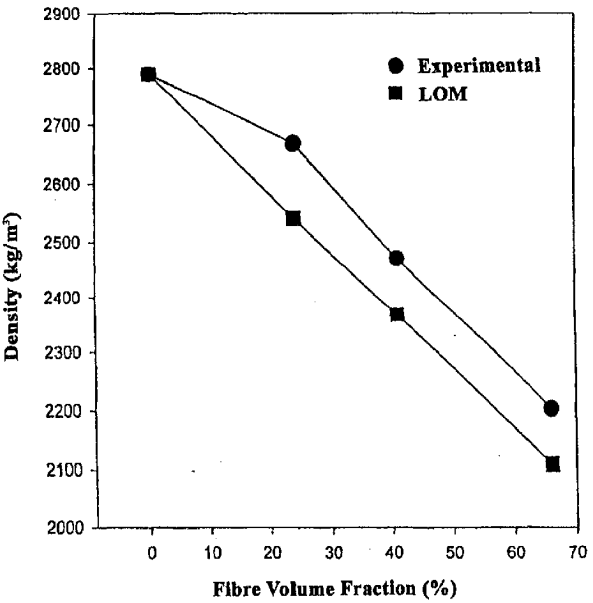

Fig. 6.1 The variation of density with fibre volume fraction for different Al-Cu/CF composites.

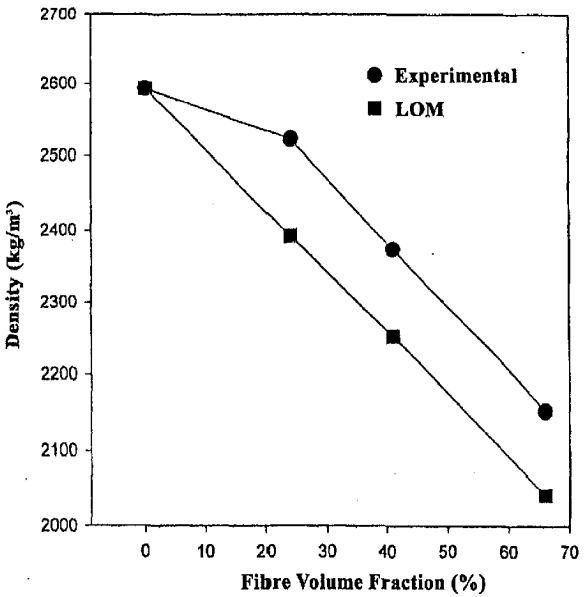

Fig. 6.2 The variation of density with fibre volume fraction for different Al-Li/CF composites.

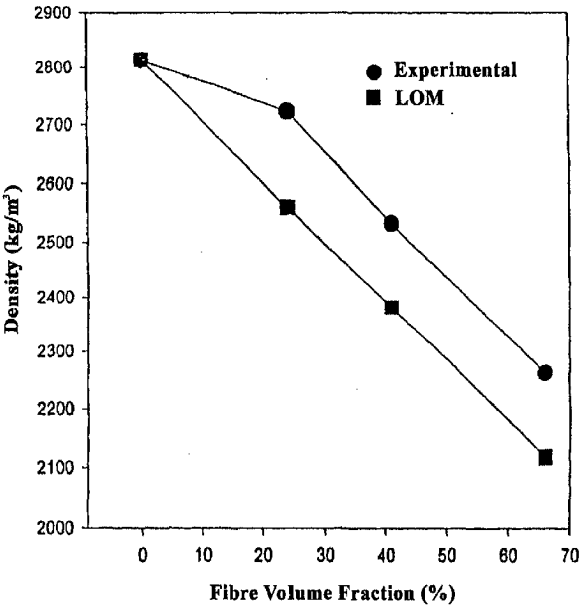

Fig. 6.3 The variation of density with fibre volume fraction for different Al-Zr/CF composites.

Table-6.1

Density of the composites

S.No.	Composite	Volume fraction (%)	Density (kg/m^3)	LOM density (kg/m^3)
1.	Al-4.5 wt.% Cu/CF	0	2789	2789
2.	Al-4.5 wt.% Cu/CF	24	2669	2524
3.	Al-4.5 wt.% Cu/CF	41	2471	2367
4.	Al-4.5 wt.% Cu/CF	66	2203	2109
5.	Al-2.3 wt.% Li/CF	0	2593	2593
6.	Al-2.3 wt.% Li/CF	24	2523	2393
7.	Al-2.3 wt.% Li/CF	41	2374	2252
8.	Al-2.3 wt.% Li/CF	66	2154	2043
9.	Al-5.2 wt.% Zr/CF	0	2813	2813
10.	Al-5.2 wt.% Zr/CF	24	2723	2560
11.	Al-5.2 wt.% Zr/CF	41	2533	2381
12.	Al-5.2 wt.% Zr/CF	66	2262	2118

6.1.2 Hardness

Figures 6.4 to 6.6 show the variation of Brinell hardness for composites with fibre volume fraction. The Brinell hardness values based on "Law of Mixtures" could not be calculated for these composites due to unavailability of hardness data for the fibres in the literature and also it was not possible to experimentally determine the hardness values of carbon fibres due to large size of indentor.

It is observed from Figs. 6.4 to 6.6 that Brinell hardness increases with increase in fibre volume fraction for all the composite systems. It is also revealed from these figures that hardness of the composites varies with alloying addition in aluminium alloy matrix as Al-Zr/CF composites show higher hardness value than Al-Cu/CF and Al-Li/CF composites, all having the same fibre volume fraction.

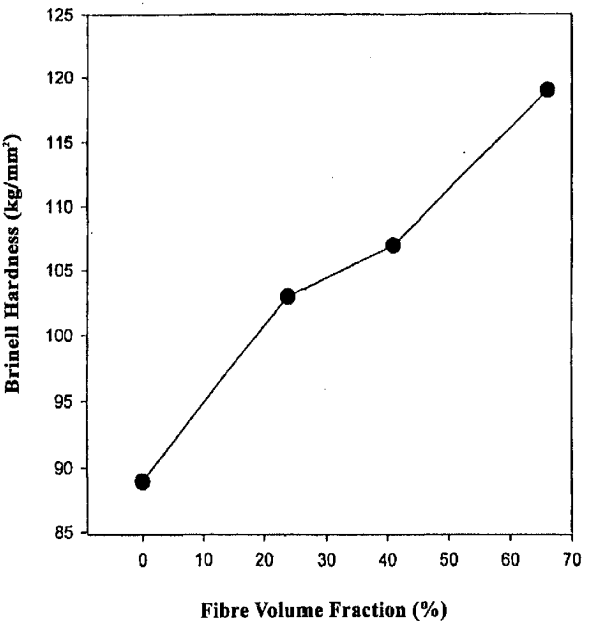

Fig. 6.4 The variation of hardness with fibre volume fraction for Al-Cu/CF composites.

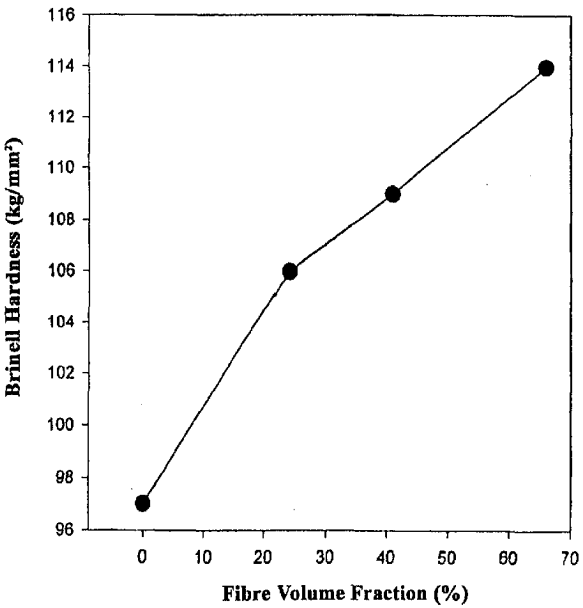

Fig. 6.5 The variation of hardness with fibre volume fraction for Al-Li/CF composites.

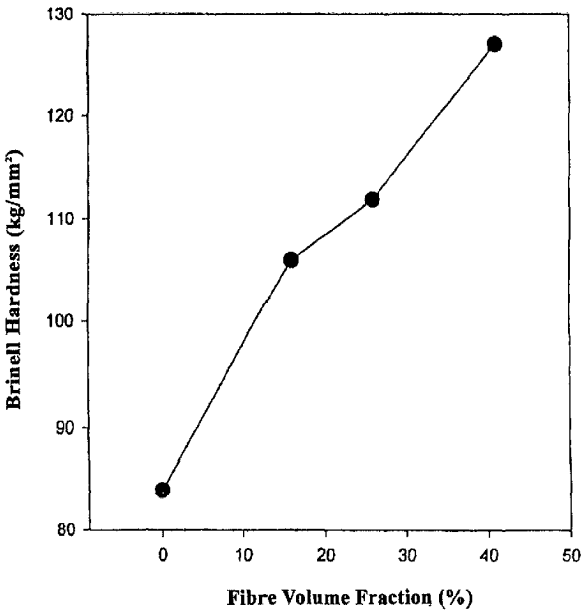

Fig. 6.6 The variation of hardness with fibre volume fraction for Al-Zr/CF composites.

The Brinell hardness of different composites and unreinforced alloys in as cast condition is given in Table 6.2.

Table-6.2

Hardness of composites

S.No.	Composite	Volume fraction (%)	Brinell hardness (kg/mm^2)
1.	Al-4.5 wt.% Cu/CF	0	89
2.	Al-4.5 wt.% Cu/CF	24	103
3.	Al-4.5 wt.% Cu/CF	41	107
4.	Al-4.5 wt.% Cu/CF	66	119
5.	Al-2.3 wt.% Li/CF	0	97
6.	Al-2.3 wt.% Li/CF	24	106
7.	Al-2.3 wt.% Li/CF	41	109
8.	Al-2.3 wt.% Li/CF	66	114
9.	Al-5.2 wt.% Zr/CF	0	84
10.	Al-5.2 wt.% Zr/CF	24	106
11.	Al-5.2 wt.% Zr/CF	41	112
12.	Al-5.2 wt.% Zr/CF	66	127

6.1.3 Fracture Strain

The variation of fracture strain with fibre volume fraction for different composites is shown in Figs. 6.7 to 6.9. It is observed from these figures that fracture strain decreases with increase in fibre volume fraction in all composites. It is also observed from these figures that fracture strain decreases very rapidly with the addition of carbon fibres in the matrix and becomes nearly steady for further increase of fibre volume fraction.

The experimentally determined fracture strain of different as cast composites and unreinforced alloys is given in Table 6.3 which clearly indicates that for same fibre volume fraction, Al-Li/CF composites show higher fracture strain as compared

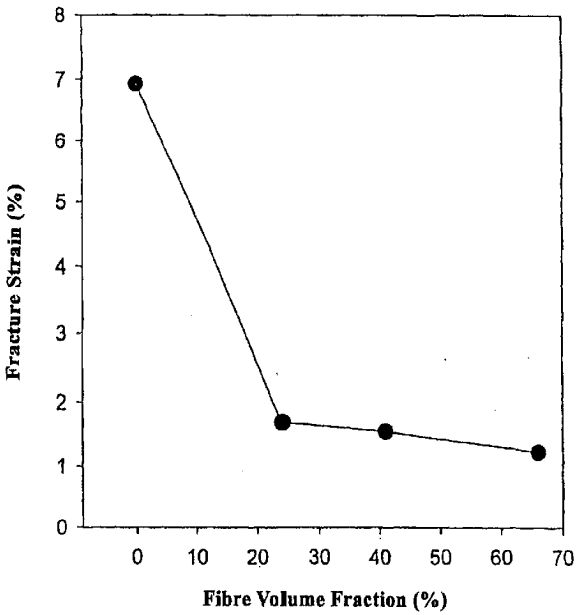

Fig. 6.7 The variation of fracture strain with fibre volume fraction for Al-Cu/CF composites.

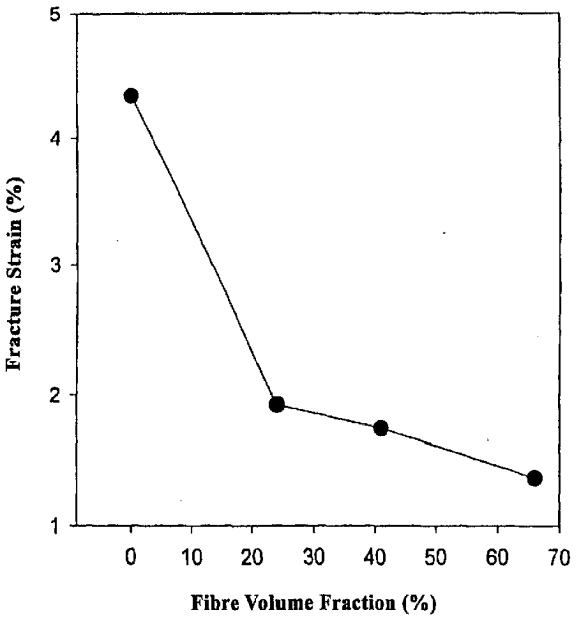

Fig. 6.8 The variation of fracture strain with fibre volume fraction for Al-Li/CF composites.

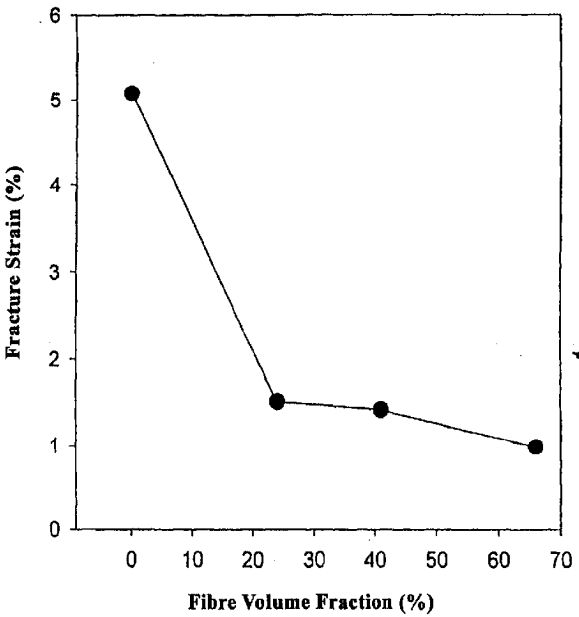

Fig. 6.9 The variation of fracture strain with fibre volume fraction for Al-Zr/CF composites.

to Al-Cu/CF and Al-Zr/CF composites. It is also revealed from Table 6.3 that Al-Li/CF composites having low fibre volume fraction show fracture strain greater than that of fibres whereas Al-Zr/CF composites having low fibre volume fraction show lower fracture strain than that of fibres. The Al-Cu/CF composites having low fibre volume fraction show fracture strain nearly equal to that of fibres.

Table-6.3

Fracture strain of the composites

S.No.	Composite	Volume fraction (%)	Fracture strain (%)
1.	Al-4.5 wt.% Cu/CF	0	6.93
2.	Al-4.5 wt.% Cu/CF	24	1.71
3.	Al-4.5 wt.% Cu/CF	41	1.56
4.	Al-4.5 wt.% Cu/CF	66	1.23
5.	Al-2.3 wt.% Li/CF	0	4.34
6.	Al-2.3 wt.% Li/CF	24	1.92
7.	Al-2.3 wt.% Li/CF	41	1.74
8.	Al-2.3 wt.% Li/CF	66	1.36
9.	Al-5.2 wt.% Zr/CF	0	5.08
10.	Al-5.2 wt.% Zr/CF	24	1.52
11.	Al-5.2 wt.% Zr/CF	41	1.43
12.	Al-5.2 wt.% Zr/CF	66	0.98

6.1.4 Ultimate Tensile Strength

The variation of experimentally determined ultimate tensile strength and theoretically calculated ultimate tensile strength with fibre volume fraction for different composites in as cast condition is shown in Figs. 6.10 to 6.12. It is observed from these figures that tensile stength increases with increase in fibre volume fraction for all the composites, however, strength values are more close to estimated strength values for low fibre volume fraction composites as compared to high fibre volume fraction composites.

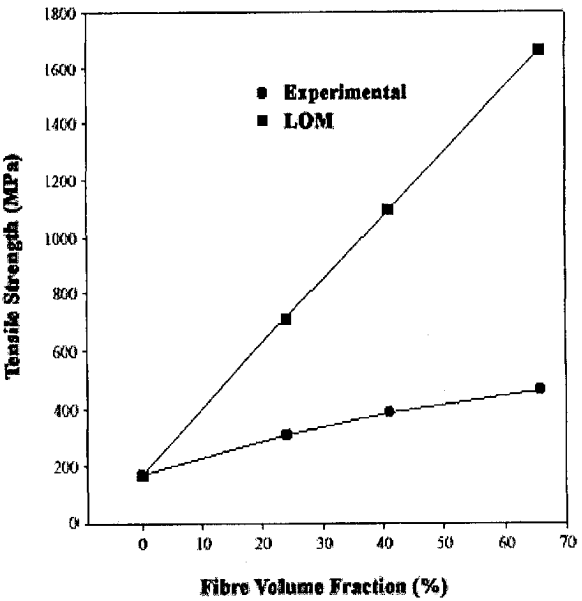

Fig. 6.10 The variation of tensile strength with fibre volume fraction for Al-Cu/CF composites.

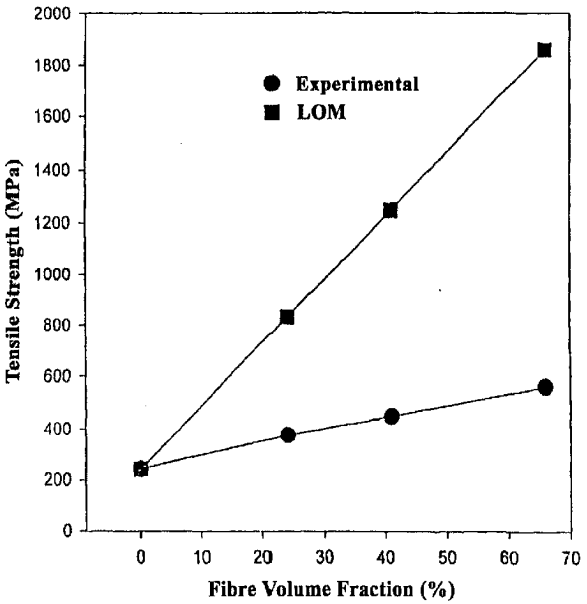

Fig. 6.11 The variation of tensile strength with fibre volume fraction for Al-Li/CF composites.

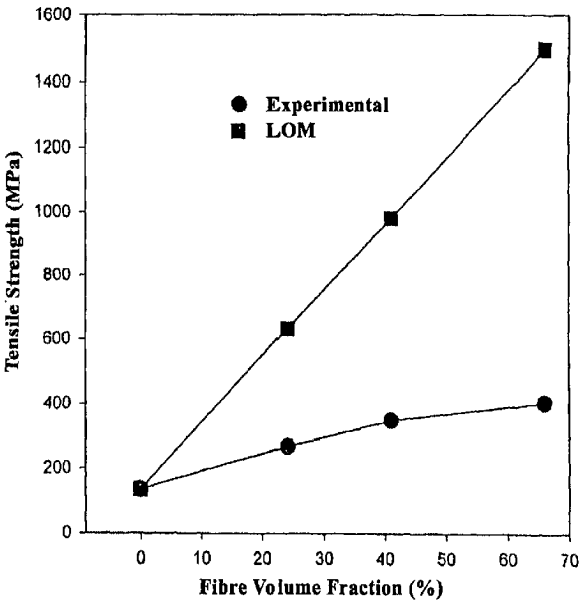

Fig. 6.12 The variation of tensile strength with fibre volume fraction for Al-Zr/CF composites.

The ultimate tensile strength of different composites and unreinforced alloys as determined experimentally and calculated theoretically by "Law of Mixtures" is given in Table 6.4. It is also clear from Table 6.4 that for same fibre volume fraction, Al-Li/CF composites show higher strength as compared to Al-Cu/CF and Al-Zr/CF composites in terms of absolute strength values. However, for low fibre volume fraction, the strength of Al-Zr composite is more close to estimated strength as compared to other composites whereas for high fibre volume fraction, the strength of Al-Li composite is more close to estimated strength as compared to other composites.

Table-6.4

Tensile strength of the the composites

S.No.	Composite	Volume fraction (%)	Tensile strength (MPa)	LOM strength (MPa)
1.	Al-4.5 wt.% Cu/CF	0	168.37	168.37
2.	Al-4.5 wt.% Cu/CF	24	309.19	711.03
3.	Al-4.5 wt.% Cu/CF	41	385.7	1095.41
4.	Al-4.5 wt.% Cu/CF	66	462.45	1660.68
5.	Al-2.3 wt.% Li/CF	0	241.46	241.46
6.	Al-2.3 wt.% Li/CF	24	376.39	830.65
7.	Al-2.3 wt.% Li/CF	41	448.03	1247.99
8.	Al-2.3 wt.% Li/CF	66	561.90	1861.73
9.	Al-5.2 wt.% Zr/CF	0	136.38	136.38
10.	Al-5.2 wt.% Zr/CF	24	277.93	631.32
11.	Al-5.2 wt.% Zr/CF	41	348.40	981.91
12.	Al-5.2 wt.% Zr/CF	66	403.67	1497.47

6.2 Tensile Strength of Carbon Fibres

The Weibull distribution of the tensile strength of preheated carbon fibres is shown in Fig.6.13. The Weibull distributions of tensile strength of carbon fibres extracted from different composites are shown in Figs.6.14 to 6.16. The value of scal parameter in the distribution indicates the degree of scattering in the distribution a

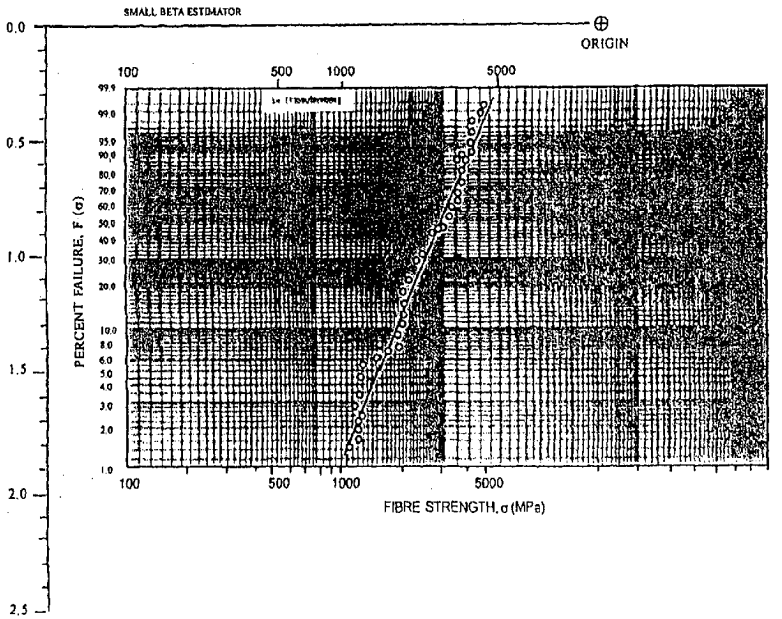

Fig. 6.13 The Weibull Distribution of strength for preheated fibres.

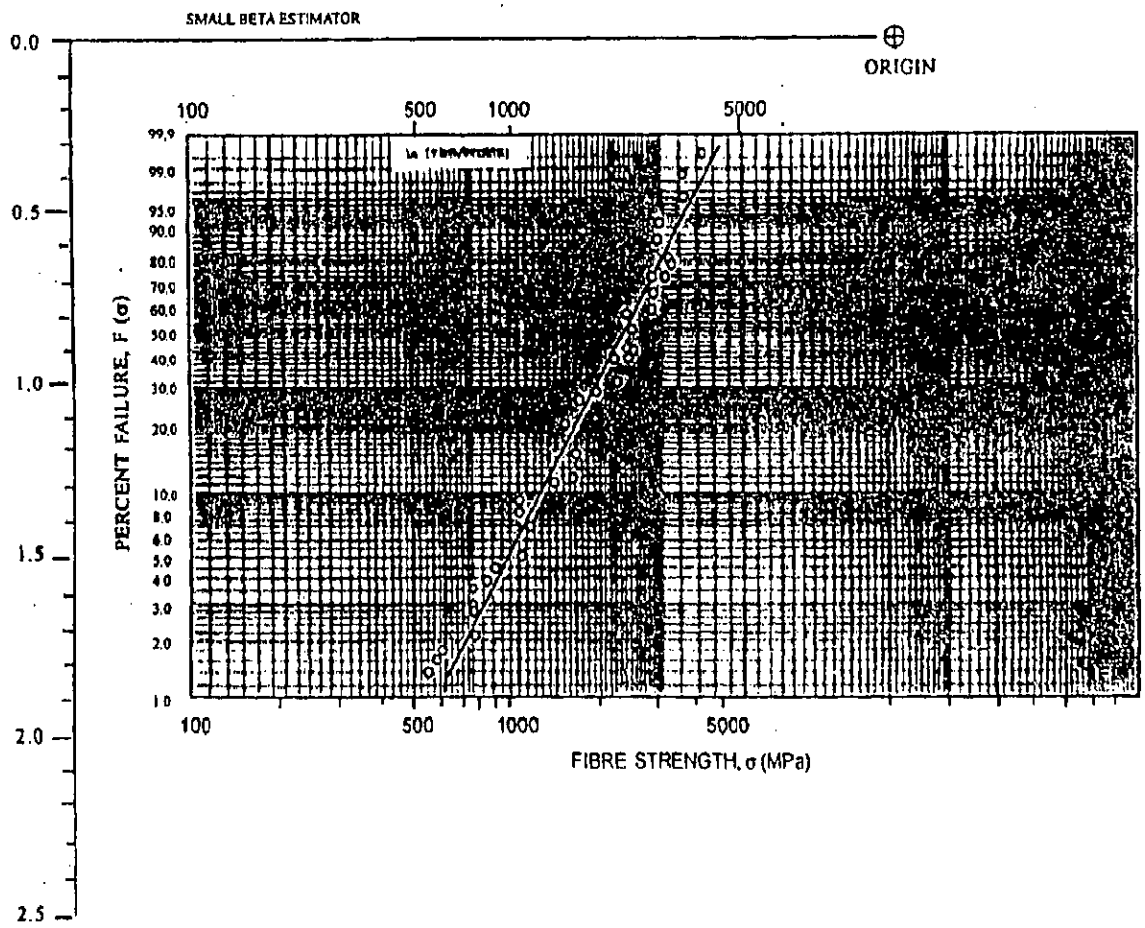

Fig. 6.14 The Weibull Distribution of strength for the fibres in Al-Cu/CF composites.

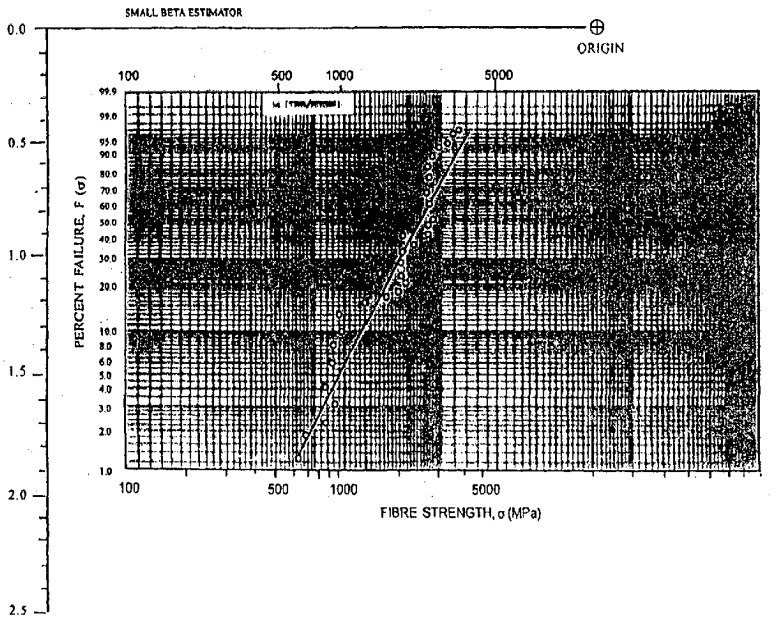

Fig. 6.15 The Weibull distribution of strength for the fibres in Al-Li/CF composites

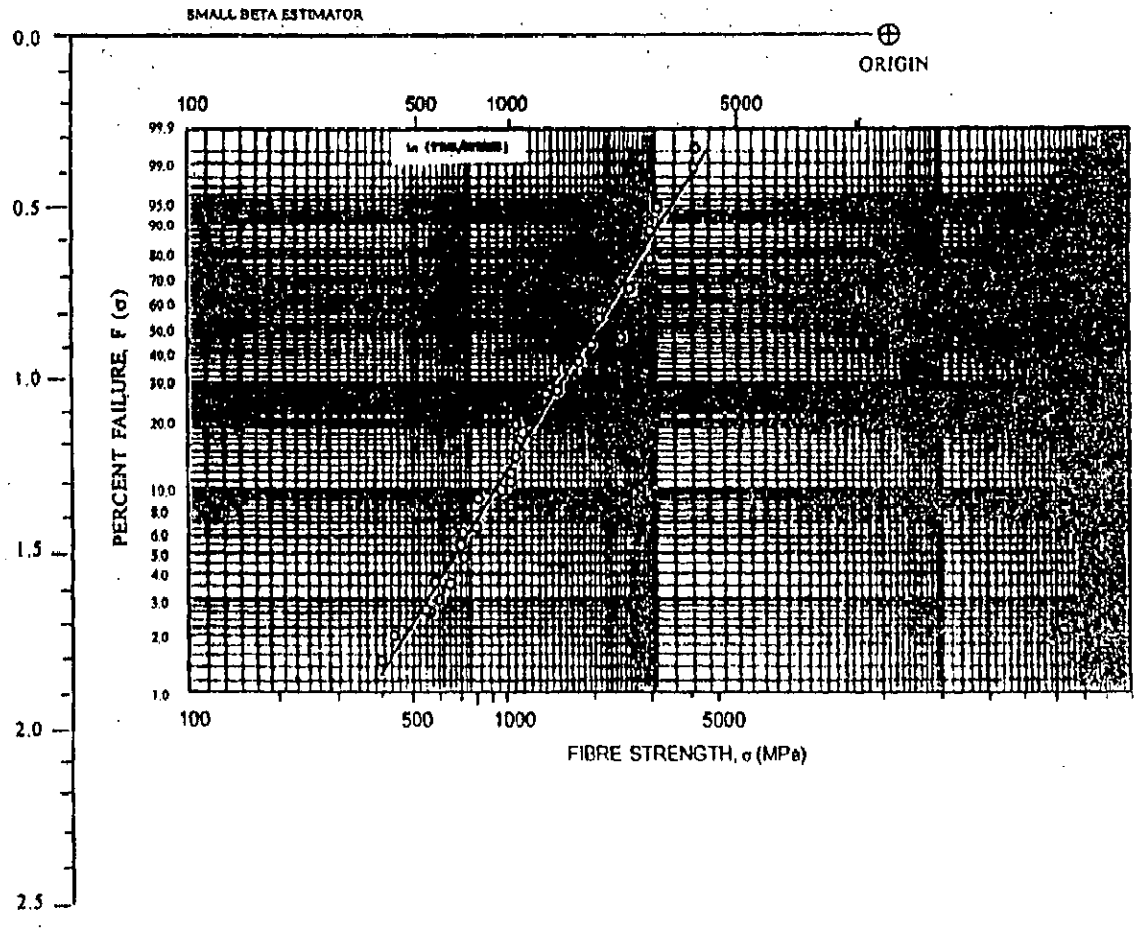

Fig. 6.16 The Weibull distribution of strength for the Al-Zr/CF composites.

larger value of scale parameter represents less scattering. The value of shape parameter gives probability of fracture at a stress level of 100 MPa and therefore, for a low value of shape parameter, the strength is considered higher. The tensile strength of various carbon fibres as determined from Weibull distribution is given in Table 6.5.

Table-6.5

Strength of carbon fibres

S. No.	Fibres	Scale parameter α (MPa)	Shape parameter β	$\Gamma(1+1/\beta)$	Fibre strength σ_f (MPa)
1.	Preheated	3250	9.038	0.9474	3079.05
2.	Al-4.5 wt.% Cu	2600	6.846	0.9344	2429.44
3.	Al-2.3 wt.% Li	2900	6.250	0.9298	2696.42
4.	Al-5.2 wt.% Zr	2400	4.801	0.9161	2198.64

The apparent and real transfer efficiency of fibre strength abbreviated as ATEFS and RTEFS respectively and as defined by Cheng et al. (12) are calculated by using the strength of the as received carbon fibres and of the fibres extracted from the as cast composites. The apparent and real transfer efficiency of carbon fibres in various composites are given in Table 6.6.

Table-6.6

Transfer efficiencies of the carbon fibres in the composites

Composite	Volume fraction	Fibre strength (MPa)	Composite strength (MPa)	ATEFS	RTEFS
Al-4.5 wt.% Cu/CF	24	2429.44	309.19	0.300	0.431
Al-4.5 wt.% Cu/CF	41	2429.44	385.70	0.287	0.413
Al-4.5 wt.% Cu/CF	66	2429.44	462.45	0.253	0.364
Al-2.3 wt.% Li/CF	24	2696.42	376.39	0.310	0.402
Al-2.3 wt.% Li /CF	41	2696.42	448.03	0.296	0.384
Al-2.3 wt.% Li /CF	66	2696.42	561.90	0.292	0.379
Al-5.2 wt.% Zr/CF	24	2198.64	277.93	0.274	0.436
Al-5.2 wt.% Zr /CF	41	2198.64	348.40	0.256	0.408
Al-5.2 wt.% Zr /CF	66	2198.64	403.67	0.225	0.359

6.1.6 Fractography and Interfacial Properties

The SEM micrographs of the fractured surfaces of tensile specimens corresponding to different as cast composites are shown in Figs. 6.17 to 6.19. It is observed from these fractographs that there are various fractographic patterns as different composites have different fibre pull out lengths, which indicate different interfacial bonding in these composites. The interfacial shear strength and shear strain of different composites, as determined after measuring the fibre pullout length from these fractographs, is given in Table 6.7.

Table-6.7

Interfacial shear strength and shear strain of composites

Composite	Fibre volume fraction	Fibre pullout length (μm)	Fibre strength (MPa)	Distance between fibres (μm)	I Shear strength	I shear strain
Al-Cu/CF	66%	3.62	2429.44	5.007	1762 MPa	0.72
Al-Li/CF	66%	13.32	2696.42	5.007	531 MPa	2.66
Al-Zr/CF	66%	1.14	2198.64	5.007	5063 MPa	0.23

6.2 DISCUSSION

The density of composites having same aluminium alloy matrix is found to decrease with increase in volume fraction of carbon fibres. It is in well agreement with the fact that density of carbon fibres (1.76 g/cm^3) is significantly lower than the density of the aluminium matrices (i.e., 2.59, 2.79 and 2.81 for Al-Li, Al-Cu and Al-Zr respectively). The same explanation can be given for the observed increase in the density of the composites as one proceeds from aluminium-lithium matrix composites to aluminium-zirconium composites having same volume fraction of carbon fibres.

The density of unreinforced alloys as given in Table 6.1 is found to be lowest for aluminium-lithium alloy (i.e., 2.593 gm/cm^3) and highest for aluminium-zirconium alloy (2.813 gm/cm^3) whereas aluminium-copper alloy has a density value in between the two (2.789 gm/cm^3). It is very well in agreement with the earlier

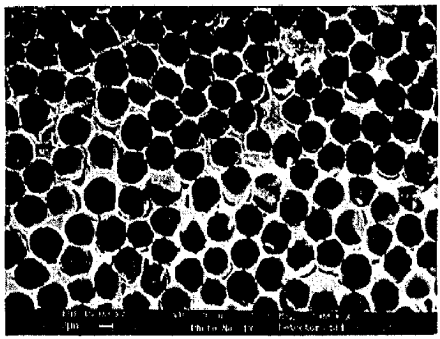

(a)

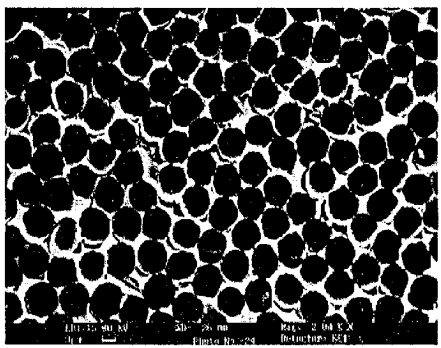

(b)

Fig. 6.17 SEM micrographs of the fractured surface in Al-Cu/CF composite having 66% fibre volume fraction (a) specimen 1 (b) specimen 2.

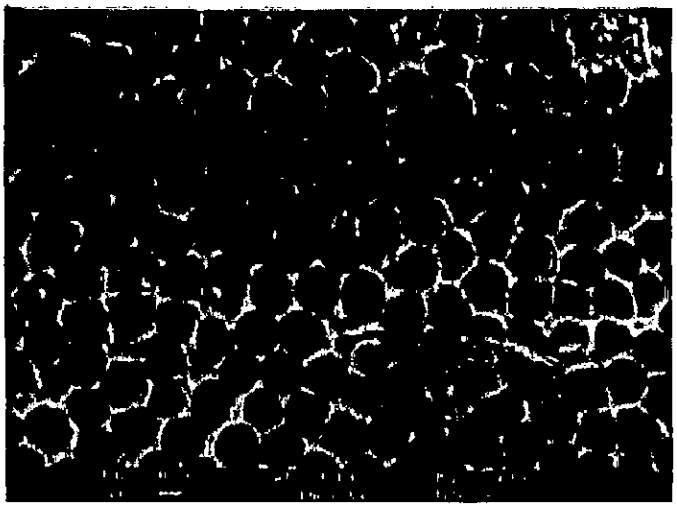

(a)

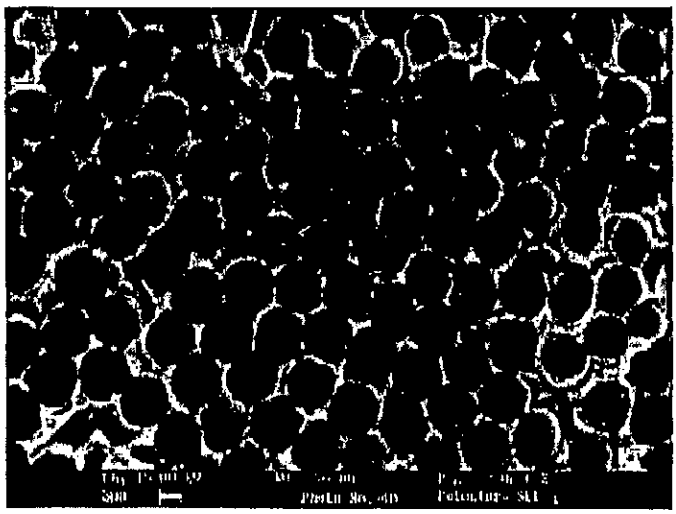

(b)

Fig. 6.18 SEM micrographs of the fractured surface in Al-Li/CF composites having 66% fibre volume fraction (a) specimen 1 (b) specimen 2.

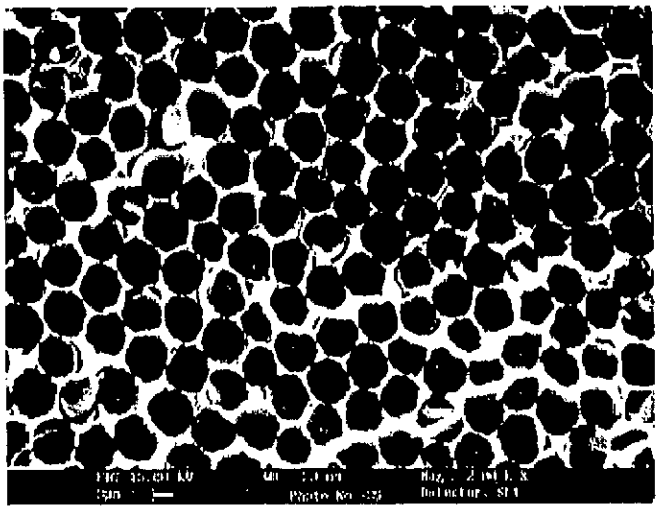

(a)

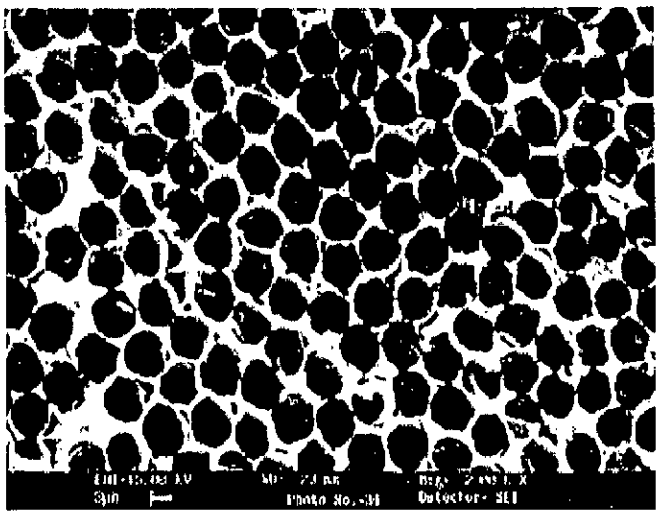

(b)

Fig. 6.19 SEM micrographs of the fractured surface in Al-Zr/CF composite having 66% fibre volume fraction (a) specimen 1 (b) specimen 2.

reported data that density of aluminium (2.70 gm/cm^3) decreases with the addition of lithium whereas it increases with the additions of copper and zirconium equally with each wt.% of these elements (218). Since addition of zirconium is more than copper, aluminium-zirconium alloy shows higher density than aluminium-copper alloy. These unreinforced alloys have been casted together with composites (processing parameters are same), hence can be considered equivalent to composite matrices.

The experimentally determined density values for as cast composites are found to be very close to the estimated density values based on law of mixtures. In most of the cases, the experimental density values are slightly higher than the estimated density values. This difference may be attributed to unavoidable incorporation of foreign particles during solidification processing of the composites and not using the precise method for density determination.

It is well understood that the mechanical properties of fibre reinforced composites largely depend upon the chemical interaction between fibres and matrix. So in the present study, it is necessary to know the extent of chemical interaction between carbon fibres and aluminium matrices. The extent of chemical interaction between fibres and different aluminium alloy matrices is evaluated in terms of the fibre strength degradation, determined by single fibre tensile test of carbon fibres extracted from composites having different matrices.

The strength of carbon fibres is found to decrease considerably by preheating treatment and the degradation rate is very high (11%). This large degradation may be attributed to the mechanical damage during preparation of fibre preform by hand and the oxidation of high strength carbon fibres during preheating at 650^{0}C in argon atmosphere as even ultra pure argon gas contains some amount of oxygen. Krishan et al. (15) have reported that graphite particles get oxidized above 400^{0}C during preheating whereas Mercier et al. (219) have shown experimentally the evolution of CO and CO_2 from carbon fibres at 650^{0}C during heating. Cheng et al. (12) have reported a degradation rate of 19% during preheating of carbon fibres at 375^{0}C in air. Therefore, it can be concluded that degradation of carbon fibres during preheating at high temperatures can be reduced by using argon or inert gas atmosphere. Kimura at al. (17) have also observed a degradation rate of 6.5% during preheating of high

modulus carbon fibres at 800^0C for 30 minutes. This lower degradation rate during preheating may be attributed to the different microstructure of high modulus carbon fibres with respect to high strength carbon fibres which generally contain more active carbon atoms exposed to the atmosphere (19).

The carbon fibres extracted from Al-Zr/CF composites show lowest tensile strength of 2198.64 MPa with a degradation rate of about 37% and carbon fibres extracted from Al-Li/CF composites show highest tensile strength of 2696.42 MPa with a degradation rate of about 23% whereas carbon fibres extracted from composites having Al-Cu/CF composites show an intermediate tensile strength of 2429.44 MPa with a degradation rate of 31%. Because of high reactivity of high strength carbon fibres with aluminium, the high strength degradation of the fibres after squeeze casting has been marked.

The light degradation of fibre strength in Al-Li/CF composites is due to the disruptive effect of lithium on the oxide layer of the aluminium metal surface. Lithium, being more electropositive than aluminium, probably substitutes aluminium in the oxide layer and brings about a weakening of the film (29). It is also reported (59) that alkali metals like lithium react with carbon and diffuse in bulk to form intercalation compounds. As the presence of intercalation compound is observed in Al-Li/CF composites, it is possible that lithium present on the surface may have diffused in carbon fibres and may have formed some intercalation compounds at the fibre surface. Most probably, this layer of intercalation compound has restricted the chemical interaction between aluminium and carbon fibres.

In case of aluminium-zirconium alloy matrix, the zirconium carbide initially formed in the free liquid due to dissolution of carbon fibres at the entrance of the preform. As the infiltration front proceeds further, the melt, which is depleted in zirconium reacts with the carbon fibres to form aluminium carbide. This aluminium carbide form a layer around the carbon fibres and due to plate like morphology grows outwardly towards the matrix. The melt is again depleted in aluminium due to formation of aluminium carbide. The zirconium present in melt then reacts with the aluminium carbide layer to form zirconium carbide.

Jarfors et al. (217) have also observed the same phenomenon during infiltration of graphite fibres by molten Al-Ti alloy. However, in this case the degradation is more than that with aluminium-lithium matrix, which may be attributed to the acceleration in the growth of zirconium carbide due to melt enrichment in zirconium.

The medium degradation of carbon fibres in Al-Cu matrix may be attributed to the fact that copper is neutral towards carbon fibres and aluminium is less reactive than zirconium in context of carbon fibres. The fact of the heavy degradation of high strength carbon fibres in aluminium alloy matrix composites is consistent with the results reported by other workers (12).

The Brinell hardness of unreinforced alloys is found to be 89, 97 and 84 kg/mm^2 for Al-Cu alloy, Al-Li alloy and Al-Zr alloy respectively. The high hardness value of aluminium-lithium alloy may be due to the presence of various intermetallic phases as this alloy contains Cu, Mg and Zr as alloying addition whereas aluminium copper alloy has $CuAl_2$ (intermetallic) in the solution and Al-Zr alloy have Al_3Zr (intermetallic) phase in the solution.

The Brinell hardness of carbon fibre-aluminium alloy matrix composites is found to increase with increase in fibre volume fraction. However, the increase in hardness is significantly higher than as one may estimate by the law of mixtures. It may be due to the formation of carbide phase at the interface of carbon fibres and aluminium alloy matrices. This hard carbide phase restricts the penetration of the indentor in the composite, although relatively soft aluminium matrix surrounding the fibres yields under the indentation load because of the pushing effect of hard carbide phase to the soft aluminium alloy matrix. The flow in aluminium alloy matrix adjacent to the carbide phase may get more restrained as the fibre volume fraction increases. It is due to the reduction in the area of interfibre region, which finally results in the increased hardness of the composites.

It is observed that for same fibre volume fraction, Al-Zr/CF composites show highest hardness values whereas Al-Li/CF composites show lowest hardness and aluminium zirconium alloy composites show hardness values in between these two. It

may be due to different amount of carbide phase present in the composites as the reactivity of carbon fibres varies with matrices. The degradation rate is a measure of the reactivity between carbon fibres and aluminium alloy matrices. A high degredation rate is indicative of high reactivity. As the carbon fibres extracted from Al-Zr/CF composites show high degradation rate, the reactivity or carbide formation will be more in these composites. On the other hand, the degradation of carbon fibres in Al-Li/CF composites is lowest, the carbide formation will be less. Since the degradation rate of carbon fibre in Al-Zr/CF composites is higher than that in Al-Li/CF and Al-Cu/CF composites, Al-Zr/CF composites show highest hardness.

The fracture strain of the fibre reinforced composites depends upon the interfacial bonding. A strong interface generally results in the planar fracture of the composite while weak interface enables the debonding of the fibres and helps in the crack blunting along the fibre axis. Thus the composites having debonded fractured surface show high fracture strain (88).

The interfacial shear strain and shear strength of the composites based on the theoretical models also confirm the above predictions. The Al-Zr/CF composites show lowest interfacial shear strain which may be responsible for the low fracture strain of this composite whereas the Al-Cu/CF and Al-Li/CF composites have sufficient debonded fibres and relatively long fibre pull out resulting in the observed higher fracture strain of these composites as compared to Al-Zr/CF composite.

The decrease in fracture strain of the composites with increasing fibre volume fraction has also been observed by other workers (5). As pointed out by Lin (101) that in a composite containing fibres of 10 μm diameter, a reaction zone of 1 μm thickness corresponds to a reaction zone to fibre volume ratio of 0.44. In other words, for a composite having 20% fibre volume fraction, there will be roughly 9vol.% reaction zone in the composite. This reaction zone is nothing but the brittle phase in the composite. The amount of this brittle phase increases with increasing fibre volume fraction, which makes the composite to be more brittle. Thus in the present investigation also, the decrease in the fracture strain of the composite with increasing

fibre volume fraction may be attributed to the increasing amount of brittle phase in the composite with fibre volume fraction.

The tensile strength of unreinforced aluminium alloys is found to vary considerably with alloying additions as unreinforced Al-Li alloy has a tensile strength of 241 MPa whereas unreinforced Al-Zr alloy and Al-Cu alloy have a tensile strength of 136 MPa and 168 MPa respectively. This variation may be attributed to the presence and distribution of different phases in these alloys. The observed increase in the tensile strength of the composites with increasing fibre volume fraction may be attributed to the high strength of carbon fibres with respect to aluminium alloy matrices.

It is also observed that for same fibre volume fraction, Al-Li/CF composites have highest strength while Al-Zr/CF composites have lowest strength. On the other hand, Al-Cu/CF composites have strength values in between these two. This behaviour can be explained on the basis of the transfer efficiency of the carbon fibres in different aluminium alloy matrix composites. The apparent and real transfer efficiencies of fibre strength, abbreviated as ATEFS and RTEFS respectively, are given in Table 6.6. The ATEFS values, as given in Table 6.6, are highest for Al-Li/CF composites and lowest for Al-Zr/CF composites whereas for Al-Cu composites, these values are slightly less than that of Al-Li/CF composites.

It is apparent from these results that the carbon fibres in Al-Li/CF composites have effectively strengthened the aluminium-lithium matrix by transferring their excellent strength to the composites. But it is not true in real sense as in case of low fibre volume fraction composites, the tensile strength of Al-Zr/CF composites is found to be more close to the theoretically estimated strength values as compared to Al-Cu/CF and Al-Li/CF composites. The real transfer efficiency (RTEFS), as given in Table 6.6, presents the true strengthening of the matrices by carbon fibres. It is found that carbon fibres have higher transfer efficiency in Al-Zr/CF composites having lower fibre volume fraction whereas these have higher transfer efficiency in Al-Li/CF composites for high fibre volume fraction. This behaviour can be explained on the basis of fibre distribution in different matrices. As shown in Fig.5.4 the fibres are

distributed more uniformly in Al-Li/CF composite as compared to Al-Cu/CF and Al-Zr/CF composites.

As shown in Table 6.4, for same fibre volume fraction the longitudinal tensile strength values vary considerably from the highest value for Al-Li/CF composites to the lowest for Al-Zr/CF composites in accordance of the tensile strength of unreinforced Al-Li which is much higher than that of Al-Zr alloy.

It is summarized so far from the above results that the reasons for the variation in the strengthening behaviour of carbon fibres with different matrices appear to be the following:

(i) Carbon fibres have been degraded by oxidation during the preheat treatment of fibre preforms.

(ii) The high strength fibres have been attacked heavily by Al-Cu and Al-Zr matrices and lightly by Al-Li matrix.

These two reasons given above are consistent with the single fibre tensile tests, however, they can not sufficiently explain the changes from the stand point of apparent and real strength transfer efficiencies of carbon fibres.

Figs. 6.17 to 6.19 show the longitudinal tensile fracture surfaces of different carbon fibre-aluminium alloy matrix composites. It can be seen that there are various fractographic patterns indicating that these composites have different interfacial bonding. On the fractured surface of Al-Li/CF composite (Fig.6.18), long and numerous fibre pullouts are observed which is a characteristic of weak interface. This long fibre pullout fracture pattern relates to a good transfer efficiency of fibre strength into the composite.

As shown in Fig.6.17, the fibre pull out on the fractured surface of Al-Cu/CF composites is much shorter than that of Al-Li/CF composite, which corresponds to a very high transfer efficiency of fibre strength and a strong interfacial bonding. It can be therefore concluded that the improvement in bonding can make a more efficient strength transfer from carbon fibres to the composites.

The fractured surface micrograph of Al-Zr/CF composites as shown in Fig.6.19 has a relatively flat fracture surface with some short fibre pullout on it. This suggests that the interfacial interactions are more pronounced between carbon fibres and matrix in these composites as compared to Al-Li/CF and Al-Cu/CF composites, discussed previously. This pattern with negligible pullout relates to a very strong interface and a lower transfer efficiency of fibre strength. From these observations, it is concluded that a very good longitudinal tensile strength corresponds to an intermediate bonding that causes an intermediate pull out.

The high strength carbon fibre-aluminium system has a high reactivity between the fibres and the aluminium matrix, which results in formation of a carbide phase at the fibre-aluminium interface. It has been reported that the reaction formed carbide phase grows as acicular inclusions that embedded themselves both in the matrix and in the fibres to make interfacial bonding very strong and cause surface defects on the carbon fibres (88). It is therefore considered that the carbide phase and the strong interfacial bonding not only result in premature fibre failure by a notch effect but also cause the unexpected planar fracture of Al/CF composites with negligible fibre pullout on the fracture surface. Fig. 6.17 is the longitudinal tensile fracture morphology of Al-Cu/CF composite showing an approximately planar fracture with little fibre pull out and partial debonding of the interface between the fibres and Al-Cu matrix. From the same figure, it can be seen that cracks originated at the brittle interfacial zone and propagated along the fibre matrix interface near the fracture surface but the cracks could not completely debond the interface to let the fibres pullout. Moreover, the notch effect of brittle products caused a high stress concentration and consequently a premature fibre failure. This planar fracture mode has made the carbon fibres unable to fully use their strength before final failure of the composite.

Further, as shown in Fig. 6.19, the crack propagation in Al-Zr/CF composite is through the carbon fibres. Because of the excess chemical interaction between fibres and the matrix, cracks originating in the interface proceed through the fibres and split them into two parts instead of debonding the interface. This implies that the interfacial strength between the fibres and the matrix was even stronger than the shear strength of the carbon fibres. The above observations indicate that cracks in Al-Zr/CF

composites can not debond the interface between carbon fibres and aluminium matrices to propagate along the fibre axis because of the strong interfacial bonding produced by the probable formation of zirconium carbide but instead propagate through the plane of fracture by breaking carbon fibres perpendicular to the fibre axis.

In general, the above results and discussion imply that the interface characteristics of carbon fibres and aluminium matrices have an important bearing on the transfer efficiency of fibre strength and the mechanical properties of Al/CF composites. An intermediate fibre pullout on the fracture surface; i.e., an intermediate interfacial bonding and no heavy interfacial reactions corresponds to a good transfer efficiency of fibre strength.

The reported law of mixtures predictions are based on the fibre strength evaluated in the present study. The flaw density of the fibre is proportional to its length. Since fibre length of 25 mm is used to determine their strength in the composites, which is less than the fibre length of 65 mm in the composite, it may be possible that fibre strength evaluated in the present study is significantly higher than the actual fibre strength in the composites. Thus, the law of mixtures predictions are quite higher than the experimental strength values. As a result, the strength of the composites is far lower than the estimated strength.

6.3 COMPARISON OF RESULTS

The strength of Al-Cu/CF and Al-Zr/CF composites having 41% fibre volume fraction is lower than the strength of Al/CF composites reported by Cheng et al. (12). This difference may be attributed to the low processing temperature and pressure used by Cheng et al. (12) as it has been reported that composite strength increases up to a pressure of 45 MPa and decreases afterwards (220). The high strength of Al-Li/CF composites in the present study may be attributed to the less degradation of carbon fibres in Al-Li alloy matrix as compared to the matrices used by Cheng et al. (12).

A MODEL TO PREDICT THE COMPRESSIVE BEHAVIOUR OF CARBON FIBRE IN THE SQUEEZE CAST Al-ALLOY MMC.

7.1 INTRODUCTION

Squeeze casting technique, used to produce fibre reinforced metal matrix composite (FMMC), can be described as a two-step process: fibre preforming followed by liquid alloy injection under pressure. While the preforming orients the fibres into a skeleton of the actual part of the ingot, the final microstructure depends to a great extent on the compaction of the preform to the desired thickness during squeezing in the molten state. Here, the matrix is important for binding the fibres together and enabling the composite to resist the effects of environment exposure thus assuring the basic strength of the material. On the other hand, the type and amount of reinforcement govern the strength and stiffness of the composite.

To facilitate the understanding of preform compaction, it is useful to review the behaviour of fibre preform under compressive loading. The bending and tensile deformations of fibres have been more extensively studied than the compressive properties. The compaction of a preform flattens the fibre bundles, reduces the pores and gaps among the fibres and results in elastic deformation and inter-layer packing. All these factors enhance the overall composite fibre volume fraction. The models proposed by researchers for predicting the compaction behaviour of fibrous materials can be divided into two categories, i.e., phenomenological and mechanistic. The former is based on empirical relationships between compaction pressure and a parameter representing either thickness or volume fraction (221,222) while the latter is based on the beam theory or analogies with the compressibility of gases (223-226).

Based on the beam theory, many theoretical compressibility models have been proposed by several investigators. In 1946, Van Wyk (223) was perhaps the first to treat the fibres as beams in Kirchhoff bending. The problem was simplified by assuming the compaction process to be dominated by fibre bending and by ignoring

the twisting, slipping and extension of fibres. Nearly four decades later, Gutowski (225) developed a simple expression similar to that of Van Wyk (223) for the compaction of lubricated aligned fibre rovings. The predictions based upon this model showed good agreement with the results of compaction experiments. Gutowski and co-workers (227-229) further developed the constitutive equation for a mass of pre-impregnated aligned continuous fibres.

Gutowski's model was also modified and extended to examine unlubricated fibre bundles by other researchers (230,231). Hoffman and Beste (221) discussed about an exponential thickness-pressure function for fibres under compressive pressure. A hyperbolic function was considered later by Bogaty et al. (224). A typical pressure-thickness curve is depicted in Fig.7.1. This curve can be divided into three parts namely, two linear parts and a non-linear part. The initial linear region corresponds to the preform compaction, primarily due to the reduction of pores and gaps among the fibres. The second non-linear region corresponds to the infiltration rate at which the infiltration of Al-alloy liquid melt takes place into the carbon fibres. Because of this effect, the initial diameter of the fibre is increased. This increase in diameter is related to the infiltration rate by Arrhenius type exponential rate equation. The third stage is dominated by the bending deformation. Matsudaira and Qin (232) used a linear equation, an exponential equation and a linear equation to regress the three parts of the compaction curve and studied the compressive properties experimentally.

The third linear relation between the preform thickness and the applied pressure is attributed to the bending deformation of the preform. The modeling of this linear portion of the curve initiates at the point $(2r_{f0}, p_0)$, where the previously applied pressure has brought the fibre diameter to $2r_f$. It should be noted that the linear elastic deformation of the preform would no longer be recoverable once the compacted fibres are impregnated within a matrix material, which then solidifies. Chen and Chou (233) presented a theoretical study of elastic deformation during the compaction of woven fabric preform in liquid composite moulding processes.

Present analysis focuses on '3D model of the unit cell' of fibre preform. This has been proposed with certain assumptions for predicting the compressive behaviour

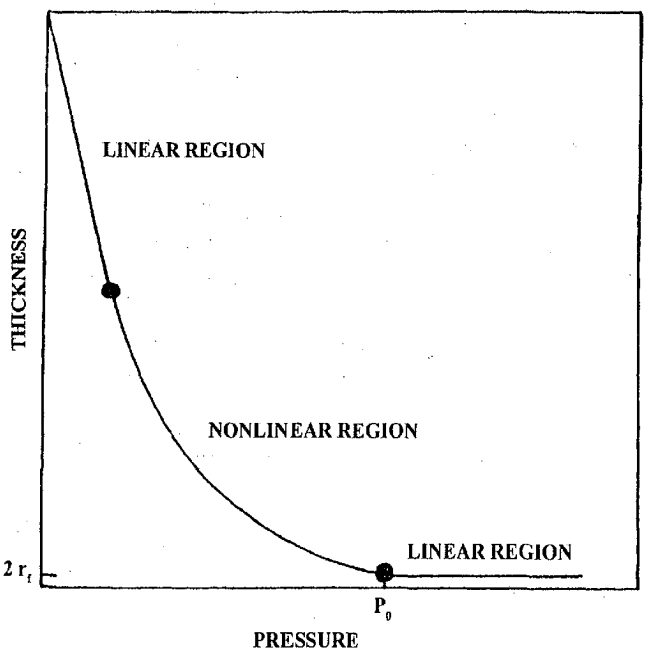

Fig. 7.1 Schematic diagram showing thickness and pressure relationship of the fibres in the mould.

of fibres. On the basis of this model, the relationship between composite fibre volume fraction and preform thickness reduction has been established. A prediction of the limiting fibre thickness reduction is also obtained.

7.2 ASSUMPTIONS AND DESCRIPTION OF COMPACTION PROCESS

A micro-mechanical model is proposed to develop the compaction behaviour of fibre preform used in the squeeze casting process. The assumptions made for the analytical study are,

(i) The unit cell repeats in the plane, which is infinite in extent.
(ii) The external compressive force is applied uniformly on the preform surface.
(iii) The elastic deformation of the fibres takes place only in its thickness direction, i.e., neglecting its effect in plane deformation.
(iv) No voids and gaps exist between the fibres in the start of the third region.
(v) During the compaction process, the fibre shape deforms, but the original cross-sectional area remains constant.

Figure 7.2 shows a schematic diagram of carbon fibre of radius, r_f, and length, l, corresponding to pressure, P_o. The fibre consists of two equal halves. The top surface is designated by the subscript, t, i.e., z_t, the bottom surface is designated by subscript, b, i.e., z_b and the contacting surface is denoted by subscript, c, i.e., z_c. Here, we see the sinusoidal cross-section shape of the fibre. Following Ito and Chou (234), the fibre surface can be defined as follows:

$$z_t = \frac{r_f}{2}\left(\sin\frac{2\pi}{a}x + \sin\frac{2\pi}{a}y\right) \tag{7.1}$$

$$z_t = \frac{r_f}{2}\left(-\sin\frac{2\pi}{a}x + \sin\frac{2\pi}{a}y\right) \tag{7.2}$$

$$z_t = -\frac{r_f}{2}\left(\sin\frac{2\pi}{a}x + \sin\frac{2\pi}{a}y\right) \tag{7.3}$$

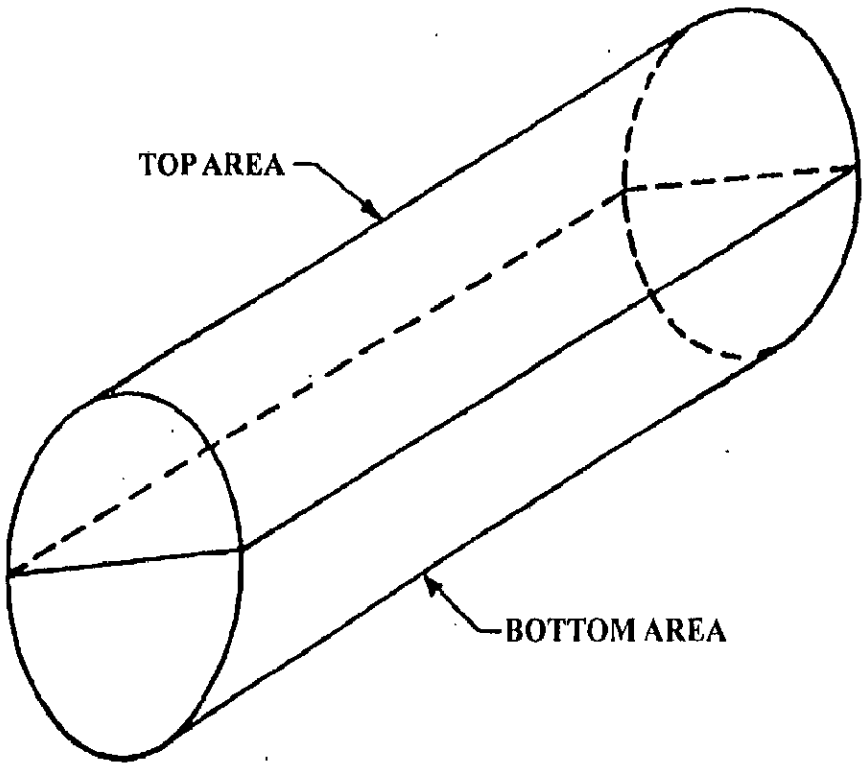

Fig. 7.2 Carbon fibre of unit length showing two distinct areas of study.

As far as the elastic deformation of the fibre is concerned, first, the compressive force acts at the highest points of the top and bottom surface of the fibre. As the compressive force increases, elastic deformation of the fibre extends and the thickness of the fibre in the preform reduces while the fibre volume fraction increases. The external force also gets distributed over the contacting area and this area expands as the external force increases. It is noted that due to the assumptions made above, the fibre cross-sectional area remains unchanged, ie., before infiltration and after complete infiltration of the fibres by liquid alloy but the shape of the fibre cross-section changes with increasing compressive forces. When the force reaches a certain value, the fibre cannot be further compressed. Ultimately, the fibre cross-section approaches to a rectangle, which represents the well-known Mosaic model for composites proposed by Ishikawa and Chou (235). Here, the maximum fibre volume fraction attained in the limiting condition is equal to the ratio of fibre volume to the unit cell volume, i.e. the packing fraction. The packing fraction is 0.785 for square packing and 0.907 for hexagonal packing. The square packing is comparatively an open structure with respect to hexagonal packing. It should be noted that the limiting case of broken fibres is not desirable in actual composite manufacturing.

7.3 FIBRE GEOMETRIC CHARACTERIZATION

7.3.1 Fibre Volume Fraction and Thickness Reduction

The fibre volume fraction, V_f^0, before compaction, V_f, during compaction and the limiting value, V_f^{max}, can be expressed in the following general forms:

$$V_f^0 = V_a \frac{V_y}{V_u(0)} \tag{7.4}$$

$$V_f = V_a \frac{V_y}{V_u(r_z)} \tag{7.5}$$

$$V_f^{max} = V_a \frac{V_y}{V_u(r_z^{max})} \tag{7.6}$$

where, V_a is the yarn packing fraction, r_z is the thickness reduction, V_y and $V_u(r_z)$ represent the fibre volume and the volume of the unit cell respectively. From the assumptions in section 7.2, Eqn.(7.1) and Eqn.(7.3), fibre volume, V_y and unit cell volume, $V_u(r_z)$ can be written as,

$$V_y = 16\int_0^{\frac{x}{4}}\int_0^{\frac{y}{4}}(z_t - z_b)dxdy = \frac{4}{\pi}a^2 r_f \tag{7.7}$$

$$V_u(r_z) = a^2(2r_f - r_z) \tag{7.8}$$

Consequently, the fibre volume fractions are as follows:

$$V_f^0 = \frac{2}{\pi}V_a \tag{7.9}$$

$$V_f = \frac{2}{\pi\left(1 - r_z/(2r_f)\right)}V_a \tag{7.10}$$

$$V_f^{max} = V_a \tag{7.11}$$

and the maximum thickness reduction is,

$$r_z^{max} = \left(1 - \frac{2}{\pi}\right)2r_f \tag{7.12}$$

which is about 36% of the original thickness $2r_f$.

7.4 VERIFICATION BY MICROSTRUCTURAL ANALYSIS

Torayla 300, PAN based carbon fibres with filament count 12K are reinforced into aluminium-copper alloy to produce a composite. To fabricate the fibre reinforced MMC, liquid alloy has been poured into the steel die containing the fibre preform prepared by placing the fibre tows parallel to each other. The fibre tows have been

immersed in ethyl alcohol before preparing the fibre preform. A pressure of 75 MPa has been applied to squeeze the liquid alloy in order to allow the liquid melt to infiltrate into the preform. The MMC has been allowed to solidify rapidly.

From the MMC thus obtained, SEM specimens have been prepared by slicing the ingot in the transverse direction of the fibres. The SEM micrograph obtained is shown in Fig.7.3. The microstructure when closely observed, distinct fibre arrangements in different region have been noticed. The schematic diagram revealing the various fibre arrangements at different region is given in Fig.7.4. In the top denoted as region 1, an open structure with square packing is observed. Hexagonal packing with different shapes of fibres has been observed in the region 2 and 3.

Due to the pressure variation along the fibre preform thickness, the different shapes and sizes of carbon fibres are observed at various regions. The increase in pressure causes greater infiltration of liquid melts into the fibres and the size of the fibres increases. One such region where the pressure is applied vertically downwards is the region marked 3 in Fig.7.1. In other regions, the turbulence of the liquid after collision with the mould wall is shown in Fig.7.5. It is clearly seen that the region marked 2 is under compression and the region marked 1 is under tension hence the arrangements of the fibres are close packed and openly packed type respectively The ratio a/b (where a is the minor axis and b is the major axis of the elliptical shaped fibres) is more appropriate term for judging the height reduction due to compaction of fibres. These ratios at different regions are determined by measuring a and b values of the fibres randomly. The values of a and b alongwith standard deviations at different regions are given in Table 7.1.

Table 7.1

Breadth to length ratio of the fibre

Region	a/b ratio	Standard deviation
1	0.55	0.015
2	0.51	0.012
3	0.39	0.019

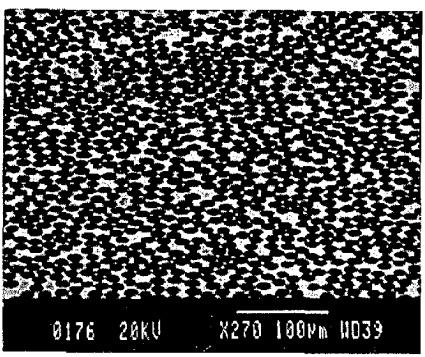

Fig. 7.3 SEM micrograph showing fibre arrangements inside the mould.

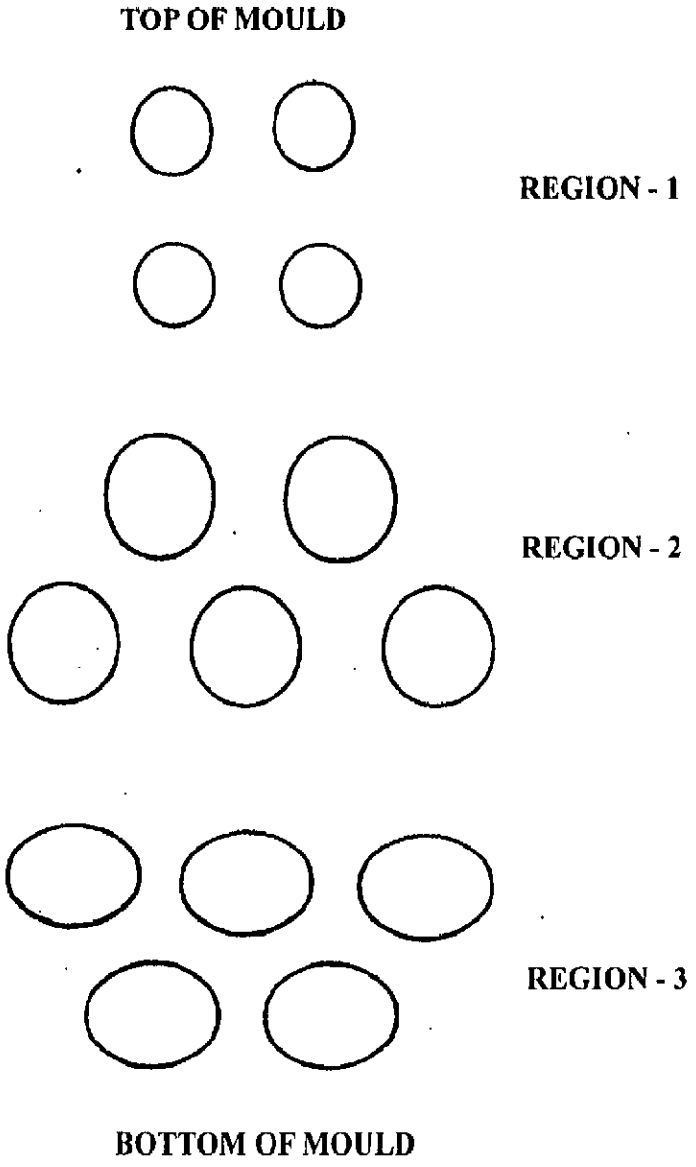

Fig. 7.4 Schematic diagram of the fibre arrangements at different regions.

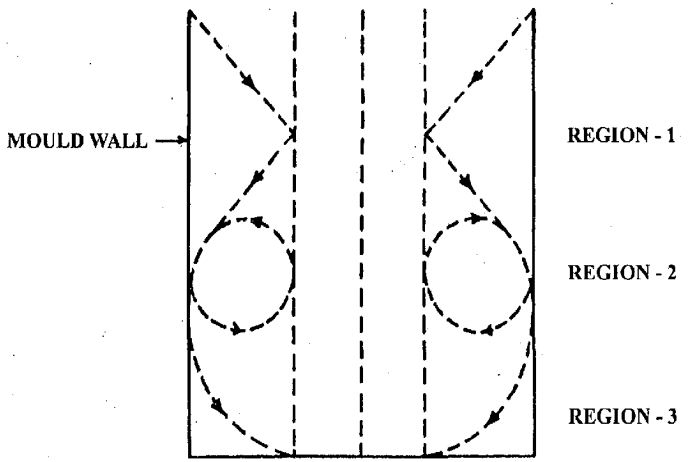

Fig. 7.5 Schematic diagram of the liquid flow inside the mould.

As shown in Fig.7.6 (the SEM micrograph), at the extreme end of the region marked 3, the 'fibre fracture' is observed in two fibres due to high reduction in height. According to the theoretical analysis, we have seen that the maximum thickness reduction is 36% and the actual experimental values, too, confirm these values.

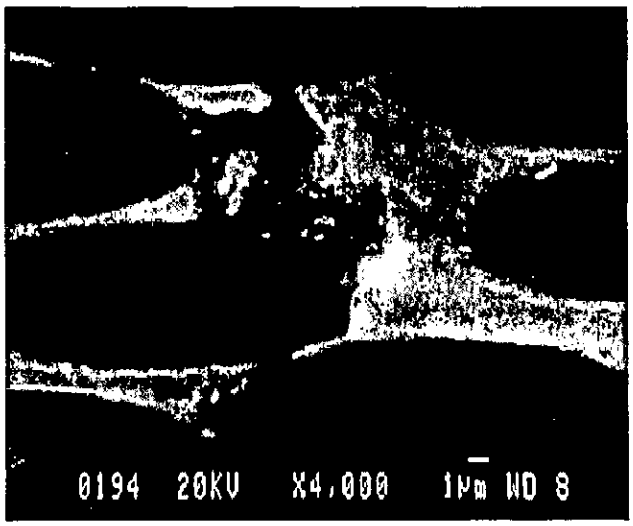

Fig. 7.6 SEM micrograph showing fibre fracture due to compression.

CONCLUSIONS

The present investigation on Al/CF cast composites and their properties have been presented in three segments as given in chapter 4, 5 and 6 outlining the results on the wettability studies, solidification processing and microstructural characterization and properties respectively. The study has led to the following conclusions pertaining to the development of Al/CF composites.

1. The deoxidation of aluminium alloys occurs more rapidly at high temperatures as compared to low temperatures. The deoxidation of alloys is mainly produced by reduction of the oxide layer by liquid aluminium with production of gaseous suboxide.
2. The contact angle of all the aluminium alloys on vitreous carbon decreases with temperature as sufficient time is left after the deoxidation of the alloys for reaction to occur at the interface between the alloy drop and the carbon substrate.
3. The addition of copper to aluminium does not improve the wettability of aluminium with vitreous carbon as contact angle decreases very slowly with temperature and reached marginally in the wetting region at high temperature.
4. The addition of lithium to aluminium improves wettability with vitreous carbon as contact angle decreases reapidly with temperature, however, the decrease is more pronounced at low temperatures as compared to high temperatures.
5. The wettability of aluminium-lithium alloy with vitreous carbon increases marginally with increase in lithium content at high temperatures whereas it increases considerably with lithium content at low temperatures.
6. The addition of zirconium to aluminium improves wettability with vitreous carbon as contact angle decreases significantly with temperature, however, the decrease is more pronounced at high temperatures as compared to low temperatures.

7. The wettability of aluminium with vitreous carbon increases substantially with increase in zirconium content at high temperatures whereas it remains ineffective with zirconium content at low temperatures.
8. The wettability of aluminium with vitreous carbon shows no improvement by the addition of small quantity of lithium and zirconium as the contact angle at high temperature is close to the contact angle of Al-Cu alloy at that temperature.
9. The improvement in the wettability of aluminium with vitreous carbon after alloying additions of copper, lithium and zirconium is due to formation of aluminium carbide, intercalation compound LiC_{16} and zirconium carbide respectively, hence chemical in nature.
10. The surface tension of all the alloys decreases with increase in temperature. The surface tension of Al-Li alloys decreases with increase in lithium content while that of Al-Zr alloys increases with increase in zirconium content.
11. The work of adhesion of all the alloys increases with increase in temperature. The work of adhesion of Al-Li and Al-Zr alloys increases with increase in lithium and zirconium content of the alloys respectively at high temperatures.
12. The increase in work of adhesion with increasing alloying additions and temperature is due to the formation of covalent bonding, ionic bonding and metallic bonding across the interface of Al-Cu/C_v, Al-Li/C_v and Al-Zr/C_v systems respectively.
13. From a practical point of view, none of the alloys shows wettability with vitreous carbon for a short holding time after melting of the alloy, even at a temperature of 1075^0C.
14. The concentration of lithium decreases significantly in Al-Li/CF composites due to oxidation whereas the concentration of copper and zirconium vary marginally in Al-Cu/CF and Al-Zr/CF composites respectively.
15. Squeeze casting of composites having low fibre volume fraction results into inhomogeneous distribution of fibres, creating fibre deficient and fibre rich regions due to pushing effect of the forced molten aluminium alloy stream during squeeze casting. However, the distribution of fibres is quite homogeneous in high fibre volume fraction composites.

16. Squeeze casting of composites results in the porosity free casting in all the composites, however, few unwetted regions are observed in Al-Zr/CF composites due to the fact that no super heat is given to melt Al-Zr alloy so that Al_3Zr crystals remain undissolved in the alloy and have blocked the interstices between the fibres.

17. The chemical interaction is more pronounced in Al-Cu/CF and Al-Zr/CF composites than that in Al-Li/CF composites as thick reaction layer is present at the interface between carbon fibre and aluminium alloy matrix in Al-Cu/CF and Al-Zr/CF composites while there is no sign of reaction layer at the interface in Al-Li/CF composites.

18. Little oxygen is absorbed due to oxidation of aluminium during squeeze casting of Al-Cu/CF composites, however, it is distributed homogeneously in the composite.

19. The alloying additions are present in sufficient quantity in different composites. Inspite of some segregation of copper and zirconium towards fibre/matrix interface in Al-Cu/CF and Al-Zr/CF composites respectively, they are distributed homogeneously in their respective composites.

20. The concentration of copper decreases from fibre to matrix in Al-Cu/CF composites resulting in copper rich interface and copper deficient matrix. In case of Al-Zr/CF composites also, interface is enriched in zirconium while matrix is deficient in zirconium.

21. Although the concentration of major alloying additions in Al-Li/CF composites is reduced significantly as compared to Al-Li alloy, they are distributed homogeneously in Al-Li/CF composites.

22. Aluminium carbide is present at the interface of Al-Cu/CF composite in the form of acicular inclusions due to the chemical reaction between aluminium alloy matrix and carbon fibres.

23. $CuAl_2$ is present as a precipitate at the interface of Al-Cu/CF composite due to uneven solute distribution in the composite. This precipitate is present in oblong shape and results in a precipitate free zone away from the fibre.

24. Dislocation network is present alongwith AlFeSi phase in Al-Cu/CF composite, however, the dislocation density is very low as copper addition reduces the thermal expansion coefficient of the aluminium matrix.

25. The density of all the composites decreases with increase in fibre volume fraction due to difference in the relative density of the aluminium alloy matrices and carbon fibres. Al-Zr/CF composites show highest density as compared to Al-Cu/CF and Al-Li/CF composites as Al-Zr alloy has higher density than other two alloys.

26. The density of the composites is higher than that estimated by law of mixtures, however, the density of high fibre volume fraction composites is more close to the estimated density than the density of low fibre volume fraction composites.

27. The Brinell hardness of the composites increases with increase in fibre volume fraction as the flow in aluminium alloy matrices adjacent to the fibre gets more restrained due to reduction in the area of interfibre region. For same fibre volume fraction, Al-Zr/CF composites show highest hardness as compared to that of other two composites due to different amount of hard carbide phase present in the composites as the reactivity of carbon fibres varies with matrices.

28. The engineering fracture strain of the composites decreases with increase in fibre volume fraction as the amount of brittle phase increases with fibre volume fraction. Al-Li/CF composites show higher fracture strain than Al-Cu/CF and Al-Zr/CF composites as the interfacial bonding is weak in Al-Li/CF composites resulting in debonding of the fibres at the interface and hence crack blunting along the fibre axis.

29. The strength of preheated carbon fibres decreases signicantly due to handling and oxidation. The strength of extracted fibres is highest in Al-Li/CF composites as compared to Al-Cu/CF and Al-Zr/CF composites due to less degradation of carbon fibres in Al-Li/CF composites.

30. The tensile strength of the composites increases with increase in fibre volume fraction, as the strength of the fibres is very high in comparison to the aluminum alloy matrices.

31. Al-Li/CF composites show higher strength than Al-Cu/CF and Al-Zr/CF composites as real transfer efficiency of fibre strength is high for Al-Li/CF composites, however, for lower fibre volume fraction composites, RTEFS is high for Al-Zr/CF composites.

32. The strength of the composites is far lower than that estimated by law of mixtures as the estimation is carried out by using the strength of extracted carbon fibres. The fibre strength is probably higher than the actual fibre strength in the composites as flaw density is proportional to the fibre length and a shorter length of fibre is used to get the Weibull distribution of fibre strength.

APPENDIX – A

Table-A1

The values of β corresponding to values of u for different values of ϕ

β	ϕ=45° α=45°		ϕ=60° α=30°		ϕ=120° α=30°		ϕ=135° α=45°	
	u=h/r	Δu	u=h/r	Δu	u=h/r	Δu	u=h/r	Δu
0.0	-0.41421		1.00000		3.0000		2.4142	
0.1	0.41922	0.00464	1.00905	0.00822	2.9586	-0.0335	2.3579	-0.0437
0.2	0.42386	0.00429	1.01727	0.00747	2.9251	-0.0286	2.3142	-0.0384
0.3	0.42815	0.00400	1.02474	0.00685	2.8965	-0.0247	2.2778	-0.0305
0.4	0.43215	0.00372	1.03159	0.00635	2.8718	-0.0213	2.2473	-0.0264
0.5	0.43587	0.00350	1.03794	0.00590	2.8505	-0.0190	2.2209	-0.0233
0.6	0.43937	0.00330	1.04384	0.00551	2.8315	-0.0171	2.1976	-0.0208
0.7	0.44267	0.00313	1.04935	0.00515	2.8144	-0.0156	2.1768	-0.0186
0.8	0.44580	0.00297	1.05450	0.00487	2.7988	-0.0141	2.1582	-0.0169
0.9	0.44877	0.00283	1.05937	0.00460	2.7847	-0.0131	2.1413	-0.0154
1.0	0.45160	0.00271	1.06397	0.00436	2.7716	-0.0121	2.1259	-0.0141
1.1	0.45431	0.00258	1.06833	0.00415	2.7595	-0.0110	2.1118	-0.0132
1.2	0.45689	0.00247	1.07248	0.00394	2.7485	-0.0105	2.0986	-0.0123
1.3	0.45936	0.00238	1.07642	0.00376	2.7380	-0.0097	2.0963	-0.0113
1.4	0.46174	0.00230	1.08016	0.00355	2.7283	-0.0092	2.0750	-0.0306
1.5	0.46404	0.00220	1.08373	0.00344	2.7191	-0.0086	2.0644	-0.0100
1.6	0.46624	0.00212	1.08717	0.00331	2.7105	-0.0081	2.0544	-0.0094
1.7	0.46836	0.00207	1.09048	0.00316	2.7024	-0.0079	2.0450	-0.0089
1.8	0.47043	0.00197	1.09364	0.00303	2.6945	-0.0072	2.0361	-0.0084
1.9	0.47240	0.00193	1.09667	0.00293	2.6873	-0.0069	2.0277	-0.0081
2.0	0.47433	0.00186	1.09960	0.00282	2.68036	-0.00664	2.01957	-0.00764
2.1	0.47619	0.00181	1.10242	0.00273	2.67372	-0.00636	2.01193	-0.00725
2.2	0.47800	0.00176	1.10515	0.00264	2.66736	-0.00608	2.00468	-0.00694
2.3	0.47976	0.00170	1.10779	0.00257	2.66128	-0.00580	1.99774	-0.00663
2.4	0.48146	0.00164	1.11036	0.00247	2.65548	-0.00557	1.99111	-0.00634
2.5	0.48310	0.00161	1.11283	0.00239	2.64991	-0.00536	1.98477	-0.00610
2.6	0.48471	0.00157	1.11522	0.00233	2.64455	-0.00512	1.97867	-0.00585
2.7	0.48628	0.00151	1.11755	0.00223	2.63943	-0.00497	1.97282	-0.00566
2.8	0.48779	0.00149	1.11978	0.00220	2.63446	-0.00478	1.96716	-0.00542
2.9	0.48928	0.00146	1.12198	0.00216	2.62968	-0.00464	1.96174	-0.00522
3.0	0.49074	0.00141	1.12414	0.00210	2.62504	-0.00446	1.95652	-0.00502
3.1	0.49215	0.00139	1.12624	0.00203	2.62058	-0.00428	1.95150	-0.00486
3.2	0.49354	0.00134	1.12827	0.00197	2.61630	-0.00418	1.94664	-0.00470
3.3	0.49488	0.00132	1.13024	0.00190	2.61212	-0.00408	1.94194	-0.00458
3.4	0.49620	0.00130	1.13214	0.00188	2.60804	-0.00391	1.93736	-0.00441
3.5	0.49750	0.00127	1.13402	0.00183	2.60413	-0.00380	1.93295	-0.00428
3.6	0.49877	0.00124	1.13585	0.00178	2.60033	-0.00368	1.92867	-0.00414
3.7	0.50001	0.00120	1.13763	0.00172	2.59665	-0.00359	1.92453	-0.00403
3.8	0.50121	0.00118	1.13935	0.00169	2.59306	-0.00351	1.92050	-0.00394
3.9	0.50239	0.00117	1.14104	0.00169	2.58955	-0.00341	1.91656	-0.00382
4.0	0.50356	0.00115	1.14273	0.00164	2.58614	-0.00333	1.91274	-0.00373
4.1	0.50471	0.00110	1.14437	0.00156	2.58281	-0.00321	1.90901	-0.00361

4.2	0.50581	0.00109	1.14593	0.00157	2.57960	-0.00316	1.90540	-0.00351
4.3	0.50690	0.00108	1.14750	0.00153	2.57644	-0.00307	1.90189	-0.00341
4.4	0.50798	0.00105	1.14903	0.00148	2.57337	-0.00295	1.89848	-0.00334
4.5	0.50903	0.00103	1.15051	0.00149	2.57042	-0.00287	1.89514	-0.00324
4.6	0.51006	0.00102	1.15200	0.00145	2.56755	-0.00284	1.89190	-0.00317
4.7	0.51108	0.00101	1.15345	0.00140	2.56471	-0.00281	1.88873	-0.00310
4.8	0.51209	0.00100	1.15485	0.00139	2.56190	-0.00270	1.88563	-0.00302
4.9	0.51309	0.00097	1.15624	0.00134	2.55920	-0.00268	1.88261	-0.00298
5.0	0.51406	0.00095	1.15758	0.00134	2.55652	-0.00260	1.87963	-0.00290
5.1	0.51501	0.00093	1.15892	0.00134	2.55392	-0.0253	1.87673	-0.00281
5.2	0.51594	0.00092	1.16026	0.00130	2.55139	-0.0249	1.87392	-0.00275
5.3	0.51686	0.00092	1.16156	0.00127	2.54890	-0.0243	1.87117	-0.00271
5.4	0.51778	0.00088	1.16283	0.00123	2.54647	-0.0240	1.86846	-0.00269
5.5	0.51866	0.00088	1.16406	0.00122	2.54407	-0.0235	1.86577	-0.00261
5.6	0.51954	0.00087	1.16528	0.00121	2.54172	-0.0230	1.86316	-0.00256
5.7	0.52041	0.00084	1.16649	0.00118	2.53942	-0.0223	1.86060	-0.00248
5.8	0.52125	0.00083	1.16767	0.00115	2.53719	-0.0222	1.85812	-0.00245
5.9	0.52208	0.00083	1.16882	0.00112	2.53497	-0.0218	1.85567	-0.00242
6.0	0.52291	0.00082	1.16994	0.00113	2.53279	-0.0213	1.85325	-0.00236
6.1	0.52373	0.00080	1.17107	0.00108	2.53066	-0.0210	1.85089	-0.00233
6.2	0.52453	0.00079	1.17215	0.00109	2.52856	-0.0206	1.84856	-0.00226
6.3	0.52532	0.00077	1.17324	0.00108	2.52650	-0.0202	1.84630	-0.00223
6.4	0.52609	0.00076	1.17432	0.00106	2.52448	-0.0198	1.84407	-0.00218
6.5	0.52685	0.00075	1.17538	0.00105	2.52250	-0.0193	1.84189	-0.00215
6.6	0.52760	0.00074	1.17643	0.00104	2.52057	-0.0190	1.83974	-0.00210
6.7	0.52834	0.00074	1.17747	0.00102	2.51867	-0.0189	1.83764	-0.00206
6.8	0.52910	0.00073	1.17849	0.00099	2.51678	-0.0184	1.83558	-0.00205
6.9	0.52983	0.00072	1.17948	0.00097	2.51494	-0.0180	1.83353	-0.00202
7.0	0.53055	0.00070	1.18045	0.00096	2.51314	-0.0178	1.83151	-0.00197
7.1	0.53125	0.00070	1.18141	0.00095	2.51136	-0.0178	1.82954	-0.00194

Table-A2

Weightage factors K for β values corresponding to different values of ϕ

β	Weightage Factor K			
	$\phi=45^{O}$	$\phi=60^{O}$	$\phi=120^{O}$	$\phi=135^{O}$
0.0	19	24	77	135
0.1	17	21	62	103
0.2	16	20	52	83
0.3	15	18	45	71
0.4	14	16	39	61
0.5	13	15	34	53
0.6	12	14	31	48
0.7	11	13	28	43
0.8	11	12	26	39
0.9	10	12	23	35
1.0	10	11	22	32
1.1	9	10	20	30
1.2	9	10	19	28
1.3	8	9	18	26
1.4	8	9	16	24
1.5	8	9	16	23
1.6	7	8	15	22
1.7	7	8	14	21
1.8	7	8	13	19
1.9	7	7	12	19
2.0	7	7	12	18
2.1	6	7	11	17
2.2	6	7	11	16
2.3	6	6	10	15
2.4	6	6	10	15
2.5	6	6	10	14
2.6	5	6	9	14
2.7	5	6	9	13
2.8	5	5	9	13
2.9	5	5	8	12
3.0	5	5	8	12
3.1	5	5	8	11
3.2	5	5	8	11
3.3	5	5	7	11
3.4	5	5	7	10
3.5	4	4	7	10

β	Weightage Factor K			
	$\phi=45^{O}$	$\phi=60^{O}$	$\phi=120^{O}$	$\phi=135^{O}$
3.6	4	4	7	10
3.7	4	4	6	9
3.8	4	4	6	9
3.9	4	4	6	9
4.0	4	4	6	9
4.1	4	4	6	9
4.2	4	4	6	9
4.3	4	4	6	8
4.4	4	4	6	8
4.5	4	4	6	8
4.6	4	4	6	8
4.7	4	4	5	8
4.8	4	4	5	8
4.9	4	4	5	7
5.0	4	4	5	7
5.1	4	4	5	7
5.2	4	4	5	7
5.3	4	3	5	7
5.4	3	3	5	7
5.5	3	3	5	7
5.6	3	3	5	6
5.7	3	3	5	6
5.8	3	3	4	6
5.9	3	3	4	6
6.0	3	3	4	6
6.1	3	3	4	6
6.2	3	3	4	6
6.3	3	3	4	6
6.4	3	3	4	6
6.5	3	3	4	6
6.6	3	3	4	5
6.7	3	3	4	5
6.8	3	3	4	5
6.9	3	3	4	5
7.0	3	3	4	5
7.1	3	3	4	5

Table-A3

Variation of p = r/b with average $\bar{\beta}$

$\bar{\beta}$	p = r / b	Δp
0.0	1.00000	-0.01579
0.1	0.98421	-0.01445
0.2	0.96976	-0.01328
0.3	0.95648	-0.01226
0.4	0.94422	-0.01139
0.5	0.93283	-0.01066
0.6	0.92217	-0.01002
0.7	0.91215	-0.00944
0.8	0.90271	-0.00894
0.9	0.89377	-0.00848
1.0	0.88529	-0.00807
1.1	0.87722	-0.00769
1.2	0.86953	-0.00735
1.3	0.86218	-0.00705
1.4	0.85513	-0.00675
1.5	0.84838	-0.00649
1.6	0.84189	-0.00625
1.7	0.83564	-0.00601
1.8	0.82963	-0.00580
1.9	0.82383	-0.00561
2.0	0.81822	-0.00542
2.1	0.81280	-0.00525
2.2	0.80755	-0.00508
2.3	0.80247	-0.00493
2.4	0.79754	-0.00479
2.5	0.79275	-0.00465
2.6	0.78810	-0.00452
2.7	0.78358	-0.00439
2.8	0.77919	-0.00428
2.9	0.77491	-0.00417
3.0	0.77074	-0.00407
3.1	0.76667	-0.00397
3.2	0.76270	-0.00387
3.3	0.75883	-0.00377
3.4	0.75506	-0.00369
3.5	0.75137	-0.00361

$\bar{\beta}$	p = r / b	Δp
3.6	0.74776	-0.00353
3.7	0.74423	-0.00345
3.8	0.74078	-0.00337
3.9	0.73741	-0.00330
4.0	0.73411	-0.00323
4.1	0.73088	-0.00317
4.2	0.72771	-0.00311
4.3	0.72460	-0.00305
4.4	0.72155	-0.00299
4.5	0.71856	-0.00294
4.6	0.71562	-0.00288
4.7	0.71274	-0.00283
4.8	0.70991	-0.00278
4.9	0.70713	-0.00272
5.0	0.70441	-0.00268
5.1	0.70173	-0.00264
5.2	0.69909	-0.00259
5.3	0.69650	-0.00255
5.4	0.69395	-0.00250
5.5	0.69145	-0.00246
5.6	0.68899	-0.00242
5.7	0.68657	-0.00239
5.8	0.68418	-0.00235
5.9	0.68183	-0.00231
6.0	0.67952	-0.00228
6.1	0.67724	-0.00224
6.2	0.67500	-0.00221
6.3	0.67279	-0.00218
6.4	0.67061	-0.00215
6.5	0.66846	-0.00212
6.6	0.66634	-0.00209
6.7	0.66425	-0.00206
6.8	0.66219	-0.00203
6.9	0.66016	-0.00201
7.0	0.65815	-0.00198
7.1	0.65617	-0.00195

Table-A4

Work of adhesion of aluminium alloys with carbon substrate at different temperature

S. No.	Alluminium alloy	Contact angle (degree)			Surface tension (mJ/m^2)			Work of adhesion (mJ/m^2)		
		775°C	925°C	1075°C	775°C	925°C	1075°C	775°C	925°C	1075°C
1.	Al-4.5 wt.% Cu	147	115	86	906.00	769.41	697.76	146.13	444.00	746.26
2.	Al-1.1 wt.% Li	136	93	78	844.92	719.16	624.73	237.42	681.76	755.92
3.	Al-1.6 wt.% Li	124	90	76	804.13	702.68	614.56	354.24	702.68	763.42
4.	Al-2.3 wt.% Li	112	81	72	784.26	669.45	602.63	490.16	773.00	789.45
5.	Al-2.1 wt.% Zr	153	109	84	879.45	757.37	680.14	95.85	511.73	751.54
6.	Al-3.4 wt.% Zr	151	105	69	921.78	804.33	688.27	115.22	596.00	936.04
7.	Al-5.2 wt.% Zr	149	102	55	945.63	815.43	701.86	135.22	645.82	1101.92

Table-A5

EDS point analysis of interfibre region in Al-Cu/CF composite

Standards :

C K $CaCO_3$

N K Not defined

O K 0

Al K Al_2O_3

Cu K Cu

Zr L Zr

Pt. No.	C K (ED)	N K (ED)	O K (ED)	Al K (ED)	Cu K (ED)	Zr L (ED)	Total
1	-	-	6.8 (12.0)	78.5 (81.7)	13.6 (6.0)	1.1 (0.4)*	100.0
2	13.3 (27.1)	-	7.4 (11.3)	59.2 (53.8)	20.3 (7.8)	-0.2 (-0.1)*	100.0
3.	17.5 (33.3)	-	3.5 (5.0)*	68.6 (58.1)	9.6 (3.4)	0.8 (0.2)*	100.0
4.	20.2 (38.6)	-	-1.2 (-1.8)*	69.4 (59.0)	11.5 (4.1)	0.2 (0.1)*	100.0
5.	23.3 (41.4)	-	-0.8 (-1.2)*	67.4 (56.1)	10.6 (3.8)	0.1 (0.0)*	100.0
6.	23.0 (42.4)	-	-1.4 (-2.0)*	68.0 (55.9)	10.3 (3.6)	0.1 (0.0)*	100.0
7.	27.4 (51.1)	-	-8.6 (-12.0)*	67.6 (56.2)	12.9 (4.6)	0.7 (0.2)*	100.0
8.	27.4 (51.6)	-	-7.6 (-10.8)*	62.4 (52.5)	18.8 (6.7)	-1.0 (-0.3)*	100.0
9.	41.6 (69.0)	-	-12.1 (-15.1)*	56.9 (42.1)	10.9 (3.4)	2.7 (0.6)*	100.0
10.	24.2 (32.8)	17.2 (20.0)	33.4 (33.9)	20.0 (12.0)	4.8 (1.2)	0.3 (0.1)*	100.0

* = <2 Sigma

Table-A6

Indexing of the SAD patterns

Fig. No.	Camera constant	R_1 (mm)	R_2 (mm)	R_3 (mm)	d_1 (Å)	d_2 (Å)	d_3 (Å)	$h_1k_1l_1$	$h_2k_2l_2$	$h_3k_3l_3$	Beam direction	Phase (s)
5.11	8.0 mmÅ	3.46	8.61	9.67	2.338	0.929	0.827	$\bar{2}\bar{2}4$	$11\bar{1}$	$\bar{1}3\bar{3}$	$-3\bar{1}\bar{2}$	Al
5.12	8.0 mmÅ	3.65	6.84	9.36	2.19	1.17	0.686	$20\bar{3}$	100	$\bar{1}03$	$0\bar{3}0$	C
5.13	11.5mmÅ	6.03	9.84	10.30	2.80	1.66	1.63	$\bar{2}01$	110	$31\bar{1}$	$1\bar{1}2$	Al_4C_3
5.14	15.0mmÅ	6.32	7.80	7.90	2.37	1.92	1.90	$\bar{2}11$	$01\bar{3}$	$20\bar{2}$	$\bar{1}\bar{3}1$	$CuAl_2$
5.15	13.0mmÅ	6.75	6.53	5.47	1.93	1.99	2.38	$\bar{3}11$	$5\bar{1}1$	202	$14\bar{1}$	AlFeSi

REFERENCES

1. M.D. Huda, M.S.J. Hashmi and M.A. El-Baradie, "MMCs: Materials, Manufacturing and Mechanical properties", Metal Matrix Composites Part 1, G.M. Newaz, H. Nebar-Aeschobacher, F.N. Wohlbier (Eds.), Trans Tech. Publications, Switzerland, (1995).
2. A. Mortensen, J.A. Cornie and M.C. Flemings, "Solidification Processing of Metal-Matrix Composites", Journal of Metals, 40, (1988), 12-19.
3. B. Terry and G. Jones, "Metal Matrix Composites", Elsevier Science Publishers Ltd., Oxford, England, 1990.
4. S. Ray, "Casting of Metal Matrix Composite Components From Slurry", J. of Indian Foundary, June 1994, 37-44.
5. J. Eliasson and R. Sanstrom, "Applications of Aluminium Matrix Composites", Metal Matrix Composites, Part I; G.M. Newaz; H.N. Aeschbacher and F.H. Wohlbier (Eds.), Trans Tech Publications, Switzerland, 1995, p. 30.
6. R.L. Trumper, "Metal Matrix Composites - Application and Prospects", Metals and Materials, 3, 1987, 662-667.
7. W.H. Hunt and T.J. Rodjom, Proc. of the 1992 Powder Metallurgy World Congress, J.M. Capus and R.M. German (Eds.), Sanfrancisco, California, U.S.A., 1992, p. 21.
8 J.E. Schoutens and K. Tempo, "Introduction to Metal Matrix Composite Materials", DOD Metal Matrix Composite Information Analysis Center, Santa Barbara, 1982, pp.3-20.
9. L. Rubin, "Application of Metal Matrix Composites : Emergency Structural Materials", SAMPE Twenty Fourth National Symposium, Sanfrancisco, California, Vol.24, 1979, p. 1236
10. J.B. Bonnet and R.C. Bansal, "Carbon Fibers", Dekker, New York, 1984, p. 52.
11. A.G. Metcalfe, "Interface in Metal Matrix Composites", Vol.1, Academic Press, New York, 1974.

12. H.M. Cheng, A. Kitahara, S. Akiyama, K. Kobayashi, Y. Uchiyama and B.L. Zhou, "Characteristics of Several Carbon Fibre-Reinforced Aluminium Composites Prepared by a Hybridization Method", J.Mat.Sci., 29, 1994, 4342-4350.

13. P.G. Sullivan and L. Raymond, "Graphite Fiber Morphology: Effect on Behaviour in Graphite-Aluminium Composites", Tenth SAMPE Symposium, New York, Vol.10, 1978, p. 466.

14. S. Towata, H. Ikuno and S. Yamada, "Mechanical Properties of Carbon Fiber-Reinforced Aluminium Alloys with Whiskers and Particulates of Silicon Carbide", Trans. JIM, 1988, 314-321.

15. B.P. Krishnan, M.K. Surappa and P.K. Rohatigi, "The UPAL Process : A Direct Method of Preparing Cast Aluminium Alloys-Graphite Composites", J. Mat. Sci., 16, 1981, 1209-1216.

16. J.P. Rocher, F. Girot, J.M. Quenisset, R. Pailler and R. Nasalin, "Memories et Etudes Scientifiques Revue de Metallurgie, 1986, pp. 69-85.

17. Y. Kimura, Y. Mishima, S. Umekawa and T. Suzuki, "Compatibility between Carbon Fibres and Binary Aluminium Alloys", J. of Mat. Sci., 19, 1984, 3107.

18. C.R. Manning and T.B. Gurganus, J. Amer. Ceram. Soc., 52, 1969, 115.

19. K Landry, S. Kalogeropoulou and N. Eustathopoulos, "Wettability of Carbon by Aluminium and Aluminium Alloys", Mat. Sci. & Engg., A254, 1988, 99-111.

20. A. Vassel, "Continuous Fibre Reinforced Titanium and Aluminium Composites : A Comparison", Mat. Sci. and Engg., A 263, 1999, 305-313,

21. T. Furuta, "Development of Composite Materials", J. of Machine Research, 33, 1981, 906-912.

22. T. W. Clyne and M.G. Bader, "Analysis of a Squeeze-Infiltration Process for Fabrication of Metal Matrix Composites", Proc. of the Fifth Int. Conf. on Composite Materials, ICCM-V, W.C. Harrigan, J. Strife and A.K. Dhingra (Eds.), San Diego, TMS-AIME, 1985, pp. 755-771.

23. B. Zantout, A.A. Das and J.R. Franklin, "Squeeze Cast Aluminium-Matrix Composite Strength at Higher Temperature", The Metallurgy of Light Alloys, Spring Residential Conf., The institute of Metallurgists, 20, 1983.

24. K. Motoki and A. Okura, "Progress in Science and Engineering of Composites", T. Hayashi, K. Kowata and S.Umekawa (Eds.), ICCM-IV, Tokyo, 1982.

25. S.D. Tsai, M. Deepak, H.L. Marcus, I.C. Noyan and J.B. Cohen, Mat. Sci. & Engg., 47, 1981, 145-149.

26. E.A. Feest, M.J. Ball, A.R. Begg and D. Biggs, Report on OSTEM visit to Japan, Oct. 1986.

27. R.R. Bowles, D.L. Mancini and M.W. Toaz, Metal Matrix Composites Aid Piston Manufacturing Engineering, 98, 1987, pp. 61-62.

28. Yu. V. Naidich and G.A. Kolesnichenko, "Surface Phenomena in Metallurgical Processes", A.I. Belyaev (Ed.), Consultants Bureau, New York, 1965, p. 218.

29. N. Eustathopoulos, J.C. Joud, P. Derse and J. M. Hicter, "The Wetting of Carbon by Aluminium and Aluminium Alloys", J. Mat. Sci., 9, 1974, 1233-1242.

30. M.G. Nicholas and D.A. Mortimer, "Carbon Fibers-Their Composites and Applications", Int. Carbon Fibres Conf., London, 1971, p. 129.

31. S.G. Warrier, C.A. Blue and R.Y. Lin, "Control of Interfaces in Al-C Fibre Composites", J. Mat. Sci., 28, 1993, 760-768.

32. S. Abraham, B.C. Pai, K.G. Satyanarayana and V.K. Vaidyan "Studies on Nickel Coated Carbon Fibres and Their Composites", J. Mat. Sci., 25, 1990, 2839-2845.

33. S. Abraham, B.C. Pai, K.G. Satyanarayana and V.K. Vaidyan, "Copper Coating on Carbon Fibres and Their Composites with Aluminium Matrix", J. Mat. Sci., 27, 1992, 3479-3486.

34. R.T. Pepper, J.W. UPP, R.C. Rossi and E.G. Kendall, "The Tensile Properties of a Graphite Fiber Reinforced Al-Si Alloy", Met. Trans., 2, 1971, 117-120.

35. R.T. Pepper and E.G. Kendall, U.S. Patent 3, 770, 488 (1973).

36. M.D. Sanctis, S. Pellitier, Y. Bienvenu and M. Guigon, "The Formation of Interfacial Carbides in a Carbon Fibre Reinforced Aluminium Composite", Carbon, 32, 1994, 925.

37. S. Towata, S.Yamada and T. Ohwaki, "Strength and Interfacial Reaction of High Modulus Carbon Fiber-Reinforced Aluminium Alloys". Trans. JIM, 26, 1985, 563-570.

38. T. Clyne, M.G. Bader, G.R. Cappleman and P.A. Hubert, "The Use of a Delta-Aluminium Fibre for Metal Matrix Composites", J. Mat. Sci., 20, 1985, 85.

39. T. Young, Phil. Trans. R. Soc., London, 95, 1805, 65.

40. A. Dupre, "Theorie Mecanique de la Chaleur", Gauthier Villars, Paris, 1869.

41. J.A. Cornie, A.S. Argon and V. Gupta, MRS Bull., 16, 1991, 32.

42. J.M. Howe, Int. Mater. Rev., 38, 1993, 257.

43. S.Y.Oh, J.A. Cornie and K.C. Russel, "Wetting of Ceramic Particulates with Liquid Aluminium Alloys: part-I, Experimental Techniques", Met. Trans., 20A, 1989, 527.

44 A. Jakobsson, M. Nasu, J. Mangwiru, K.C. Mills and S. Seetharaman, "Interfacial Tension Effects on Slag-Metal Reactions",Phill. Trans. R. Soc., London, A, 1998, 356, 995-1001.

45. A. Jakobsson, N.N. Vishwanathan, Du Sichen and S. Seetharaman, "Interfacial Phenomenon in some Slag-Metal Reactions", Accepted Met. Trans., 2000.

46. A. Jha and C. Dometakis, "The Dispersion Mechanism of TiB_2 Ceramic Phase in Molten Al and Its Alloys", Materials and Design, 18, 1997. 297-301.

47. C. Dometakis and A. Jha, "Flux Assisted Dispersion of Ceramic Phases in Molten Aluminium Alloys", Conf. Proc., Design Fundamentals of High Temperature Composites, Intermetallics and Metal-Ceramic Systems, R.Y. Lin, Y.A. Chang, R.G. Reddy and C.T. Liu (Eds.), TMS Publications, Anaheim, California, Feb 4-8, 1996.

48. S. Takahashi and O. Koboi, "Study on Contact Angles of Au, Ag, Cu, Sn, Al and Al Alloys to SiC", J. Mat. Sci., 31, 1996, 1797.

49. P. Kozakevitch and G. Urbain, Memoires Scientifiques Rev. Metallurgy, 58, 1961, 401.

50 A. Mortensen, "Proceedings of the 9th Riso International Symposium on Metallurgy and Materials Science, S.I. Ansersen, H. Lilholt and O.B. Pedersen (Eds.), Roskilde, Denmark, 1988, p. 141.

51. V. Laurent, D. Chatain, C. Chatillon and N. Eustathopoulos, Acta Metall., 36 1988, 1797.

52. D.J. Wang and S.T. Wu, Acta Metall. Mater., 42, 1994, 4029.

53. C. Zhongyu, W. Jinbo, and H. Xiangui, "Interfaces in Metal-Ceramics Composites", R.Y. Lin, R.J. Arsenault, G.P. Martins and S.G. Fishman (Eds.), The Minerals, Metals and Materials Society, 1989. p. 223.

54. V.I. Kostikov, Y.I. Koshelev, E.F. Filmonov, E.M. Taitevskaya and R.N. Ponkratova, Poroshk. Metall., 226, 1981, 79.

55. J. Israelachvili, "Intermolecular and Surface Forces", 2nd Edition, Academic Press, London, 1991, p. 176.

56. D.A. Widdows and M.G. Nicholas, "The Wetting of Graphite by Liquid Aluminium and Aluminium-Based Alloys", UKAEA Report, AERE-R 5625, U.K. Atomic Energy Authority, Harwell, 1967.

57. K. Nogi, K. Ohnishi and K. Ogino, Keikenzoku, 38, 1988, 588.

58. D. Weirauch, W. Balaba and A. Perrotta, "Kinetics of the Reactive Spreading of Molten Aluminium on Ceramic Surfaces", J. Mater. Res., 10, 1995, 640.

59. Y.V. Naidich, Y.N. Chubashov, N.F. Ishchuk and V.P. Krasovskii, Poroshk. Metall., 246, 1983, 67.

60. A. Mortensen, and J.A. Cornie, "On the Infiltration of Metal Matrix Composites", Met. Trans. A, 18A, 1987, 1160-1163.

61. M. Humenik Jr., "Ceramic-Metal Composites and Their Uses", The Science of Materials used in Advanced Technology, E.R. Parker and U. Colombo (Eds.), Wiley-Interscience Publication, 1973, p. 297.

62. V. Agarwala and D. Dixit, "Fabrication of Aluminium Base Composite by Foundry Technique", Trans. JIM, 8, 1981, 521.

63. R.C. Rossi, R.T. Pepper, J.W. Upp and W.C. Riley, Ceramic Bulletin, 50, 1971, 484.

64. N. Sobczak, Z.Gorny, M.Ksiazek, W. Radziwill and P. Rohatgi, "Interaction Between Porous Graphite Substrate and Liquid or Semi-liquid AlTi6 and AlTi10 Alloys", ICCE2, New Orleans, L.A, USA, 1995.

65. E. Delamotte, K. Phillips, A.J. Perry and H.R. Kallias, J. Mat. Sci., 7, 1972, 346.

66. K. Kuniya et al., U.S. Patent 3 871 834, 1975.

67. R.V. Sara, U.S. Patent 4 347 083, 1982, or 4 402 744, 1983.

68. J.V. Naidich, Prog. Surf. Membr. Sci., 14, 1981, 484.

69. D.A. Mortimer and M.Nicholas, "The Wetting of Carbon and Caribides by Copper Alloys", J. Mat. Sci., 8, 1973, 640.

70. L. Froyen and A. Deruytter, "Proceedings of 4th European Symposium on Materials Science and Microgravity", T.D. Guyenne and J. Hunt (Eds.), Madrid, ESA SP-191, Noordwljk, 1983, p. 31.

71. A.C. Ferro, and B. Derby, Proceedings of the 1st International Conference on High Temperature Capillarity, N. Eustathopoulos (Ed.), Smolenice Castel, May 1994, Reproprint, Bratislava, 1995, p. 29.

72. F. Delannay, L. Froyen and A. Deruyttere, "Review: The Wetting of Solids by Molten Metals and its Relation to the Preparation of Metal-matrix Composites", J. Mat. Sci., 22, 1987, 1.

73. N. Mori, H. Sorano, A. Kitahara, K. Ogi and K. Matsuda, J. of the Japan Institute of Metals, 47, 1983, 1132.

74. S.M. Wolf, A.P. Levitt and J. Brown, Chemical Engineering Progress, 62, 1966, 74.

75. Mitsubishi Industries, Japanese Patent 5, 834, 148, 1983.

76. A.G. Kulkarni, B.C. Pai and N. Balasubramaniam, "The Cementation Technique for Coating Carbon Fibers", J. Mat. Sci., 14, 1979, 592.

77. M. Yoshida, S. Ikegami, T. Ohosaki and T. Ohokita, "Studies on Ion-plating Process for Making Carbon fiber Reinforced Aluminium and Properties of the Composites", Nat. SAMPE Symp., 24, 1979, p. 1417.

78. K.I. Paultnoi, S.E. Salibekov, I.L. Svetlov and V.M. Chubarov, "Structure and Properties of Composite Materials", 1979.

79. D.M. Goddard, "Interface Reactions During Preparation of Aluminium-Matrix Composites by the Sodium Process", J. Mat. Sci., 13, 1978, 1841.

80. O.S. Yourchenko, Sov. Powder Metall. Met. Ceram., 10, 1971, 35.

81. R.A. Huggins, J. Compos. Mater., 4, 1970, 434.

82. A. Miyase and K. Piekarski, "Compatibility of Chromium Carbide Coated Graphite Fibers with Metallic Matrices", J. Mat. Sci., 16, 1981, 251.

83. D.D. Himbeault, R.A. Varin and K. Piekarski, "Carbon Fibers Coated with Chromium Carbide Using the Liquid Metal Transfer Agent Technique", Met. Trans., 20A, 1989, 165.

84. M.S. Rashid and C.D. Wirkus, Ceramic Bulletin, 51, 1972, 836.

85. D.A. Mortimer, M.G. Nicholas and R.M. Crispin, "Int. Conf. On Carbon Fibers, Their Place in Modern Technology", The Plastic Inst., London, 1974, p. 101.

86. D.D. Himbeault, R.A. Varin and K. Piekarski, Met. Trans., 19A, 1988, 2109.

87. S. Morooka, J.I Hayashi, K. Kusakabe, H. Marda and B.K. Sea, Carbon, 34, 1996, 179.

88. Y.Q. Wang and B.L. Zhou, "Behaviour of Coatings on Reinforcements in Some Metal Matrix Composites", Composites PartA, 27A, 1996, 1139.

89. G.R. Cappleman, J.F. Watts and T.W. Clyne, "The Interface Region in Squeeze-Infiltrared Composites Containing Delta-Alumina Fibres in an Aluminium Matrix", J. Mat. Sci., 20, 1985, 2159.

90. J.P. Rocher, J.M. Quenisset, R. Pailler and R. Naslain, European Patent Office, Patent 0 105 890, 1983.

91. W.H. Pfeifer, "Graphite/Aluminium Technology Development", Hybrid and Select Metal Matrix Composites, W.J. Renton (Ed.), Chapter-6, American Institute of Aeronautics and Astronautics, 1977.

92. W.L. Lackman, R.A. Penty and A.F. Jahn (Fiber Materials Inc.), U.S. Patent 3894863, 1978.

93. W.C. Harrigan and R.H. Flowers, "Failure Modes in Composites IV", Cornie and Crossman (Eds.), TMS-AIME, 1977, p. 319.

94. W. Meyerer et al., Proc. of the Int. Conf. on Composite Materials, ICCM-2, AIME, 1978, p. 141.

95. L. Coudurier, J. Adorian, D. Pique and N. Edutathopoulos, Rev. Int. Hautes Temperate. Refract., 21, 1984, 81.

96. H.L. Marues, D.L. Hull and M.F. Amateau, "Failure Modes in Composites IV", Cornie and Crossman (Eds), TMS-AIME, 1977, p. 308.

97. J. Obinata and N. Komatsu, Keikinzoku, 14, 1964, 226.

98. R.Standing, and M.G. Nicholas, "The Wetting of Alumina and Vitreous Carbon by Copper-Tin-Titanium Alloys", J. Mat. Sci., 13, 1978, 1509-1514.

99. K. Landry, C. Rado, R. Voitovich, N. Eustathopoulos, Acta Mater., 45, 1997, 3079.

100. P.K. Ghosh, "Ph.D. Thesis", Department of Metallurgical Engineering, University of Roorkee, Roorkee, U.P., India, 1986.

101. R.Y. Lin, "Interface Evolution in Aluminium Matrix Composites During Fabrication", Metal Matrix Composites Part 2, G.M. Newaz, H. Nebar-Aeschobacher, F.N. Wohlbier (Eds.), Trans Tech. Publications, Switzerland, 1995.

102. J.W. Dinwoodie and I. Horsfal, "Proceedings of the Sixth International Conference on Composite Materials", ICCM VI, F.L. Matthews, N.C.R. Buskell, J.M. Hodginson and J. Morton (eds.), Elsevier Applied Science, London, 1987, p. 2390.

103. M. Gallernault and D.J. Lloyd, ASM/TMS-AIME Conference, Cincinnati, 1987.

104. E.G. Kendall, Composite Materials Vol.IV, Metallic Matrix Composites, L.J. Broutman and R.H. Krock (Eds.), Acad. Press, 1974, p. 319.

105. H.N. Hashemi and J. Seyyedi, "Study of the Interface and Its Effect on Mechanical Properties of Continuous Graphite Fiber Reinforced 201 Aluminium", Met. Trans., 20A, 1989, 727-739.

106. S.G. Warrier and R.Y. Lin, J. of Metals, 45, 1993, 24.

107. S.G. Warrier and R.Y. Lin, Met. and Mater. Trans., 3, 1995, 456.

108. M.F. Amateau, J. Compos. Mater., 10, 1976, 279.

109. S.M. Savvateeva and P. Sebo, Proceedings of International Symposium on Composite Materials, Paper No.21, 1978.

110. B. Veprik, M. Kurilev, E. Shtersel and V. Mukazhenov, Moscow International Conference on Composites, MICC 90, Proceedings Conf. MICC90, Moscow, USSR, Elsevier Science Publisher Ltd. 1990.

111. P. Bracke, H. Schurmans and J. Verhoest, "Inorganic Fibers and Composite Materials–A. Survey of Recent Developments", Pergamon International Information Corporation, Pergamon, 1984.

112. T.W. Chou and A. Kelly and A. Okura, "Fibre Reinforced Metal Matrix Composites", Composite, 16, 1985, 187.

113. J.T. Moore, D.V. Wilson, and T.W. Roberts, "Formability Limits of Metal-Metal composites on Rolling in the Direction of Fibre Alignment", Mater Sci. and Engg., 48, 1981, 107-112.

114. O. Watanabe, "The Compatibility and Mechanical Properties of the Carbon Fibre-Metal Composite Materials", Proc. of 1st Japan-USSR Symp. on Composite Materials, Moscow University Press, 1979, pp. 226-237.

115. L.O.K. Larsson and R. Warren, "Tungsten Wire Reinforced Metals for High Temperature Application", Advanced Fibres and Composites for Elevated Temperatures, op cit, pp.108-125.

116. G.A. Doble and I.J. Toth, "Roll Diffusion Bonding of Boron Aluminium Composites", Proc. ICCM-I, The Metallurgical Society of AIME, 1975, pp. 775.

117. S.T. Mileiko, "Fabrication of Metal-Matrix Composites", Fabrication of Composites, A. Kelly and S.T. Mileiko (Eds.), North Holland, Chapter-5, 1983, pp. 221-294.

118. J. Karwan-Bacezewska, T. Dymkowski and S. Seetharaman, "Sintered Intermetallic Compounds Type Fe-Al-Ni", Advances in Powder Metallurgy and Particulate Materials, Vol.4, Part 15, 1996.

119. J. Karwan-Bacezewska, T. Dymkowski and S. Seetharaman, "Manufacturing of Intermetallics Alloys by Conventional Powder Metallurgy and Thermochemical Treatment", Proc. of Int. Conf. on Non-Ferrous Metals and Alloys, Cracow, Poland, 1999.

120. F.V. Lenel, "Powder Metallurgy: Principles and Applications", Metal Powder Industries Federation, Princeton, New Jersy, USA, 1980.

121. S. Riaz and H.M. Flower, "Phase Transformation upon Heat Treatment of Ti6Al4V/TiC Composites Produced by Powder Metallurgy", Accepted for Publication in J. Mat. Sci. and Tech., 2000.

122. K.I. Portnoi, A.A. Zabolotskii and N.I. Timofeeva, Metal Science and Heat Treatment, 22, 1980, pp. 813-815.

123. J.R. Vinson and T.W. Chou, "Composite Materials and Their Use in Structures", Elsevier-Applied Science Publishers Ltd., London, 1975.

124. K.G. Satyanarayna, R.M. Pillai and B.C. Pai, Handbook of Ceramics and Composites, Vol. I, p. 495.

125. P.R. Beeley, "Foundary Technology", Butterworths, London, 1972.

126. C. Williams and K.M. Fisher, "Solidification Technology in the Foundry and Casthouse", The Metals Soc., 1983, p. 137.

127. H. Hu, "Squeeze Casting of Magnesium Alloys and Their Composites", J. Mat. Sci., 33, 1998, 1579-1589.

128. A.A. Das and S. Chatterjee, "Squeeze Casting of an Aluminium Alloy Containing Small Amounts of Silicon Carbide Whiskers", The Metallurgist and Materials Technologist, March 1981, pp. 137-142.

129. P.C. Carman, Soil Science, 52, 1941, 1-14.

130. S. Ergun, Chemical Engineering Progress, Vol.48, 2, 1952, 89-94.

131. V. Stanek and J. Szekely, J. AIChE, 20, 5, 1974, 974-980.

132. J.E. Drummond and M.I. Tahir, Int. J. Multiphase Flow, 10, 1984, 515-540.

133. A.S. Sangani and A.Acrivos, Int. J. Multiphase Flow, 8, 1982, 195-206.

134. L.J. Masur, A. Mortensen, J.A. Cornie and M.C. Flemings, "Infiltration of Fibrous Preforms by a Pure Metal: Part II, Experiment", Met. Trans., 20A, 1989, 2549-2557.

135. S. Yajima, J. Tanaka, K. Okamura, H. Ichikawa and T. Hayase, Rev. Chim. Miner., 18, 1981, 412.

136. G. Girot, J.P. Rocher, J.M. Quinisset and R. Nasalin, Proc. E-MRS Meeting, Fall, 1985.

137. A.A. Baker, D.M. Braddick and P.W. Jackson, "Fatigue of Boron-Aluminium and Carbon-Aluminium Fibre Composites", J. Mat. Sci., 7, 1972, 747-762.

138. I.H. Khan, "The Effect of Thermal Exposure on the Mechanical Properties of Aluminium-Graphite Composites", Met. Trans., 7A, 1976, 1282-1289.

139. Imprescia et al., "Carbide Coated Fibers in Graphite Aluminium Composites", NASA-CR-2711, LX-6181-PR, 1976.

140. A.A. Baker, "Carbon Fibre Reinforced Metals-A Review of Current Technology", Mater. Sci. and Engg., 17, 1975, 177-208.

141. M.C. Flemings, "Solidification Processing", McGraw-Hill, Inc., New York, 1974.

142. R.G. Dixon, M.Sc. Thesis, Dept. of Mat. Sci. and Engg., MIT, USA, 1985.

143. P.K. Rohotgi, R. Asthana and S. Das, Int. Met. Rev., 31, 1986, 115-139.

144. L.J. Masur, A. Mortensen, J. A. Cornie and M.C. Flemings, Proceedings of the Sixth International Conference on Composite Materials, ICCM-VI, F.L. Mathews, N.C.R. Buskell, J.M. Hodginson and J. Morton (Eds.), Elsevier Applied Science, London, 1987, pp. 2.320-2.329.

145. T.W. Clyne, Proceedings of the Sixth International Conference on Composite Materials, ICCM-VI, F.L. Mathews, N.C.R. Buskell, J.M. Hodginson and J. Morton (Eds.), Elsevier Applied Science, London, 1987, pp. 2.275-2.286.

146. A. Mortensen, J.A. Cornie and M.C. Flemings, "Columnar Solidification in a Metal Matrix Composite", Met. Trans, 19A, 1988, 709-721.

147. S. Towata and S. Yamada, J. Japan Institute of Metals, 48, 1984, 1192.

148. V.I. Kostikov, Y.I. Koshelev, E.F. Filimonov, E.M. Tatievskaya and R.N. Ponkrotova, Soviet Powder Metallurgy and Metal Ceramics, 20, 1981, 732-735.

149. W.H. Hunt, "Interfaces in Metal Matrix Composites", A.K. Dhingra, and S.G. Fishman (Eds.), Proc. Conf., New Orleans, TMS-AIME, 1986, pp. 3-25.

150. A. Mortensen, Ph.D. Thesis, Dept. of Material Science and Engineering, Massachusetts Institute of Technology, U.S.A., 1986.

151. M.N Gungor, J.A. Cornie and M.C. Flemings, Interfaces in Metal Matrix Composites", A.K. Dhingra, and S.G. Fishman (Eds.), Proc. Conf., New Orleans, TMS-AIME, 1986, pp. 185-202.

152. T. Erturk, J.A. Cornie and R.G. Dixon, "Interfaces in Metal Matrix Composites", A.K. Dhingra, and S.G. Fishman (Eds.), Proc. Conf., New Orleans, TMS-AIME, 1986, pp. 239-253.

153. S. Towata, S. Yamada, Trans. JIM, 27, 1986, 708.

154. O.B. Pederson, Proc. of the Fifth Int. Conf. on Composite Materials, ICCM-V, W.C. Harrigan, J. Strife and A.K. Dhingra (Eds.), San Diego, TMS-AIME, 1985, pp. 1-19.

155. S. Riaz, P.S. Sidky and M.G. Hocking, "Residual Stress Measurement After Thermomechanical Cycling of TiAlV-SiC Fibre Composites", Ist Int. Conf. of Composite Materials, Hargadha, Egypt, 1998.

156. T. Mori and M. Taya, "Composites'86: Recent Advances in Japan and the United States", K. Kawata, S. Umekawa and A. Kobayashi (Eds.), Proc. Japan-U.S. CCM-III, Tokyo, 1986, pp. 563-570.

157. J.C. Williams and G. Garmong, Met. Trans., 6A, 1975, 1699-1909.

158. J. England and I.W. Hall, Scripta Metallurgica, 20, 1986, 697.

159. S. Riaz, H.M. Flower and D.R.F. West, "Thermomechanical Behaviour of TiC Reinforced Ti Composites Produced by Different Routes", Accepted for Publication in J. Mat.Sci. and Engg., 2000.

160. M.H. Kural and B.K. Min, J. Compos. Mater., 18, 1984, 519-535.

161. S.R. Nutt and R.W. Carpenter, Mat. Sci. and Engg., 76, 1985, 169-177.

162. K. Tu and D. Turnbull, Acta Metall., 15, 1967, 3619.

163. G. Meyrick, Scripta Metall., 10, 1976, 649.

164. J.M. Howe, H.I. Aaronson and R. Gronsky, Acta Metall., 33, 1985, 649-658.

165. C. Laird and H.I. Aaronson, Acta Metall., 17, 1969, 505.

166. K.K. Chawla, "Composite Materials-Science and Engineering", B. Ilschner and N.J. Grant (Eds.), Springer-Verlag, New York Inc., 1987, p. 110.

167. L.J. Broutman and R.H. Krock, Composite Materials, Vol.1, Interfaces in Metal Matrix Composites, A.G. Metcalfe (Ed.), Academic Press, New York, 1974, p. 4.

168. A.T. Di Benedetto and L. Nicolais, "Interfaces in Composites", Advances in Composite Materials, G. Piatti (Ed.), Applied Science Pub. Ltd., London, 1978, pp. 153-181.

169. S.J. Baker and W. Bonfield, "Fracture of Aluminium Coated Carbon Fibres", J. Mat. Sci., 13, 1978, 1329-1334.

170. O. Kubaschewski and C.B. Alcock, "Metallurgical Thermochemistry, 5th Ed.", Pergamon Press, Oxford, U.K., 1983.

171. R. Everett, W. Henshaw, D.G. Simons and D.J. Land, "Composite Interfaces", H. Ishide and J.L. Koeing (Eds.), Elsevier, New York, 1986, p. 213.

172. D.M. Riggs, R.J. Shuford and R.W. Lewis, "Hand Book of Composites", Van Nostrand Reinhold, 1992, p. 196.

173. S.H. Lo, S. Dionne, G. Carpenter and D. Zimcik, "Interfaces in Metal-Ceramics Composites", The Mineral Metals and Mater. Soc., Anaheim, California, 1990, p. 165.

174. M. Yang and V.D. Scott, "Carbide Formation in a Carbon Fibre Reinforced Aluminium Composites", Carbon, 29, 1991, 877.

175. A.P. Diwanji and I.W. Hall, "Fibre and Fibre Surface Treatment Effects in Carbon/Aluminium Metal Matrix Composites", J. Mat. Sci., 27, 1992, 2093-2100.

176. G.J.C. Carpenter and S.H. J. Lo, "Characterization of Graphite Aluminium Composites Using Analytical Electron Microscopy", J. Mat. Sci., 27, 1992, 1827.

177. X.Q. Chen and G.X. Hu, Interfaces in Polymer, Ceramic and Metal Matrix Composites, H. Ishide (Ed.), Elsevier, New York, 1988, p. 381.

178. B. Maruyama, F.S. Ohuchi and L.Rabenberg, Interfaces in Metal Matrix Composites, A.K.Dhingra and S.G.Fishman (Eds.), AIME, Warrendale, PA, 1986, p. 233.

179. S. Lo, D. Finello, M. Scherling and H.L. Marcus, "Mechanical Behaviour of Metal Matrix Composites", Sym. Proc., AIME-ASM, Dallas, Texas, 1982.

180. S.E. Salibekov, A.A. Zabolotskii, V.A. Turchenkov, J.A. Kantserich, and E.M. Fadyukov, Sov. Powder Met. Ceram., 1977, 124.

181. C. Visconti, "Basic Design for Structural Applications of Composites", Advances in Composite Materials, G. Piatti (Ed.), Applied Science Publishers Ltd., London, 1978, pp. 75-89.

182. W. Voigt, Lehrbuch der Kritallphysik, Teubner, Leipzig, 1910.

183. A Reuss, Z. Angew. Math. Mech., 9, 1929, 49.

184. D.L. McDanels, R.W. Jech and J.W. Weeton, Trans. Metal. Soc., AIME, Vol.233, 1965, pp.636-642.

185. A Kelly and G.J. Davies, "The Principles of the Fibre Reinforcement of Metals", Met. Rev., 10, 1965, 37.

186. K.M. Prewo and K.G. Kreider, Met. Trans., 3, 1972, 2201-2211.

187. T. Kyono, I.W. Hall and M.Taya, "The Effect of Isothermal Exposure on the Transverse Properties of a Continuous Fibre Metal-Matrix Composite", J. Mater. Sci., 21, 1986, 4269-4280.

188. B.W. Rosen, AIAA Journal, 2, 1964, 1985-1991.

189. C. Zweben, AIAA Journal, 6, 1968, 2325-2331.

190. B.D. Coleman, J. Mech. Phys. Solids, 7, 1959, 60-70.

191. J.A. Dicarlo, J. of Metals., 37, 1985, 44.

192. L.W. Davis and P.G. Sullivan, "Exploratory Development of Graphite-Aluminium Composites", Final NETCO Report under contract No. 0024-75-C-5002 to Naval Sea Systems Command, U.S.A., 1976.

193. J.R. Singh, "The Role of Composites as an Enabling Materials Technology for Transition to 300 mm Precision Systems", Future Fab. Int., Issue 5, July 1998.

194. J.R. Singh, "Metal Matrix Composites: An Enabling Materials Technology for Precision Semiconductor Equipment Manufacturers", SEMI Executive Summary Report VII, 3, 1997, pp.4-7.

195. T. Ohsaki, M. Yoshida, Y. Fukube and K. Nakamura, Thin Solid Films, 45, 1977, 563.

196. A. Kelly and K.N. Street, Proc. R. Soc. London, 328A, 1972, p. 283.

197. M. Lilholt, "Fatigue and Creep of Composite Materials", Third Riso International Symposium, Riso, Denmark, 1982.

198. M. Mclean, Proc. Of the Fifth Int. Conf. on Composite Materials, ICCM-V, TMS-AIME, Warrendale, PA, 1986, p. 37.

199. M.F. Amateau and W.D. Hanna (Aeroopace Corp.), "Fatigue Behaviour of Aluminium Alloy-30% Graphite Fiber Composites", Report ART-75 (9450)-1, 1975.

200. K.D.Shimmin and I.J.Toth, "Failure Modes in Composites I", I.J.Toth (Ed.), The Metallurgical Society-American Institute of Mining, Metallurgical and Petroleum Engineers, 1973, p. 357.

201. J.L.Christian, ASTM STP 569, American Society for Testing and Materials, 1975, pp.280-292.

202. G. Rosenkranz, V. Gerold, D. Stockel and L. Tillmann, "Fatigue Behaviour of Metallic Fibre Reinforced Materials: A Study of Steel Fibre Reinforced Silver, Part-I Low Cycle Fatigue", J. Mat. Sci., 17, 1982, 264.

203. C.R. Crowe, R.A. Gray and D.F. Hasson, Proc. of the Fifth Int. Conf. on Composite Materials, ICCM-V, TMS-AIME, Warrendale, PA, 1986, p. 843.

204. J. Dinwoodie, E. Moore, C.A.J. Langman and W.R. Symes, The Properties and Applications of Short Staple Alumina Fibre Reinfroced Aluminium Alloys, Fifth Chemical International Conference on Composite Materials, San Diego, California, U.S.A., 1985.

205. S.B. Lasday, "Ceramic Fibre Utilization in Metal Matrix Composites", Industrial Heating, 54, 1987, 20-21.

206. R. Wilson, "Aluminium Metal Matrix Composites for High Speed Diesel Pistons, Engines and Drives", Diesel Progress, 54, 1988, 4-6.

207. S.Y. Zhang, "A Simple Approach to the Evaluation of Fibre/Matrix Interfacial Shear Strength and Fracture Toughness", Composite Science and Technology, 60, 2000, 145-148.

208. S.Y. Zhang, "A New Model for the Energy Release Rate of Fibre/Matrix Interfacial Fracture", Composite Science and Technology, 58, 1998, 163-166.

209. M.R. Piggot, "Debonding and Friction at Fibre-Polymer Interfaces I: Criteria for Failure and Sliding", Composite Science and Technology, 30, 1987, 295-306.

210. V. Con, O. Allix, P. Sigety and M.H. Auvray, "Compressive Performance of Carbon Fibres: Experiment and Analysis", Composite Science and Technology, 58, 1998, 1649-1658.

211. A. Kelly and W.R. Tyson, "Tensile Properties of Fibre Reinforced Metals: Copper/Tungsten and Copper/Molybdenum", J. Mech. Phy. Solids, 13, 1965, 329-350.

212. L.D. Lucas, Physiochemical Measurements in Metals Research, R.A. Rapp (Ed.), Interscience Publishers, New York, 4, 1970, p. 210.

213. Secrist and Winsyl, Acta Cryst., 15, 1962, 1042.

214. R. Hultgren, P.D. Desai, D.T. Hawkins, M. Gleiser, K.K. Kelly and D.D. Wagman, Selected Values of the Thermodynamic Properties of the Elements, American Society for Metals, Metals Park, Ohio, 1973.

215. A.I. Belyaev and E.A. Zhemchugina, Poverkhnostie Yavleniya V Metalluggichek Protssessakh-Metallurgizdat, Moscow, 1952.

216. B. Dervet, S. Kalogeropoulou and N. Eustathopoulos, Acta Metall. Mater., 41, 1993, 3119.

217. A.E.W. Jarfors, L. Svendsen, M. Wallinder and H. Fredriksson, Metallurgical Transactions A, 24A, 1993, 2577.

218. L.F. Mondolfo, Aluminium Alloys: Structure and Properties, Butterworths, London, U.K., 1976, p. 18.

219. S. Mercier, P. Ehrburger and J. Lahaye, "Interfacial Reactivity of Aluminium/Fibre Systems During Heat Treatments", J. Mat. Sci., 30, 1995, 4770-4774.

220. H. Fukunaga and M. Kuriyama, Bulletin of JSME, 25, 1982, 842.

221. R.M. Hoffman and L.F. Beste, "Some Relation of Fiber Properties to Fabric Hand", J. Text. Res., 21, 1951, 66-67.

222. R. Gauvin and M. Chibani, "Modelization of Clamping Force and Mold Filling in Resin Transfer Molding", Proceedings of the Society for the Plastics Industry, Reinforced Plastics-Composites Institute, 43rd Annual Conference, Session 22C, Cincinati, OH, 1988, pp. 1-4.

223. C.M. Van Wyk, "Note on the Compressibility of Wool", J. Text. Inst., 37, 1946, T285-T-292.

224. H. Bogaty, N.R.S. Hollies, J.C. Hintermaier and M. Harris, "The Nature of a Fabric Surface: Thickness-Pressure Relationships", J. Text. Res., 23, 1953, 108-114.

225. T.G. Gutowski, "A Resin Flow/Fiber Deformation Model for Composites", SAMPE Quart, 16, 4, 1985, 58-64.

226. S. De Jong, J.W. Snaith and N.A. Michie, "A Mechanical Model for the Lateral Compression of Woven Fabrics", J. Text. Res., 57, 1986, 759-767.

227. Z. Cai and T.G. Gutowski, "The 3-D Deformation Behaviour of a Lubricated Fibre Bundle", J. Comp. Mater., 26, 1992, 1207-1237.

228. T.G. Gutowski and G. Dillon, "The Elastic Deformation of Lubricated Carbon Fibre Bundles: Comparison of Theory and Experiments", J. Comp. Mater., 26, 1992, 2331-2347.

229. T.G. Gutowski and G. Dillon, "The Elastic Deformation of Fibre Bundles", Advanced Composites Manufacturing, T. G. Gutowski (Ed.), John Wiley and Sons, NY, 1997, pp. 115-156.

230. P. Simacek and V.M. Karbhari, "Notes on the Modelling of Preform Compaction: I-Micromechanics at the Fiber Bundle Level", J. Reinf. Plast. Comp., 15, 1996, 86-122.

231. V.M. Karbhari and P. Simacek, "Notes on the Compaction of Preform Compaction: II-Effects of Sizing on Bundle Level Micromechanics", J. Reinf. Plast. Comp., 15, 1996, 837-861.

232. M. Matsudaira and H. Qin, "Features and Mechanical Properties of a Fabric's Compressional Property", J. Text. Inst., 86, 1995, 476-486.

233. B. Chen and T.W. Chou, "Compaction of Woven Fabric Preforms in Liquid Composite Moulding Processes: Single-Layer Deformation", Composite Science and Technology, 59, 1999, 1519-1526.

234. M. Ito and T.W. Chou, "An Analytical and Experimental Study of Strength and Failure Behaviour of Plain Weave Composites", J. Comp. Mater., 32, 1998, 2-30.

235. T. Ishikawa and T.W. Chou, "Stiffness and Strength Behaviour of Woven Fabric Composites", J. Mater. Sci., 17, 1982, 3211-3220.